SENSING MATERIALS BASED ON IONIC LIQUIDS

A Thesis
Presented to
The Academic Faculty

by

Amir H. Saheb

In Partial Fulfillment
of the Requirements for the Degree
Doctor of Philosophy in the
School of Chemistry and Biochemistry

Georgia Institute of Technology
August 2008

SENSING MATERIALS BASED ON IONIC LIQUIDS

Approved by:

Dr. Jiří Janata, Advisor
School of Chemistry and Biochemistry
Georgia Institute of Technology

Dr. Uwe Bunz
School of Chemistry and Biochemistry
Georgia Institute of Technology

Dr. Mira Josowicz
School of Chemistry and Biochemistry
Georgia Institute of Technology

Dr. Paul Kohl
School of Chemical Engineering
Georgia Institute of Technology

Dr. David Collard
School of Chemistry and Biochemistry
Georgia Institute of Technology

Date Approved: June 30, 2008

To my parents,

ACKNOWLEDGEMENTS

I would like to express my sincere gratitude to my thesis advisors Professor Jiří Janata and Dr. Mira Josowicz for their guidance, support, and constant encouragement that has made this quest a success. I would also like to thank Dr. Uwe Bunz, Dr. David Collard, and Dr. Paul Kohl for their willingness to serve on my thesis advisory committee and for their helpful comments. I would like to thank the Janata research group members for their friendship and assistance. The support by the grant of the National Science Foundation (CHE 0137391 and CHE 0452045) is also gratefully acknowledged. Finally, I also thank my mother and father for providing me with the foundation for who I am and all my achievements.

TABLE OF CONTENTS

LIST OF TABLES

LIST OF FIGURES

SUMMARY

The first chapter of this thesis describes the motivation behind using room temperature ionic liquids (RTILs) in gas sensor research and provides the reader with background knowledge of RTILs and a review of current applications of RTILs in various sensors.

The second chapter describes electrochemical polymerization of aniline in room temperature 1-butyl-3-methylimmidazolium (BMI) ionic liquids without addition of any acid. It is shown that the polymerization of aniline in BMI(BF_4) does require small but controlled amounts of water whereas the polymerization in BMI(PF_6) and in BMI(TF_2N) does not require any water addition. Differences in the cyclic voltammograms during polymerization of aniline are observed. In addition, all the synthesized polyaniline films show stable electroactivity in a wide potential range.

The third chapter describes the construction of reference electrodes for RTIL applications that have a known and reproducible potential versus the ferrocene/ ferrocenium couple. They are based on reference electrodes of the first kind, Ag/Ag^+ couple type, or of the second kind, based on Ag/AgCl in M^+Cl^-. The former uses $AgNO_3$ salt and the latter tetrabutylammonium chloride, $Bu_4N^+Cl^-$, dissolved in acetonitrile which are then introduced to the ionic liquid of choice for a final concentration of 0.1M. The stability, reproducibility, and temperature behavior of the two reference systems have been characterized in the following ionic liquids: 1-butyl-3-methylimidazolium tetrafluoroborate [BMI(BF_4)], 1-butyl-3-methylimidazolium bis(trifluoromethane-

sulfonyl)imide [BMI(TF_2N)], and 1-butyl-3-methylimidazolium hexafluorophosphate [BMI(PF_6)].

The fourth chapter describes the electrochemical preparation and spectral analysis of gold clusters by adding gold atoms one-by-one ("bottom up" approach) through polyaniline's ability to form a strong complex with chloroaurate at the protonated imine sites. It is contrasted with the "top down" approach in which the growth of multi-atom Au clusters was also controlled electrochemically. Our results confirm that both the amount and the size of gold clusters affects the properties of the composite material.

The fifth chapter describes the development and characterization of a CHEMFET sensing layer based on a composite of CSA-doped polyaniline (PANI), and the room temperature ionic liquid 1-butyl-3-methylimidazolium bis(trifluoromethanesulfonyl)-imide, BMI(TF_2N) for the sensing of ammonia gas. The work function responses of the cast films with and without IL are analyzed by "step-wise" changes of ammonia gas concentration from 0.5 to 694 ppm in air as a function of the mole fraction of IL to PANI. The PANI·CSA/BMI(TF_2N) layers shows enhanced sensitivities, lower detection limit and shorter response times. There is a strong indication that ammonia also forms a charge transfer complex with imidazolium cation in which it acts as an electron acceptor.

The final chapter describes the preparation and characterization of field-effect transistors with mixed ionic-electronic conductors that have been created by varying the ratio of room temperature ionic liquid and emeraldine salt of polyaniline. Transistor with sufficiently high electronic conductivity (32mol% ES-PANI) and Au gate contact exhibited theoretical behavior of insulated gate field-effect transistor. On the other hand

the purely ionic gate behaved irreproducibly, indicating that a capacitive divider has been formed in the gate.

CHAPTER I

INTRODUCTION

1.1 Advantages of Ionic Liquids

Polyaniline can be synthesized chemically or electrochemically in a wide range of aqueous and organic electrolytes.[1,2] However, changes in the concentration of dopants and organic solvents, due to evaporation, result in physical and chemical instability of the PANI material, limiting PANI applications in devices such as sensors.

The goal of this thesis was to develop a chemical sensing interface which promotes faster diffusion of gaseous species and has enhanced mechanical and chemical stability. Development of this interface will be based on the conducting polymer polyaniline (PANI) which has room temperature ionic liquids (RTILs) incorporated into the polymer matrix to result in a permeable gel.

Dopable π-conjugated polymers such as polyaniline (PANI), polypyrrole (PPy), and polythiophene (PT) have attracted attention for application in various electrochemical devices including batteries, capacitors, electrochromic displays, actuators, photovoltaic cells, and sensors.[3] While significant effort has been spent toward the development of new high-performance π-conjugated polymer materials, less attention has been paid to the importance of the electrolyte in determining device performance. The realization of useful, long-lived π-conjugated polymer electrochemical devices thus remains a difficult goal because of performance limitations that include poor environmental stability, slow switching speeds, and short lifetimes when electrochemically cycling between oxidation states. These problems are derived in part from the electrolytes used in the devices. Improved electrolytes are needed that concurrently satisfy the requirements of high ionic

conductivity (>10^{-4} S cm^{-1}), large electrochemical windows (>1 V) over which the electrolyte is neither reduced nor oxidized at an electrode, low volatility, and environmental stability. Certain members of the family of materials known as ionic liquids meet all these conditions.

To date, most of the research on π-conjugated polymer actuators has been carried out in aqueous electrolytes. Unfortunately, these systems suffer from narrow electrochemical potential windows and high volatility. These factors limit the lifetime and performance of a device. For example, electrochemical degradation of polyaniline occurs after only a few cycles in some aqueous electrolytes because of nucleophilic attack on, and hydrolysis of, the polymer. Nonaqueous electrolytes, e.g., lithium salts in propylene carbonate can be used to improve the performance of polyaniline and other π - conjugated polymer electrochemical actuators. Propylene carbonate has a relatively high boiling point (241.7°C), low vapor pressure (0.039 mm Hg), high dielectric constant (64.4), high ionic conductivity with dissolved lithium salts (0.1 to 1.0 mS/cm), and a relatively broad electrochemical window (–1.9 to +1.7 V versus saturated calomel electrode). Nevertheless, organic electrolyte systems are still susceptible to evaporation, thus limiting the operational voltage range and device lifetime.

1.2 Ionic Liquid Structures

An alternative to organic electrolytes are ionic liquids. Typically, ionic liquids consist of nitrogen containing organic cations and inorganic anions. As they are nonvolatile and nonflammable, have high thermal stability, and are relatively inexpensive to manufacture, ionic liquids are now finding applications in chemical synthesis, catalysis, separation technology, and the fabrication of conventional electrochemical

devices.[4] Ionic liquids are salts that are fluid over a wide temperature range, including room temperature, with higher viscosities (10^{-2} to 10^{0} Pa s) than either aqueous (>10^{-3} Pa s) or organic (~6 x 10^{-3} Pa s) electrolytes at room temperature.

Room temperature ionic liquids consist of bulky and asymmetric organic cations such as 1-alkyl-3-methylimidazolium, 1-alkylpyridinium, N-methyl-N-alkylpyrrolidinium and ammonium ions. A wide range of anions is employed, from simple halides, which generally inflect high melting points, to inorganic anions such as tetrafluoroborate and hexafluorophosphate and to large organic anions like bistriflimide, triflate or tosylate. There are also many interesting examples of uses of ionic liquids with simple non-halogenated organic anions such as formate, alkylsulfate, alkylphosphate or glycolate. As an example, the melting point of 1-butyl-3-methylimidazolium tetrafluoroborate or BMI(BF_4) with an imidazole skeleton is about -80 °C, and it is a colorless liquid with high viscosity at room temperature.

The cations of the ionic liquid include organic and inorganic cations. The cation employed in this thesis is a dialkylimidazolium ion and this cation can be used with a number of different anions, Figure 1.1. The anion includes organic and inorganic anions such as PF_6^-, $CF_3SO_3^-$, CF_3COO^-, *etc*.

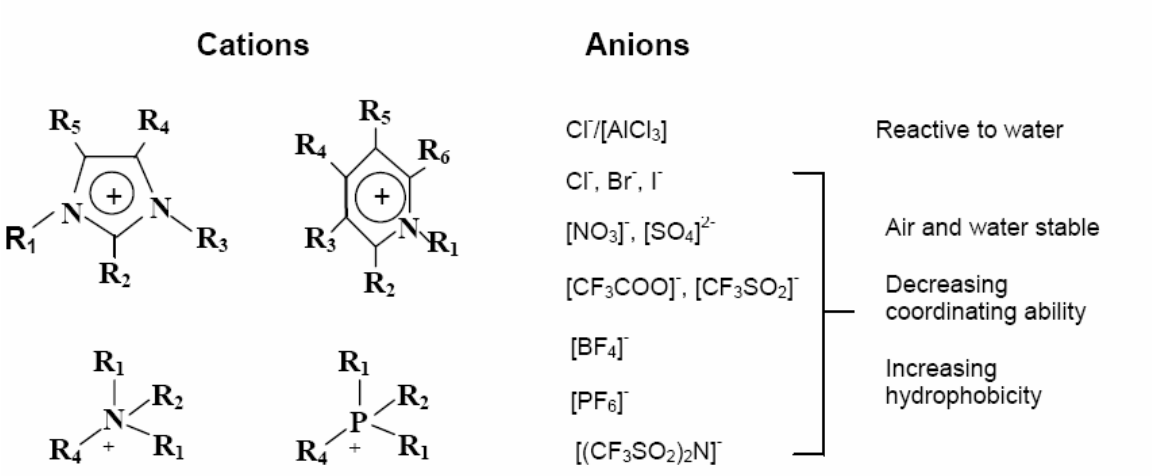

Figure 1.1: Examples of common cations and anion pairs used in the formation of ionic liquids, and general progression of changes in IL properties with anion type.

1.3 Basic Properties of Ionic Liquids

The physical and chemical properties of ionic liquids can be varied over a wide range by the selection of suitable cations and anions. Some of the properties that depends on the cation and anion selection includes: melting point, viscosity, and solubility characteristics.[5]

One of the more important properties for the assessment of an ionic liquid is its melting point. The solid-liquid transition temperatures of ionic liquids can be below ambient temperature. The dominant force in ionic liquids is Coulombic attraction between ions. Reports in the literature show that factors such as, low symmetry, weak intermolecular interactions (such as the avoidance of hydrogen bonding), and a good distribution of charge in the cation are the main factors that influence the melting point of the salts, as generic classes.[6-9] Within a similar series of salts, however, small changes in the shape of uncharged, covalent regions or the ions can have an important influence on the melting points of the salts, Table 1.1.

Table 1.1: Melting points of various chlorides.

Salt		Melting point (°C)
NaCl		803
KCl		772
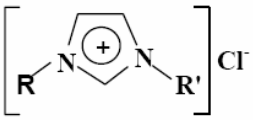	R=R' = methyl (MMIM)Cl	125
	R= methyl, R'= ethyl (EMIM)Cl	87
	R= methyl, R'= n-butyl (BMIM)Cl	65

Besides the cation, the anion influences the melting point, too. As the size of the anion increases, the melting point of the salt decreases, Table 1.2.

Table 1.2: Influence of different anions on the melting point of imidazolium salts.

Salt	Melting point (°C)
(EMIM)Cl	87
(EMIM)NO_2	55
(EMIM)NO_3	38
(EMIM)$AlCl_4$	7
(EMIM)BF_4	15
(EMIM)CF_3SO_3	-9
(EMIM)CF_3CO_2	-14

Another important property of ionic liquids is their inherent viscosity. In ionic liquids the viscosity is determined by their tendency to form hydrogen bonding and by the strength

of their van der Waals interactions and hydrogen bonding.[7] The viscosities of many ionic liquids are strongly dependent upon temperature.

Morever, by changing the nature of the ions present in an IL, it is possible to change the resulting properties of the IL. For example, the miscibility with water can be varied from complete miscibility to almost total immiscibility, by changing the anion from Cl^- to PF_6^-. [5]

1.4 Nanoparticles and Ionic Liquids

It has been shown that many synthetic processes using transition metal catalyst, metal nanoparticles play an important role as the actual catalyst or as a catalyst reservoir. It also been shown that ILs are an appealing medium for the formation and stabilization of catalytically active transition metal nanoparticles. More importantly, ILs can be made that incorporate co-ordinating groups, for example, with nitrile groups on either the cation or anion (CN-IL).[10] In various C-C coupling reactions catalyzed by palladium catalyst, it has been found the palladium nanoparticles are better stabilized in CN-IL compared to non-functionalized ionic liquids; thus enhanced catalytic activity and recyclability are realized.[11]

Incorporation of nanoparticles into a sensing layer would have viable applications for sensing as nanoparticles have catalytic properties which lead to enhanced sensitivity and selectivity of certain analytes. The fourth chapter of this thesis describes an electrochemical approach for the preparation of such clusters in a polyaniline matrix.

1.5 Sensors Based on Ionic Liquids

Extensive efforts have been made to develop new materials and transducers for gas sensing both at room and at high temperatures with particular emphasis on optimizing interface properties among the gas phase, the sensitive materials, and the transducer. IL thin

films perform well as sensor interfaces and provide additional control over selectivity and sensitivity when interacting with analytes in the gas phase.

Due to the entire ionic composition, ILs are unique compounds to be used in the development of stable electrochemical sensors for gaseous analytes such as O_2, CO_2, and NH_3.[12-18] The superoxide radical ($O_2^{\bullet-}$) which is generated in situ by the reduction of O_2 was found to be stable in ILs at glassy carbon, gold (Au) or platinum (Pt) electrodes.[12-15] This allows for amperometric detection of O_2 and the O_2 gas sensor based on porous polyethylene supported EMI(BF_4) membrane has a wide detection range, high sensitivity and reproducibility.[12] With increasing levels of CO_2 in the sample, cyclic voltammetry showed increased cathodic peak current from the creation of $O_2^{\bullet-}$ radicals together with the decreased peak current from the reverse scan of oxidation providing an amperometric way to detect CO_2.

In addition, the electrochemical oxidation of the nitrite ion (NO_2^-) and nitrogen dioxide gas (NO_2) in EMI(Tf_2N) have been studied by cyclic voltammetry on Pt electrodes of various sizes.[19] Using chronoamperometrical techniques, the following solubility values were calculated: 7.5 mM for NO_2^- and approximately 51 mM for NO_2, demonstrating this IL is a potential media for sensing NO_2 gas.

Moreover, determination of ammonia based on the electrooxidation of hydroquinone in dimethylformamide (DMF) and EMI(Tf_2N) has also been conducted.[17] Ammonia can remove protons from the hydroquinone molecules reversibly and thus assists in the oxidation process resulting in a peak at less positive potentials. Similar responses were found both in dimethylformamide and EMI(Tf_2N).

The viscosity of an IL is generally higher than that of organic solvents resulting in a considerably slower mass transport. Even though the slow mass transport will cause a longer response time of the gas sensors based on IL, it is still sufficient in many practical applications. Such sensors will have potential applications mainly in more extreme operating conditions, such as high temperature and pressure where conventional solvents would evaporate or decompose. The low-volatility and remarkable thermal stability make ILs suitable for gas sensing especially at high temperature.

Furthermore, ILs are a new class of sensing materials for detection of organic vapors when using the quartz crystal microbalance (QCM) technique.[21-23] QCM is a mass sensor and the working principle of QCM is based on the change in frequency that is measured between a reference state and when the quartz crystal is exposed to a sample vapor. In an ideal case, the frequency change is only caused by the change in mass loading on the surface of the vibrating crystal. However, Liang et al. showed that changes in viscosity of the IL film upon absorption of organic vapors at room temperature was the main cause for the change in frequency rather than change in the mass of the IL film.[21] The sensing mechanism of a QCM sensor using ILs is based on the fact that the viscosity of the IL membrane decreases rapidly due to solvation of the analytes in the ILs. However, the change of viscosity caused by the gas absorption becomes rather small at high temperature and the frequency changes are then mainly due to changes in mass of the IL film.

One of the added benefits of using ILs is they offer many options for chemical modifications allowing greater flexibility in designing molecular recognition sites in their structures. These possibilities offer opportunities to explore the applications of ILs in high sensitive and selective determination of trace analytes using ILs in sensor arrays. For

example, a task specific IL with an amine group on the cation has been designed to capture CO_2 and was reported to enhance significantly the solubility of CO_2 in that particular IL.[27] A set of diverse ILs showed selective responses to different organic vapors due to structural differences in the used ILs. Therefore, a sensor array of ILs would be able to effectively differentiate different vapors in using pattern recognition methods, and having increased selectivity to organic vapors both at room and high temperatures.[22] Since the physicochemical properties of ILs can be tuned to fit in particular applications the ILs can provide high solubility of analytes and hence short response and desorption times, as well as an quick baseline recovery after exposure to sample vapors.

CHAPTER II

ELECTROPOLYMERIZATION OF ANILINE FROM IONIC LIQUIDS

2.1 Introduction

Polyaniline (PANI) is probably the most studied conducting polymer because its structural flexibility allows a broad tuning of physical and chemical properties. It can be synthesized chemically or electrochemically in a wide range of aqueous and organic electrolytes. However, changes in conductivity, morphology and mechanical stability of the PANI material are often related to gradual changes in concentration of acid or organic solvent due to evaporation. This instability sometimes limits PANI applications in device fabrication, such as batteries, supercapacitors, actuators, sensors, etc. Degradation of the polymer due to over-oxidation is also observed if the applied potential exceeds 1V vs. SHE. That behavior limits the use of PANI as an electrochromic material. In order to overcome some of these problems, we investigated the use of room temperature ionic liquids (RTIL) as the electrolytes for electropolymerization of PANI. Electrochemical synthesis of conducting polymers, such as polypyrrole and PEDOT in pristine ILs and PANI in BMI(BF_4) in the presence of acid, e.g. CF_3COOH, as a proton source has been reported.[28] In this study the electropolymerization of aniline in BMI(BF_4), BMI(PF_6) and BMI(Tf_2N) without addition of any acid is investigated.

Ionic liquids especially those based on the 1,3 dialkylimidazolium cations and BF_4^-, PF_6^-, and Tf_2N^- anions have a negligible vapor pressure, large viscosity, high polarity, high thermal and chemical stability, high intrinsic conductivity, and wide electrochemical window.[13,29] They are emerging as a new class of electrolytes for synthesis, extraction and catalysis.[29-33] Moreover, the properties of the BMI ionic liquid

can be tuned using different anions; BF_4^- is water soluble at room temperature, whereas PF_6^- is much less water miscible.[33,34] Presence of trace amounts of water in BMI(PF_6) or in BMI(BF_4) might form HF acid. The BMI(Tf_2N) has a higher density, lower surface tension and lower viscosity than BMI(PF_6).[34,35] The BMI(Tf_2N) exhibits the highest hydrogen bond acidity.[36] It is expected that the anion may have a significant effect on reactivity of aniline during the electropolymerization.

2.2 Experimental

2.2.1 Chemicals

Aniline and ferrocene were obtained from Aldrich and were used without further purification. Both, 1-butyl-3-methylimmidazolium tetrafluoroborate, BMI(BF_4), and 1-butyl-3-methylimmidazolium bis(trifluoromethanesulfonyl)imide BMI(Tf_2N), were synthesized by us according to standard procedures.[37] The presence of colored impurities was examined by UV-visible absorption spectroscopy. No absorbance was observed between 400 and 700 nm suggesting absence of any impurities. According to the literature, the BMI(PF_6)-based liquid contains a moderate amount of water, ranging from 150 to 360 ppm. The BMI(Tf_2N) has the lowest water content of 80 ppm.[38,39] Examination of the ^1H NMR before and after drying was also conducted, showing the removal of impurities, Figure 2.1.

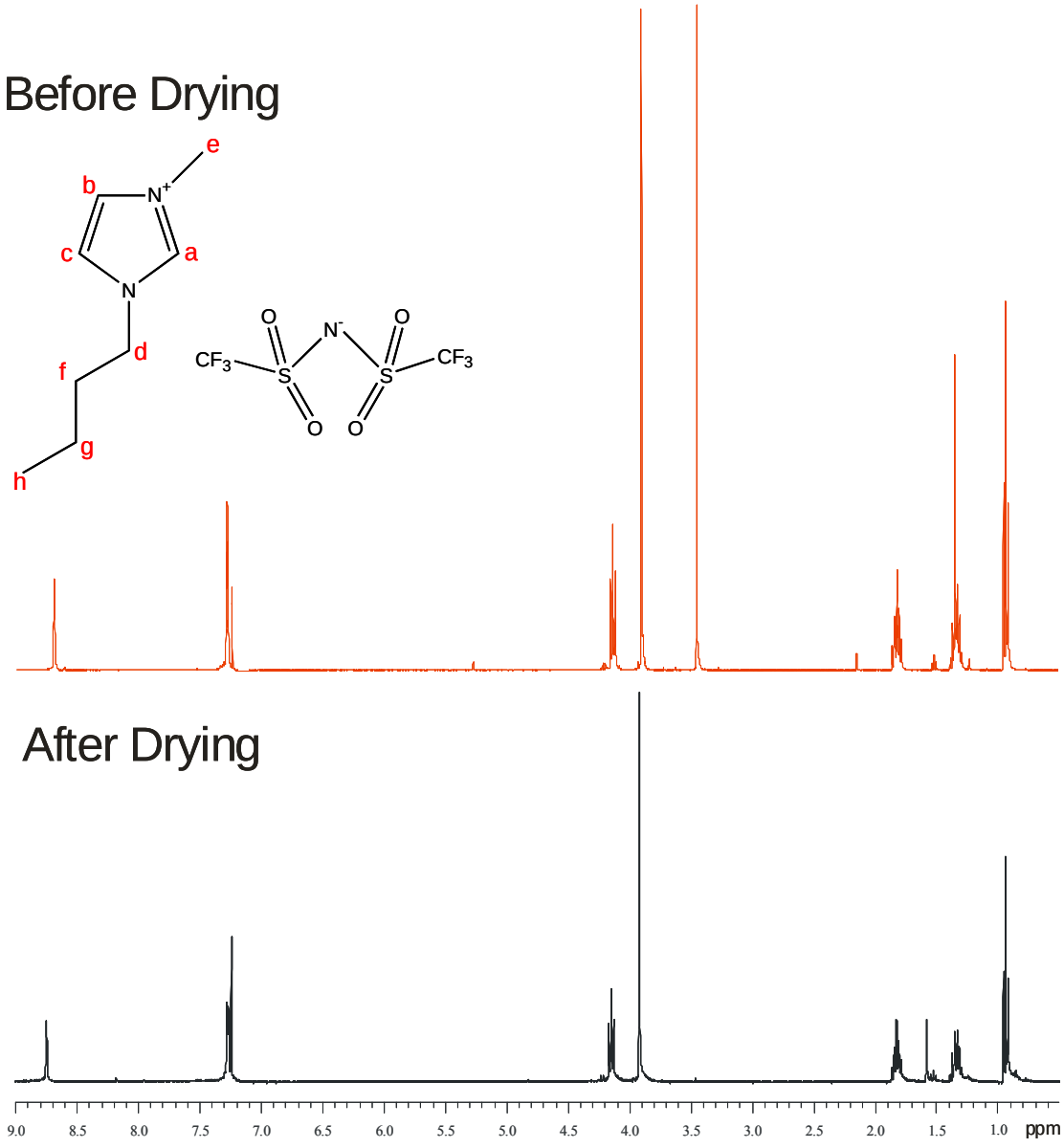

Figure 2.1: ^{1}H NMR of BMI(Tf_2N) before and after drying at 60^{o}C under vacuum.

2.2.2 Instrumentation

All CVs were recorded using CH, Inc. (Model 401) potentiostat. The electrochemical cell consisted of Pt-electrode as a working electrode (diameter 1.0 mm), Pt wire coil as a counter electrode and silver wire as a quasi-reference electrode. Potential of the reference redox couple ferrocene/ferrocenium (Fc/Fc^{+}) at Pt electrode was determined to be 0.34 V in BMI(BF_4), 0.26 V in BMI(PF_6)and 0.28 V in BMI(Tf_2N). That places the reference potential of the Ag electrode vs SHE for BMI(BF_4) at 0.74 V, BMI(PF_6) at 0.66V and BMI(Tf_2N) at 0.68 V, respectively.

FT-IR spectra were collected on a BIORAD FTS-6000 spectrometer with a BIORAD UMA 500 IR microscope run in the ATR mode using a germanium crystal. All the FT-IR spectra of the cast films were measured using a gold substrate as a background.

2.2.3 Electropolymerization of Aniline

Electropolymerization of PANI was always carried out from 0.1 M aniline in the ionic liquid of choice. Polymerization in BMI(BF_4) was also conducted with additions of deionized water. The water was added into the ionic liquids by weighing. The mol fractions of water in BMI(BF_4) were 0.06, 0.11, 0.16, and 0.20 that correspond to molar concentrations of 0.34 M, 0.68 M, 1.02 M, and 1.36 M, respectively. The samples were vigorously shaken and allowed to equilibrate for 24 hours prior to polymerization. All polymerized PANI films on Pt-electrode were always rinsed with the ionic liquid from which they were electropolymerized. The CVs of the deposited PANI films were recorded under the same electrochemical conditions as those used for polymerization.

2.3 Results and Discussion

2.3.1 Electrochemical Behavior of Ionic Liquids

To explore the possibility for polymerization of aniline on Pt electrode in ionic liquids, cyclic voltammetric measurements in pristine ionic liquids were first conducted. Figure 2.2 shows the electrochemical window in BMI(BF_4) and BMI(PF_6) from +2.5 V to -2.0 V and from +2.9 V to -2.0 V in BMI(Tf_2N). At the cathodic limit irreversible reduction of 1-butyl-3-methylimmidazolium cation sets in and at the anodic limit the decomposition of the anion is observed.[7,40]

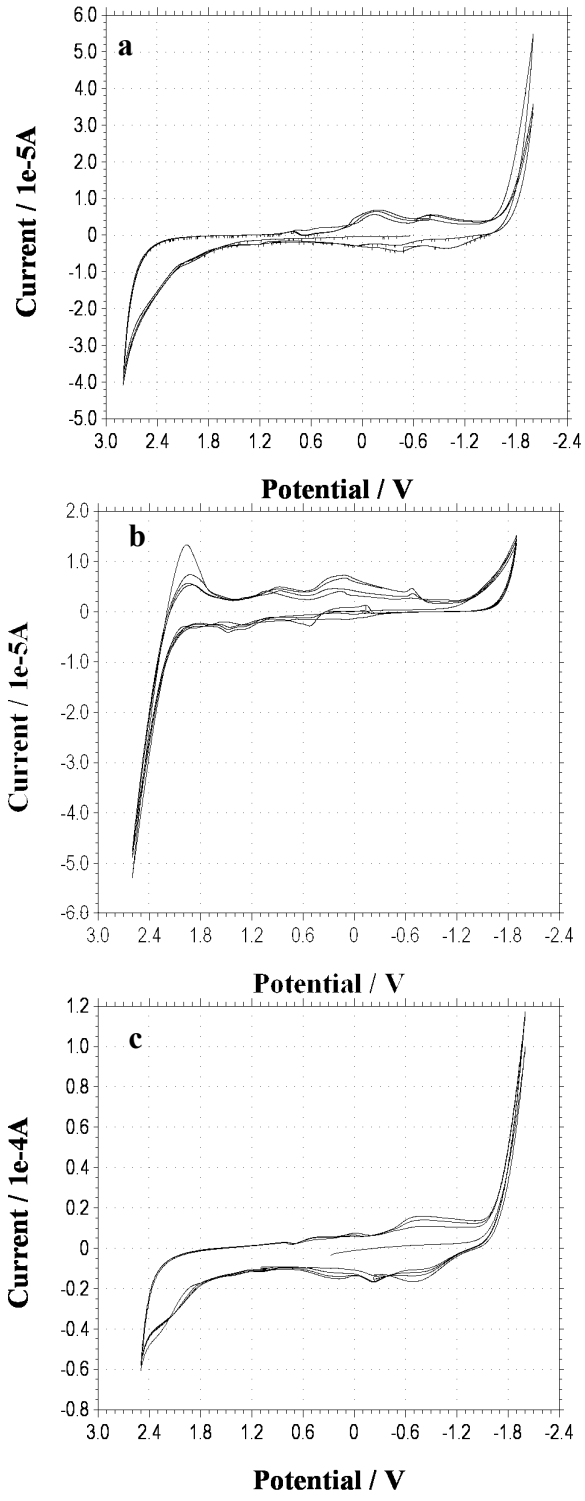

Figure 2.2: Cyclic voltammograms of Pt electrode in a) BMI(Tf_2N), b) BMI(PF_6) and c) BMI(BF_4), all recorded at the sweep rate 20 mV/s vs. Ag reference electrode.

BF_4^- is less polarizable and is a harder base than the fairly large, polarizable and less basic PF_6^- ion. Therefore, BF_4^- has the ability to form a tighter interaction with the hydrogen atoms of the imidazolium cation than the PF_6^- ion and it is less sensitive to solvation effects than the hydrogen atoms of BMI(PF_6).[41,42] It is seen that in all ionic liquids, around -0.7 V, a small shoulder appears. After purging oxygen through the BMI(BF_4) this shoulder is developing to a quasi-reversible redox peak. The potential separation between the reduction and re-oxidation of the O_2 species is ca. 110 to 160 mV at 40 mV/s (Figure 2.3). By adding 0.35 M water to the ionic liquid, the reduction potential of O_2 is shifting slightly into the negative direction and the peak current is increasing. This confirms that the redox potential of O_2/ O_2^- depends on the degree of solvation of O_2^-.[43,44] It was observed that the degree of solvation of O_2^- increases as the acceptor number of the medium increases.[45] The influence of adding water on the oxidation of ferrocene was also monitored. The effect is not significant.

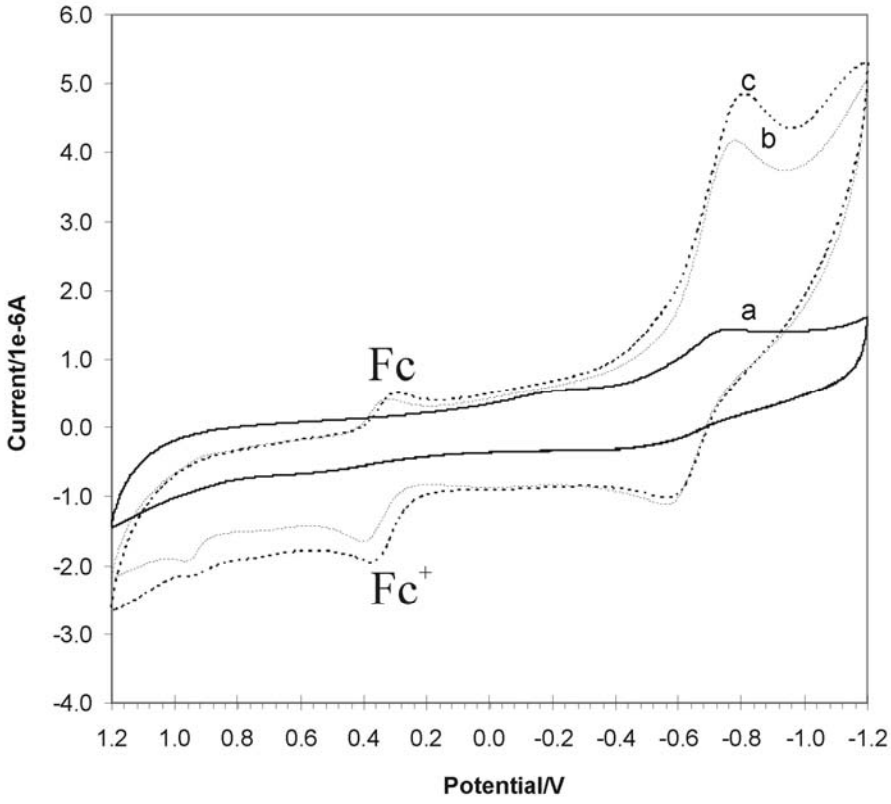

Figure 2.3: Cyclic voltamograms obtained on Pt electrode in the presence of 10 mM of Fc/Fc^+ vs. Ag reference electrode with scan rate 40 mV/s ; a) in pristine $BMI(BF_4)$, b) after purging oxygen through the $BMI(BF_4)$ and c) after adding 0.34 M water to (b). To the electrolytes (b) and (c) 2 mM of ferrocene was added.

Polymerization of aniline in ionic liquids was carried out within the potential limit of 1.4 to -0.2 V vs. the Ag-reference electrode. As seen in Figure 2.2 and 2.3, within these potential limits the reduction/reoxidation of O_2 is not taking place.

2.3.2 Electropolymerization of Aniline from $BMI(Tf_2N)$

Figure 2.4 shows successive cyclic voltammograms that have been recorded for the polymerization of aniline. The polymerization is initiated with anodic scan of the first cycle. The anodic current rising at electrode potential of +0.9 V vs. Ag reference electrode indicates the oxidation of aniline. The one-electron abstraction from aniline

possibly forms a primary intermediate, cation radical, that undergoes deprotonation and dimerization to 4-aminodiphenylamine. This compound is the key intermediate in the formation of green precipitate at the electrode surface during continued electrolysis of acidic aniline solutions because the oxidation potential of aniline is higher than those of the 4-aminodiphenylamine.

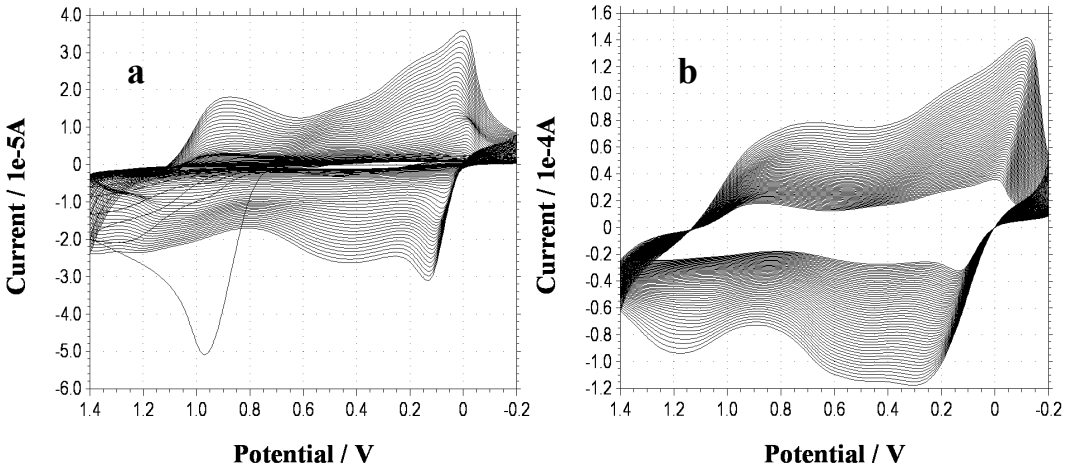

Figure 2.4: Polymerization of 0.1 M aniline in BMI(Tf_2N) carried out with 20 mV/s ; a) 1 to 50 cycles and b) 50 to 100 cycles.

Continued scanning of the modified electrode leads to voltammograms showing two broad, reversible waves. The shape of the CVs is similar to the one reported for aniline polymerized in strong aqueous acids. Recent comprehensive studies demonstrate that $(Tf)_2NH$ ranks among the strongest Brønsted acids.[46] The high acidity is attributed to the strong electron delocalization within the tetrahedral arrangement of the bis(trifluoromethanesulfonyl)imide anion (shown in Figure 2.1) that facilitates the dissociation of proton. Furthermore, with the increase of the peak current, the peak potential is shifting. This indicates that uncompensated resistance exists within the polymer film and/or slowing redox kinetics.

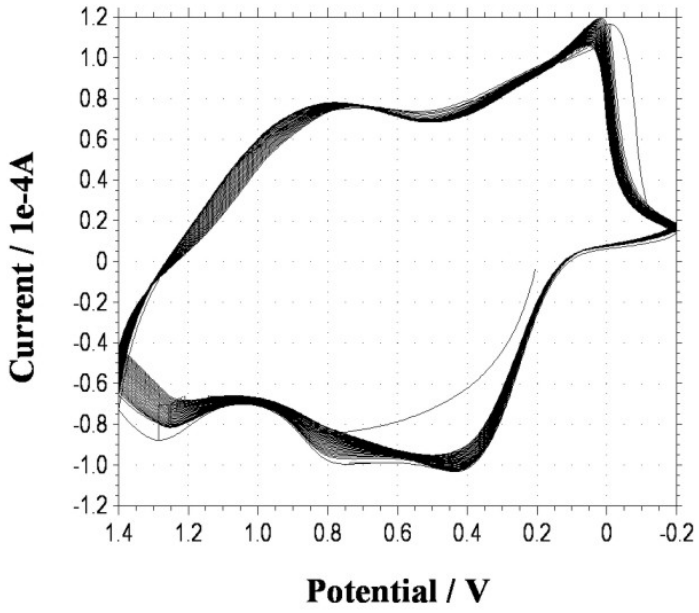

Figure 2.5: Cyclic voltammograms of the deposited PANI(Tf_2N) on Pt-electrode in BMI(Tf_2N) recorded with scan rate of 20 mV/s.

A PANI film, well adhered to the electrode surface was obtained after one hundred cycles, Figure 2.4b. Figure 2.5 shows the electrochemical response of this PANI film in the pristine BMI(Tf_2N). The coloration of the polymer film is changing between yellow in the reduced, green in the semiquinone, and purple in the fully oxidized state. The redox activity of the as grown polymer remains fairly constant and it follows the reversible redox couples as observed during the film growth. This behavior suggests that the ionic liquid remains in the PANI film.

2.3.3 Electropolymerization of Aniline from BMI(PF_6)

By maintaining the same polymerization conditions as discussed above aniline was polymerized from BMI(PF_6) Figure 2.6a. A substantial difference between these CVs and those recorded in BMI(Tf_2N) (Figure 2.4a) during the PANI growth is observed.

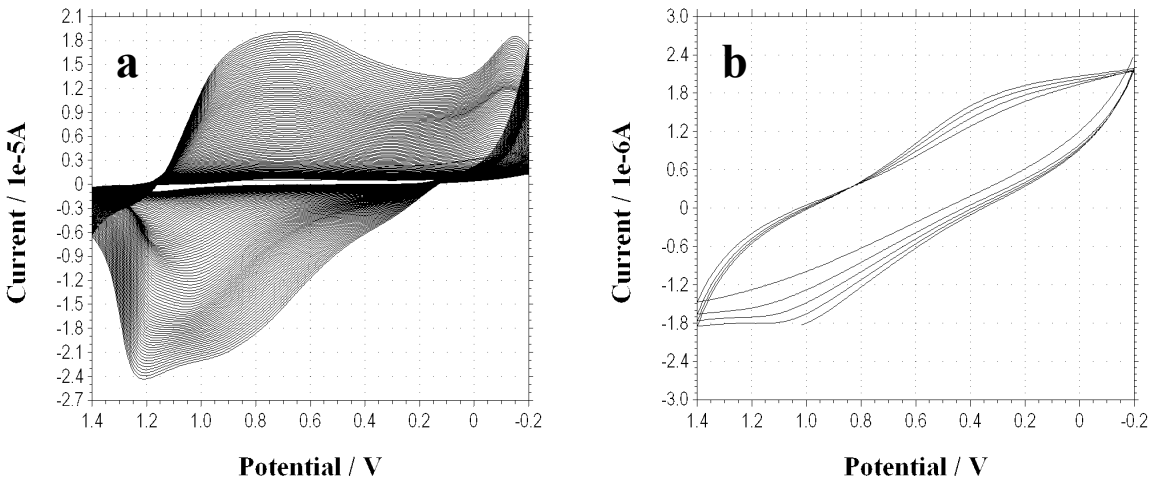

Figure 2.6: a) Electropolymerization of aniline from 0.1M aniline in BMI(PF_6) on Pt electrode (100 cycles) and b) CVs of the deposited PANI(PF_6) film in BMI(PF_6) in the absence of aniline. All CVs were recorded with a scan rate of 20 mV/s.

BMI(PF_6) has higher viscosity than BMI(Tf_2N) (319 cP as compared to 52 cP).[47] The difference in viscosity is affecting mass transport of ions during CVs. The presence of small amounts of water in BMI(PF_6) may lead to formation of HF and introduce some competing acid catalyzed polymerization reactions.[48] One possibility could be that in the presence of acid (2-4 M) formation of N-phenyl-1,4 benzoquinonedeimime takes place that is accompanied by its hydrolysis.[49] After the polymer formation (in pernigraline form), hydrolysis is not likely to take place due to the presence of aniline. The redox activity of the as grown polymer is observed to increase with each subsequent cycle. However, the current density after 100 cycles is by a factor of 10 lower than it is seen in Figure 2.4b. Consequently, after 100 cycles only a very thin layer of the PANI film is deposited from BMI(PF_6). Cycling of the PANI PF_6 using BMI(PF_6) as electrolyte changes the shape of the CV, Figure 2.6b. This different shape and the accumulated charge under the CVs lets us assume that the redox responses observed in Figure 2.6a can be attributed to the interactions of the grown film with aniline present in the electrolyte.

The oxidation of aniline generates protons. In the absence of aniline in the electrolyte (see Figure 2.6b) the grown polyaniline film is not protonated, therefore the color of the film remains purple.

2.3.4 Electropolymerization of Aniline from BMI(BF_4)

The physical and electrochemical properties of IL can be further affected by the presence of water. Whereas BMI(PF_6) is only partially miscible with water, BMI(BF_4) is fully miscible. In order to obtain information how the uptake of moisture may affect the polymerization of aniline we first conducted an experiment in a dried BMI(BF_4), Figure 2.7. The first potential scan produces an irreversible oxidative wave near +0.9 V. Similar observation was already made for the BMI(Tf_2N). However, further repetitive sweeping of the potential within the same range as shown in Figures 2.4 and 2.5, does not lead to growth of PANI film on the Pt-electrode.

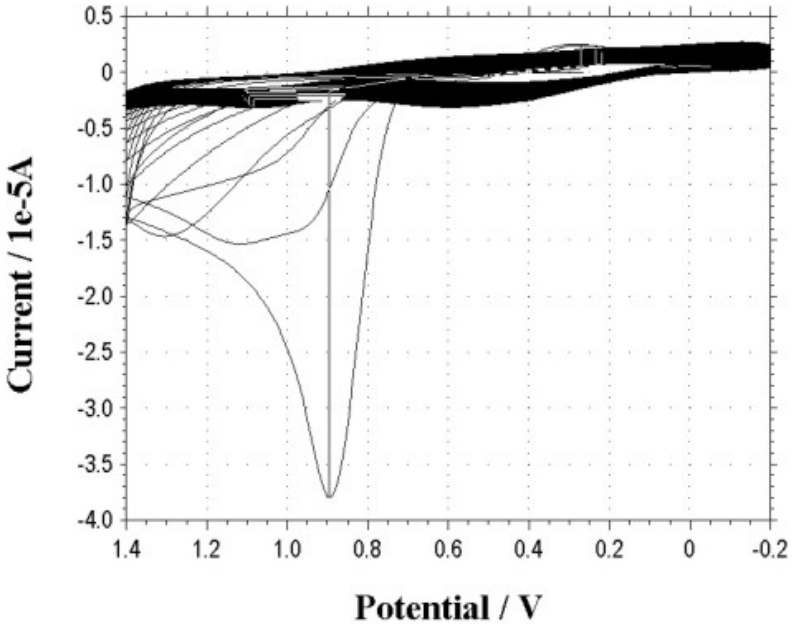

Figure 2.7: Cyclic voltammograms of Pt–electrode in 0.1 M aniline in BMI(BF_4) with a scan rate of 20 mV/s vs. Ag-reference.

The relatively high solubility of water in the BMI(BF_4) is important for the design of the electrochemical experiment. As seen in Figure 2.8, the uptake of water accelerates and increases the voltammetric signal due to water reduction. Addition of water leads to an increase of conductivity (and decrease in viscosity).[49] It has been suggested that electrostatic attraction between the ions of the BMI^+ and BF_4^- are decreased when water is present in equimolar amount (x = 0.5).

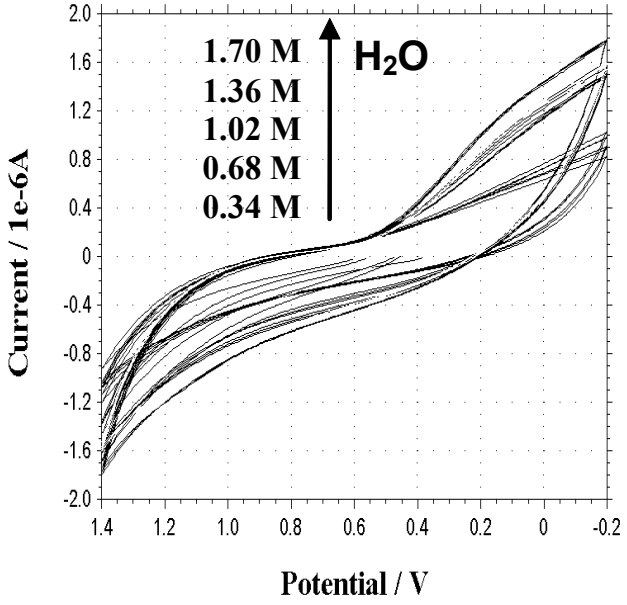

Figure 2.8: Stepwise addition of water to BMI(BF_4).

Further addition of water may initiate solvation of ions and result in appearance of water molecules not hydrogen bonded to the salt but as "free water".[50] These "free water" molecules were apparent in the FT-IR spectra with absorption peaks at 3640 and 3560 cm^{-1} obtained as shown in Figure 2.9.

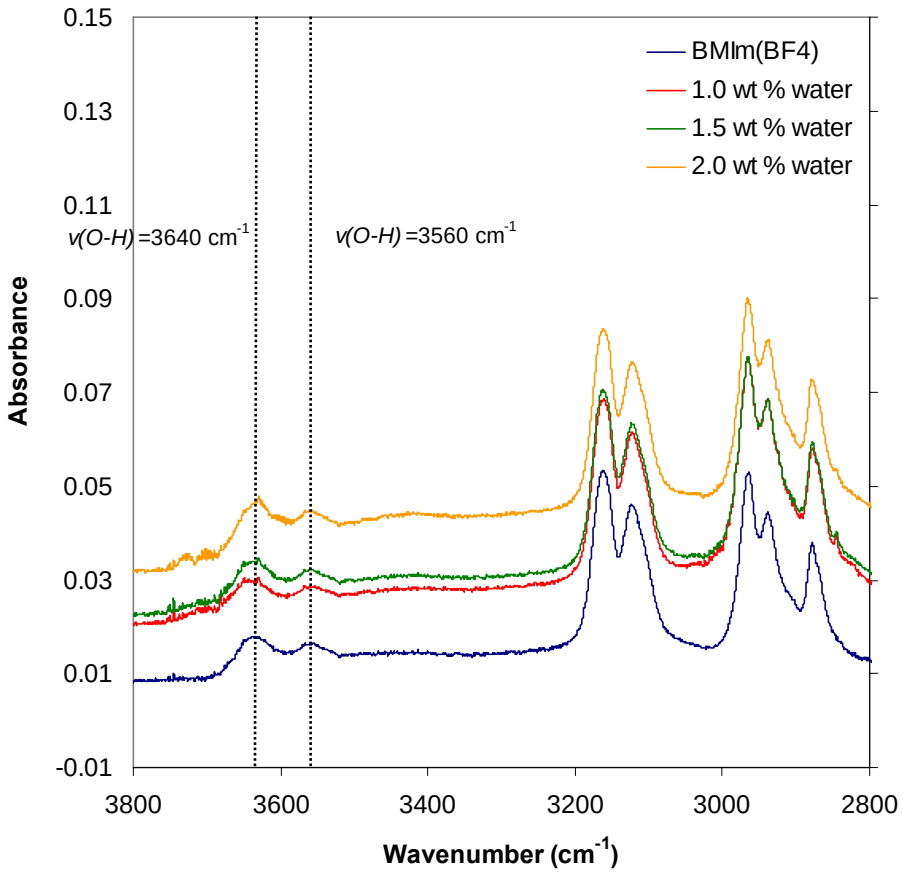

Figure 2.9: FT-IR spectra of BMI(BF_4) with addition of water.

The impact of the water addition on the hydrolysis of the BF_4^- anion follows the following reactions:[50-55]

$$BF_4^- + H_2O \rightarrow BF_3OH^- + H^+ + F^-$$

$$BF_3OH^- + H_2O \rightarrow BF_2(OH)_2^- + H^+ + F^-$$

$$BF_2(OH)_2^- + H_2O \rightarrow BF(OH)_3^- + H^+ + F^-$$

The hydrolysis becomes faster as the reaction progresses, liberating the F^- anion. The growth of polyaniline is accelerated with the addition of water. In Figure 2.10 the growth of PANI in the presence of 0.68 M of water is shown.

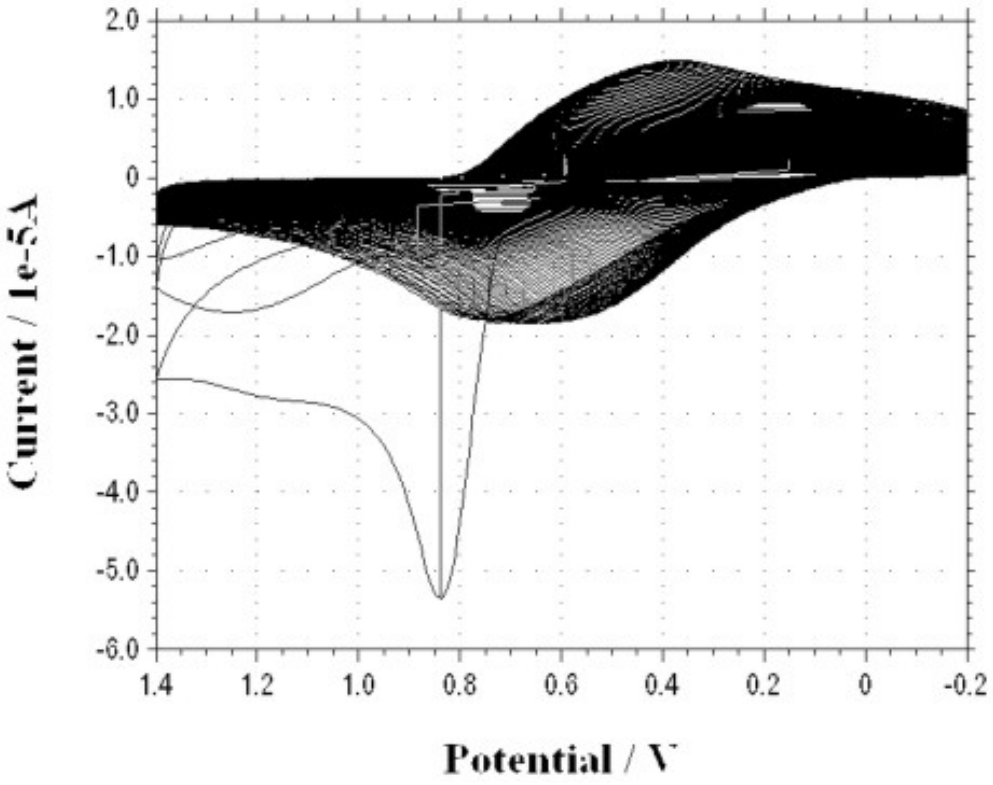

Figure 2.10: Growth of PANI film from BMI(BF_4) in the presence of 0.68 M H_2O.

Similar CVs have also been recorded for 0.34 M, 1.02 M and 1.36 M water in BMI(BF_4). In Figure 2.11, only the final CVs after one hundred cycles are shown. The interesting part of this experiment is that there is a range of water concentrations where the water changes from a "reagent" to a "medium". That is, if there is too much water, the system behaves as an aqueous solution of BMI^+ and BF_4^-. At the other end, water is a reagent that has a high affinity for solutes that it can solvate. As it is seen, the fastest

growth of PANI is observed when the added H_2O is 0.68 M. The anilinum ion that is a stronger Brønstead acid than water and the presence of F^- in a high enough molar concentration promote the polymerization of aniline. On the other hand the additions of BMI(BF_4) as a reagent to water did not promote any growth of polyaniline. However protons can be formed with the addition of water and be involved in the PANI redox reaction.

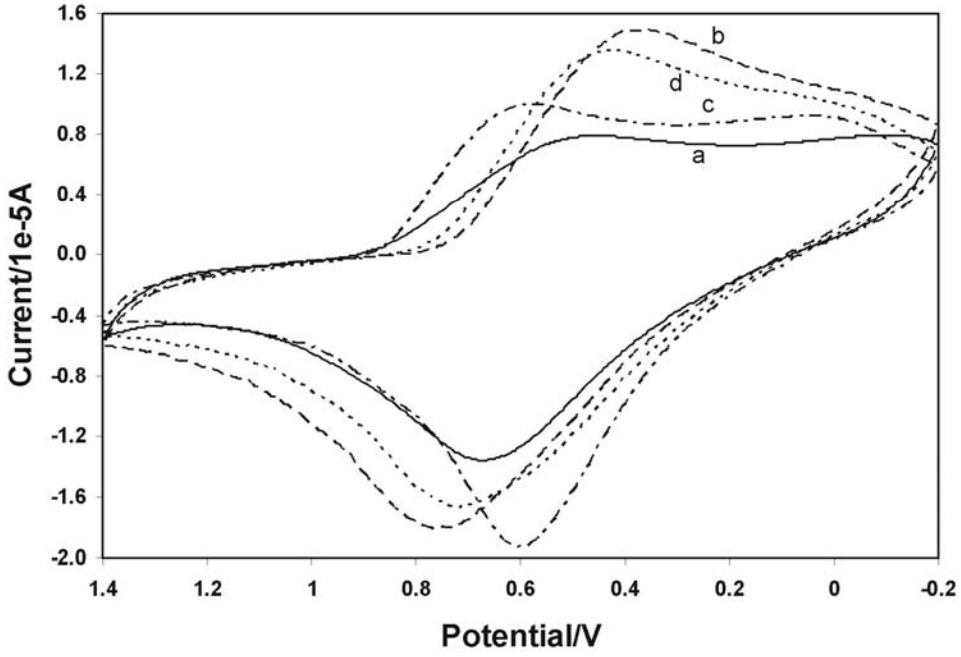

Figure 2.11: Final CVs of the 100 cycles of the aniline polymerization in the presence of water for a) 0.34 M, b) 0.68 M, c) 1.02 M and d) 1.36 M H_2O recorded with a scan rate of 20 mV/s vs. Ag reference electrode.

In Figure 2.12, the stability of the grown PANI film in the absence of aniline in IL is shown.

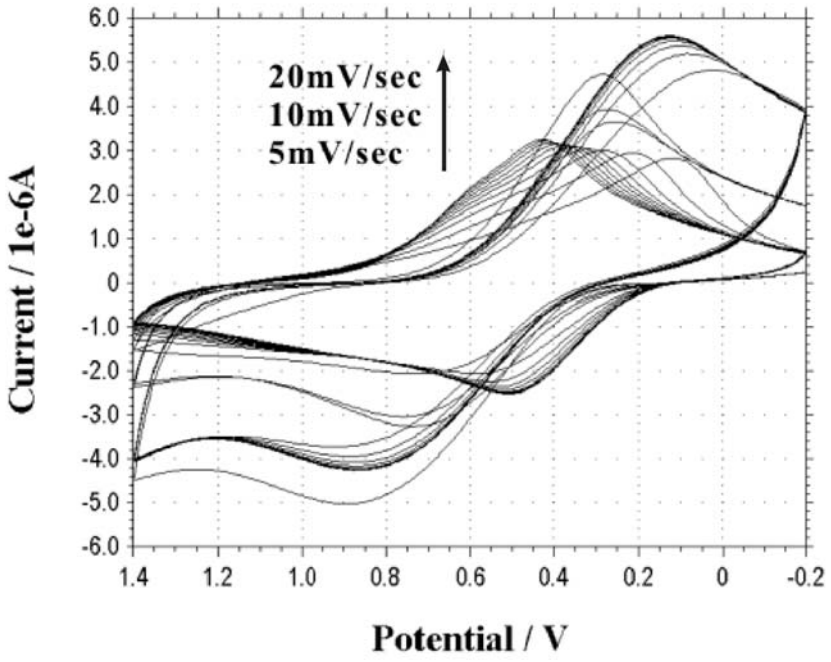

Figure 2.12: Cyclic voltammograms of PANI film grown from 0.1 M aniline in BMI(BF_4) in the presence of 0.32 M H_2O. The CV's were recorded only in BMI(BF_4).

With increasing scan rate the separation between the redox peaks is increasing from 60 to 600 mV for the scan rate of 5 and 20 mV/s, respectively. This may be attributed to the resistivity of the deposited layer. It may also limit the growth of the polymer as the number of cycle increases.

The coloration of the polymer film is changing between yellow in the reduced state, and only green in the fully oxidized state. The deposited polymers are insoluble in the strong base such as NaOH or NH_4OH.

2.4 Conclusion

It has been demonstrated that it is possible to electropolymerize aniline in pure IL. Aniline polymerization in BMI(BF_4), BMI(PF_6), and in BMI(Tf_2N) exhibit different redox electrochemistry. The CVs of aniline polymerization from BMI(Tf_2N) are comparable to those recorded in aqueous strong acid solutions. The presence of small amounts of water in BMI(BF_4) results in good, adherent PANI films. The growth of PANI in BMI(PF_6) is different, presumably due to formation of a different aniline oxidation intermediate. No degradation of the PANI films were observed when the oxidation potential exceeded one volt.

CHAPTER III

REFERENCE ELECTRODE FOR IONIC LIQUIDS

3.1 Introduction

Room Temperature Ionic Liquids (RTIL) are based on salts of bulky, substituted N-alkypyridinium or N,N,-dialkylimidazolium cation with variety of anions such as BF_4^-, PF_6^-, $CF_3SO_3^-$, Tf_2N^-. Different cation/anion combinations have different properties, such as viscosity, melting point, water miscibility and density. They are non-volatile and their unique physico-chemical properties e.g., Lewis and/or Brønsted acidity/basicity, hydrogen-bonding stability, and π-π interactions are of increasing interest to various electrochemical applications. However, the control of the potential of the working electrode in RTIL is not trivial. Quasi-reference electrodes such as Pt or Ag wire[56-60] are commonly used even if they do not allow to compare voltammetric data or to compare them to those obtained in conventional solvents.[61] A better approach is to use an inert metal quasi-reference electrode in combination with a redox couple, such as I^-/I_3^-, Li^+/Li, ferrocene/ferrocenium, $[Fe(Cp)_2]/ [Fe(Cp)_2]^+$, cobaltocenium/cobaltocene, $[Co(Cp)_2]^+/[Co(Cp)_2]$ that define the reference potential.[57] However, the use of the known redox potential of such a voltammetric reference standard still requires extrapolation to the standard, NHE potential scale. Also, it is not convenient to use a voltammetric reference potential in applications requiring a reference electrode that works at zero current, i.e. in potentiometry. This necessity requires some non-thermodynamic assumptions to be made, namely that the redox process taking place at the quasi-reference electrode is electrochemically and chemically reversible, stable and

does not interact with other redox species in the electrolyte. A further limitation of this reference redox system is the unknown solubility of such redox couples in RTILs.[57]

Herein we present reference electrodes of the first and of the second kind that were tested to behave well in selected RTILs and therefore have the potential to allow development of a practical reference potential scale for RTILs. These reference electrodes are based on the Ag/Ag^+ couple or Ag/AgCl always in contact with a soluble salt, such as silver nitrate or tetrabutylammonium chloride, respectively. These salts are able to remain in a relatively high concentration (0.1 M) when first dissolved in acetonitrile, ACN, and then added to the ionic liquid of choice.

3.2 Experimental

3.2.1 Chemicals

Ferrocene (98%), acetonitrile anhydrous (99.8%), silver nitrate (99+%), and tetrabutylammonium chloride hydrate (98%) were obtained from Aldrich and used without further purification. The ionic liquids 1-butyl-3-methylimidazolium tetrafluoroborate, BMI(BF_4) 1-butyl-3-methylimidazolium bis(trifluoromethanesulfonyl)-imide, BMI(Tf_2N) and 1-butyl-3-methylimidazolium hexafluorophosphate, BMI(PF_6) were synthesized by us, according to the standard procedures.[37] No absorbance was observed between 400 and 700 nm suggesting absence of any impurities. In addition, the ionic liquids were characterized by ^1H NMR and showed no significant organic impurities.

3.2.2 Equipment

Cyclic voltammograms, CVs, were recorded using a CH, Inc. (Model 401) potentiostat and electrochemical cell in three electrode configuration. A platinum disk-electrode with a diameter of 1.2 mm from Bioanalytical System (BAS) was used as the working electrode. Platinum wire coil ($A > 0.5\ cm^2$) was used as the counter electrode. The stability studies of the reference electrode potential were conducted using the PHM 240 pH/Ion meter (Radiometer Copenhagen). The temperature effects on the reference electrodes was examined using a Neslab RTE 211 water thermostat that controls the temperature to better than ± 0.1 ^oC.

3.2.3 Fabrication of the Reference Electrodes

The internal system solution was prepared by dissolving 50 µL of a 1M solution of $AgNO_3$ (or 1M Bu_4NCl) in acetonitrile into 450 µL of the RTIL, to give a final concentration of 0.1 M salt in the internal system. Flint glass Pasteur pipets (5 ¾'', from Fisher Scientific) were cut to a length of 5.5 cm and used as reference compartments with a total capacity of 0.5 mL. Liquid junctions were realized by sealing a thin strand of asbestos fiber at the end of the low-melting point glass pipets. The inner reference compartment was then filled with 250 µL of the respective internal system solution in which silver wire (or Ag/AgCl wire) with a diameter of 1mm and length of 3 cm was immersed in the internal solution and held in place with a plastic septum. A double junction arrangement was used in most cases in which the internal system was inserted into a second compartment containing only the respective RTIL, completing the half-cell as depicted in Figure 3.2. In addition, the Ag/AgCl wire was prepared by submerging the silver wire in a saturated solution of $FeCl_3$ (aq) for a few minutes.

3.3 Results and Discussion

3.3.1 Reference Electrodes

Two stable reference electrodess are reported here:

Ag/Ag^+, 0.1M $AgNO_3$ in RTIL//RTIL// sample … (Reference **A**)

and

Ag/AgCl, 0.1M Bu_4NCl in RTIL//RTIL// sample … (Reference **B***)* .

Successful fabrication and use of these electrodes is predicated by the good miscibility of acetonitrile with most RTIL given by its high polarity.[62,63] Typically, 50 µL of ACN were added to 450 µL of RTIL (~ 10 % by vol.). Note, that the same RTIL used as the background electrolyte has also been used as the solution in the inner compartment of the reference system and in the double junction compartment.

Reference **A** is based on the most widely used reference Ag/Ag^+ couple, where silver nitrate dissolved in acetonitrile maintains the concentration at 0.1 M in RTIL. The ionic contact with the external solution is made using fiber liquid junction.

The construction of Reference **B** is based on the most commonly used Ag/AgCl couple, where the electrical contact with the silver chloride is made by chlorination of the silver wire while ionic contact with the external solution is made using asbestos fiber liquid junction. The inner electrolyte system consists of RTIL and tetrabutylammonium chloride hydrate (Bu_4NCl) previously dissolved in acetonitrile to maintain a final concentration of 0.1 M in RTIL.

3.3.2 Comparison of the Reference Electrodes

To be able to compare emf data of both reference electrodes, cyclic voltammograms of 2.5 mM ferrocene dissolved in BMI(PF_6), BMI(BF_4), BMI(Tf_2N) respectively, were recorded. Typical CV of the ferrocene/ferrocenium (Fc/Fc^+) couple recorded on Pt electrode using the Reference **B** is shown in Figure 3.1.

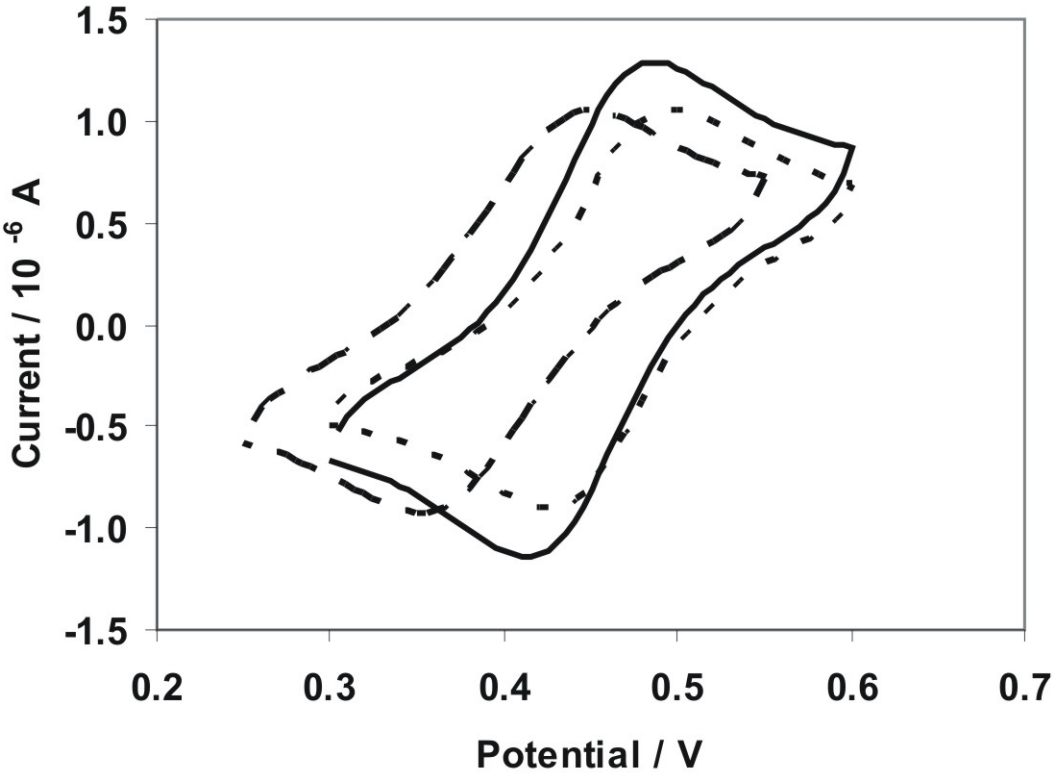

Figure 3.1: Cyclic voltammograms of Fc/Fc^+ couple recorded on Pt electrode using Reference **B** (Ag/AgCl-type). The reference electrodes were assembled and tested with the ionic liquid (——)BMI(Tf_2N), (- - - -)BMI(BF_4) and (— —)BMI(PF_6). All CVs were recorded in 2.5 mM ferrocene in the selected IL with the scan rate of 50 mV/s. For clarity only the last CVs from at least 10 consecutive scans are shown.

As expected the reduction, Ep_{red}, and oxidation peak, Ep_{ox}, potentials of Fc/Fc^+ shift along the potential axis when the reference system is changed. The recorded CVs are stable, with no potential shift observed between the first and the final CV approaching reproducibility less than $^{\pm}$1 mV for experiments conducted over a period of three days.

The measured and calculated values obtained for 2.5 mM of ferrocene in all the three RTILs are given in Table 3.1.

Table 3.1: Experimental voltammetric data for Fc/Fc^+ in different ionic liquids recorded on Pt-Electrode using the same set-up as in Figure 3.1 with Reference **B**. The number of electrons, n, was calculated using the equation $E_{p/2} - E_p = 2.2\ (RT/nF)$ at T = 295 K.

	Ip_{ox}/Ip_{red}	Ep_{ox} (mV)	Ep_{red} (mV)	E (mV)	$Ep/2_{ox}$ (mV)	$Ep/2_{red}$ (mV)	n
$BMIm(BF_4)$	1.245	495	430	463	440	480	0.932
$BMIM(CF_3SO_2)_2N$	1.085	485	410	448	430	470	0.932
$BMIm(PF_6)$	1.051	450	350	400	385	420	0.860

It should be noted that the type of ionic liquid affects the redox process of ferrocene at the Pt electrode. Similar observations were made by others and rises the need to test the feasibility of a redox couple as a voltammetric reference standard before it used.[57,64] The Ip_{ox}/Ip_{red} ratio for the $Fc^{o/+}$ redox does obey criteria of electrochemical-reversibility in almost all tested ionic liquids. The discrepancy from $Ip_{ox}/Ip_{red} = 1$ indicates a difference in the diffusion rate of the oxidized and reduced form of ferrocene.[64] From peak–to-peak potential separation value, $\Delta E = Ep_{red} - Ep_{ox}$ that is larger than the 59 mV/n we are gaining the information that in the redox reaction more than one electron is involved. The discrepancy in the formal redox potential, $E^{'} = \Delta Ep_{1/2}\ (Ep_{red} + Ep_{ox})/2$ mirrors the physico-chemical differences between the tested ionic liquids.

Because the ionic liquid-ferrocene system has not changed in these experiments, the conversion of formal potentials has been made using the standard potential of 400 mV vs NHE for ferrocene/ferricinium.[65] The data are summarized in Table 3.2.

Table 3.2: Potentials of Reference Electrodes A and B vs. NHE at 25.0°C.

	Reference **A** (mV)	Reference **B** (mV)
BMI(BF_4)	632	-63
BMI(Tf_2N)	582	-48
BMI(PF_6)	622	0

3.3.3 Determination of the Temperature Coefficient

Just like single electrode potentials, the true temperature coefficients of single potentials cannot be determined experimentally. Only the changes in electrode potential can be experimentally obtained by observing the change in cell potential when non-isothermal conditions are deliberately created. In Figure 3.2, two reference half-cells at different temperatures were used with the temperature of one reference half-cell varying while the other reference half-cell remained constant. The salt bridge and the reference electrodes contained identical ionic liquids. This symmetrical cell-arrangement indicates that differences in the liquid junction potential on both sides of the reference systems including the thermal gradient formed within the salt bridge are minimal.

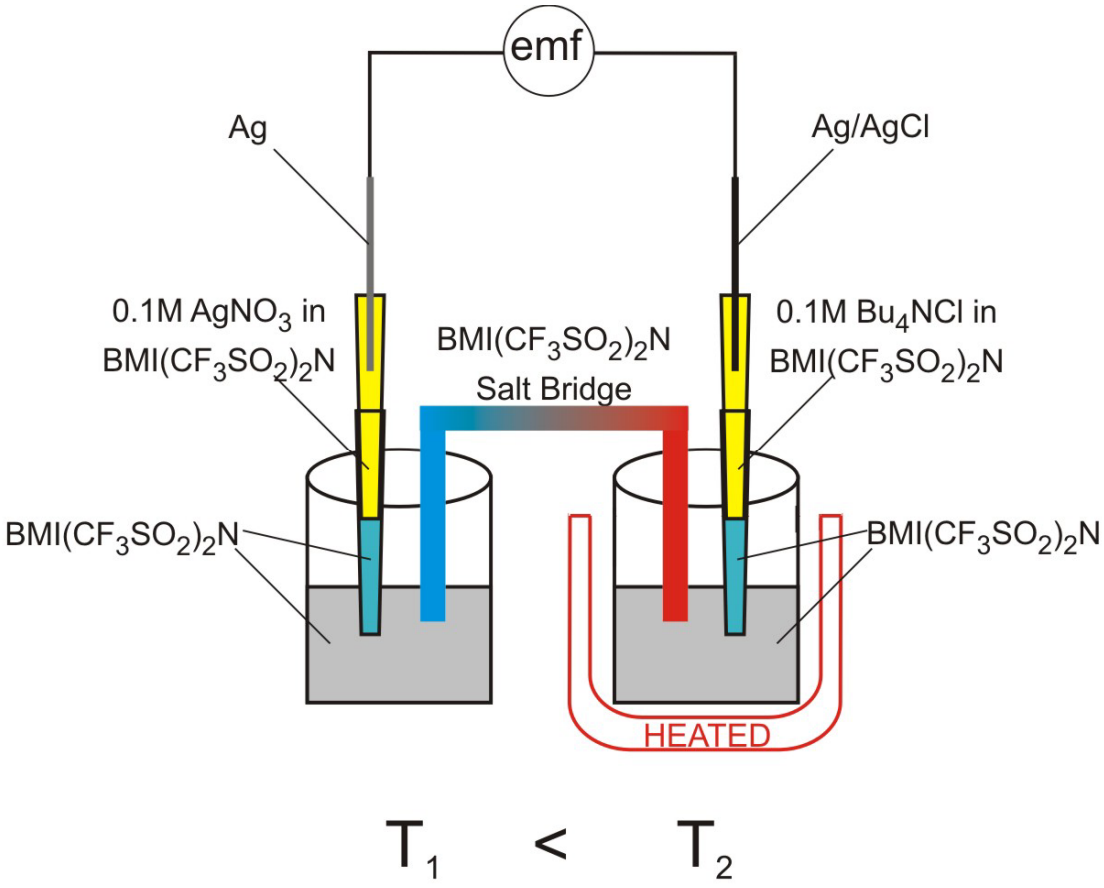

Figure 3.2: Schematic of the experimental set-up used for determining temperature effects on the reference system. During the experiments always only one cell was heated while the other cell was kept at room temperature.

Figure 3.3 shows the results of the changes of the emf cell when Reference **B** was heated from 25 to 60 ^{o}C while Reference **A** was kept at room temperature. The overall change of the cell voltage is $\Delta E/\Delta T$ = 0.0437 mV. The same result is obtained in the reversed experiment in which the reference half-cell **A** is heated and reference half-cell **B** is kept at room temperature.

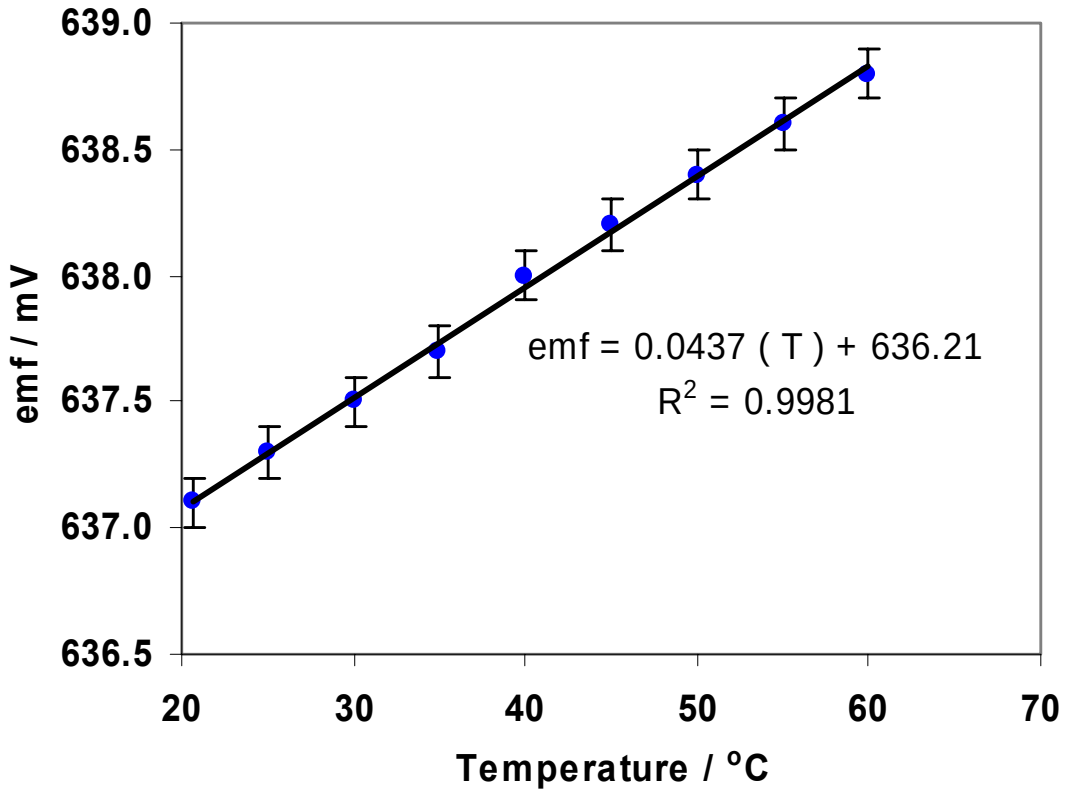

Figure 3.3: Temperature calibration curve determined for the heated Reference **B** compartment (Ag/AgCl) in comparison to the room temperature Reference **A**. The potential difference, $\Delta E = Ep_{Ref\,B} - Ep_{Ref\,A}$.

The CVs shown in Figure 3.4 were obtained in 3-electrode cell arrangement during heating the cell compartment. This data agrees with the reported decrease in viscosity of ionic liquids with increasing temperature that in turn may affect the diffusion coefficient.[66] Increase of temperature leads to the increase of measured redox peak current ratio confirming that the temperature affects the diffusion coefficient but not the redox potential, Table 3.3.

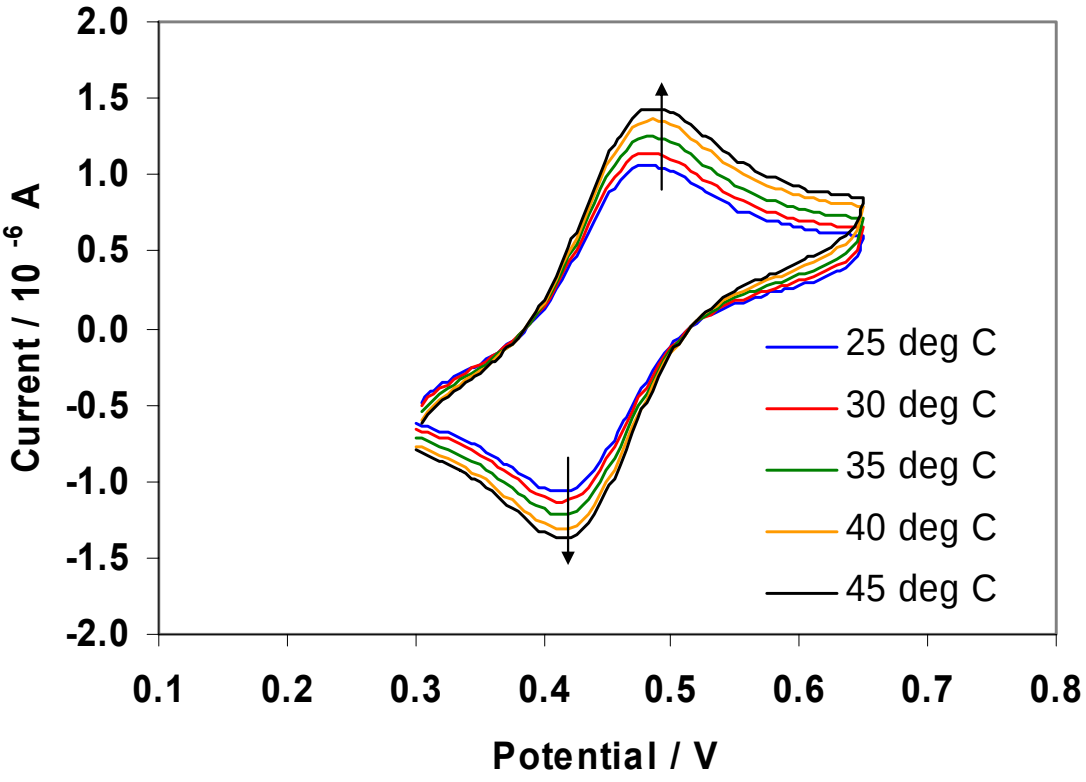

Figure 3.4: Overlay of cyclic voltammograms recorded at different temperatures within the range of 25 ^{o} C up to 45 ^{o} C in a BMI(Tf_2N) solution with 2.5 mM ferrocene, using Reference **B** . The CVs were recorded with a scan rate of 50 mV/s.

Table 3.3: Peak current ratios and formal reference potentials E' for ferrocene CVs at varying temperatures using Reference **B**.

Temp. (^{o}C)	I_{ox}/I_{red}	E (mV)
25	0.761	448
30	0.751	448
35	0.741	450
40	0.756	450
45	0.766	450

3.3.4 Effect of Acetonitrile Concentration in Reference A

In addition, the potential change was measured as a function of the concentration of acetonitrile in the internal system, as shown in Figure 3.5. From the plot it can be concluded that the reference potential is independent of ACN concentration in the range 10 to 15 vol %.

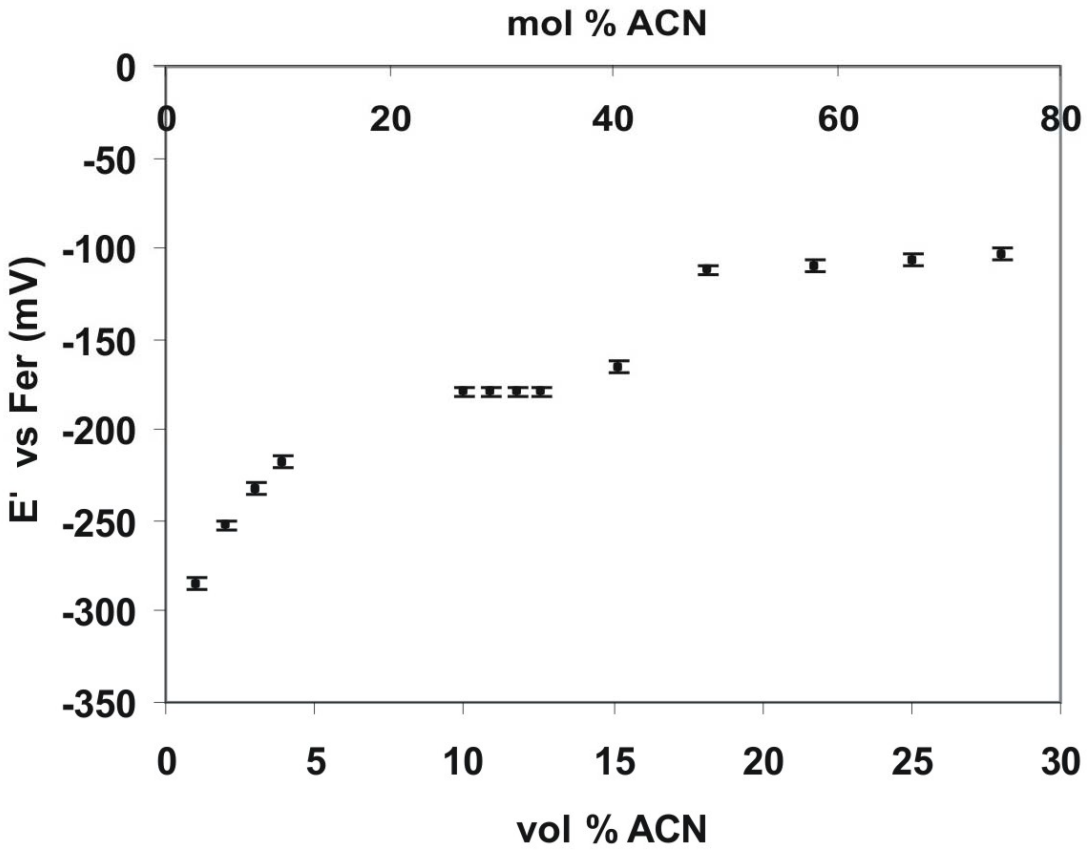

Figure 3.5: Dependence of the formal reference potential E' vs. Fc^0/Fc^+ with changing amount of acetonitrile in the reference electrode compartment containing BMI(Tf_2N).

3.4 Conclusions

A more or less universal approach of a practical reference electrode that allows comparison of potential scales in different RTILs is realized. Reference electrodes of the *first kind* and of the *second kind* have been made and tested. Their performance have been verified against voltammetric ferrocene/ferrocenium reference. This approach is based on the widely accepted *metallocene assumption*[67] which recognizes the fundamental impossibility of measurement of a single electrode potential while *assuming* minimal difference in solvation energy of the ferrocenium ion between different media. Our reference electrode systems offer implementation of a reference potential based on this assumption in a practical liquid junction format.

CHAPTER IV

CONTROLLING SIZE OF GOLD CLUSTERS IN POLYANILINE FROM TOP DOWN AND FROM BOTTOM UP

4.1 Introduction

Incorporation of nanoparticles into a sensing layer would have viable applications for sensing as nanoparticles have catalytic properties which lead to enhanced sensitivity and selectivity of certain analytes. Preparation of metal clusters, their characterization, their properties and their practical applications, all depend on their size. When the size is on the order of tens of nanometers and larger, the clusters contain millions and millions of atoms, they exhibit properties of a continuous metal phase. The atoms at the surface of such clusters are viewed as surface atoms while the rest have properties characteristic of organized bulk phase. The relationship of clusters to electronically conducting neighboring phases is governed by the difference of work functions, leading to formation of contact potential and three-dimensional space charge regions at the interface. Their interaction with electromagnetic radiation leads to size and wavelength-dependent plasmon resonance observed in nanometer sized particles. The subject has been recently reviewed by El-Sayed.[68] Preparation of such clusters is typically done in the "top-down" manner, essentially starting from a large object and using the size as the controlling parameter during the various scaling-down processes.[69] It is worth mentioning that when the size of e.g. gold cluster reaches 1 nm diameter, such a particle still contains approximately 30 metal atoms.

Another approach is to build metal clusters from the "bottom-up", by assembling individual atoms one-by-one, into a multiatomic unit, by a more or less controlled growth process. The product is then typically viewed as a "molecule" consisting of metal oligomers and having certain distinct chemical properties. There is no clear dividing line separating these two approaches, but a one nm diameter cluster is probably a good measure. The aggregation of the small particles following their initial formation is often the factor that determines their final size and the number of atoms they contain. Such aggregates often exhibit unique physical and chemical properties.[68] The literature covering metal nanoclusters is exponentially growing and reaches into thousands of original reports per year.[68] The subject of nanomaterials has been covered in specialized textbooks[70-72] and will not be elaborated here.

Polyaniline is one of the most studied conducting polymers. It has a rich and complex redox and acid/base chemistry and the literature concerning all aspects of this material is very extensive.[73] Here we limit ourselves only to the selected publications directly relevant to the electrochemical preparation of gold/polyaniline composite materials (Au/PANI). Controlling the size of the unprotected Au clusters from the top-down or from the bottom up is predicated on the templating ability of PANI to sequester chloroaurate anion, on control of electrochemical potential of PANI and on control of concentration of the chloroaurate in the electrolyte during various stages of the preparation. Polyaniline exists in three redox states shown in Figure 4.1:

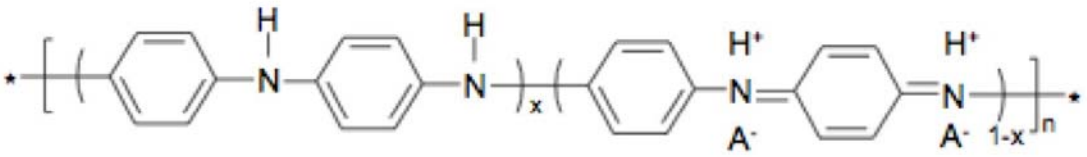

Figure 4.1: Protonated form of polyaniline in 1 M strong acid.

In moderately acidic medium (i.e. 1 M strong acid), the imine nitrogens are protonated yielding corresponding polyaniline salt forms: fully reduced leucoemeraldine salt (LES, x=1), semi-oxidized emeraldine salt (ES, x~0.5) and fully oxidized pernigraniline salt (PNS, x=0). Thus, there are six main forms of polyanline, three for protonated and three for the basic form, of which only the emeraldine salt (ES) is electronically conducting, all other forms are non-conducting.[69,74] The potential ranges of existence of these forms depend on the composition of the electrolyte.

Both the cations and the anions contribute to maintaining the charge neutrality inside the polymer. The electrochemical ion insertion is known as “doping” or “redox switching”. Not surprisingly, the voltammetric patterns of polyaniline in different electrolytes appear to be very different.[74] Polyaniline can be viewed also as a special kind of bulk ion exchanger with very high affinity for certain halo complexes.[75] It is a relatively open, porous network of chains which is accessible to most ions from the solution. Not surprisingly, the open cell potential of polyaniline coated electrodes also depends on the electrolyte and is typically around +0.4 V vs Ag/AgCl in 1 M KCl. That means that emeraldine salt is the most stable form of polyaniline. Because the ES

network is conducting its bulk is electrically neutral and all the faradaic electrochemistry takes place at the polymer/solution interface.[69,76]

The reactions relevant to this work can be summarized as follows:

$$LES = ES + 2e^- + 2H^+ \qquad E <-0.2V;+0.5V> \qquad (1)$$

$$ES = PNS + 2e^- + 2H^+ \qquad E <+0.5V;+0.9V> \qquad (2)$$

Above approximately +0.9V polyaniline is irreversibly, oxidatively damaged. Introduction of chloroaurate anion into this system brings additional complexity. Chloroaurate ion has exceptionally high affinity for polyaniline, presumably for the imine nitrogens of ES and PNS.[77]

$$ES \text{ (or PNS)} + AuCl_4^- = [ES\ ^*AuCl_4^-] \qquad K = 10^{10} \qquad (3)$$

It also contributes with its own redox behavior. The standard potential of $AuCl_4^-$ also depends on the concentration of chloride ion. Under the conditions employed in this work the formal potential was slightly above +0.8 V.

$$AuCl_4^- + 3e^- = Au(0) + 4\ Cl^- \qquad E >+0.8V \qquad (4)$$

Reduction of polyaniline/chloroaurate salt occurs at +0.5V yielding metallic gold

$$[ES\ ^*AuCl_4^-] + 3e^- = Au(0) + ES + 4Cl^- \quad E = +0.5V \qquad (5)$$

A typical cyclic voltammogram of gold/polyaniline composite is shown in Figure 4.2. The anodic peak at +0.2 V corresponds to the expulsion of protons.[74] It is somewhat suppressed in the presence of Au(0). It can be used to quantify the amount of polyaniline

originally deposited at the electrode. The anodic peak at +0.75 V corresponds to the uptake of the anions in the film. Its position and shape are strongly dependent on the type of the anion.[74] The peak at +0.5 V corresponds to the reduction of the [ES *$AuCl_4^-$] complex. It does not vary with the composition of the electrolyte.[78]

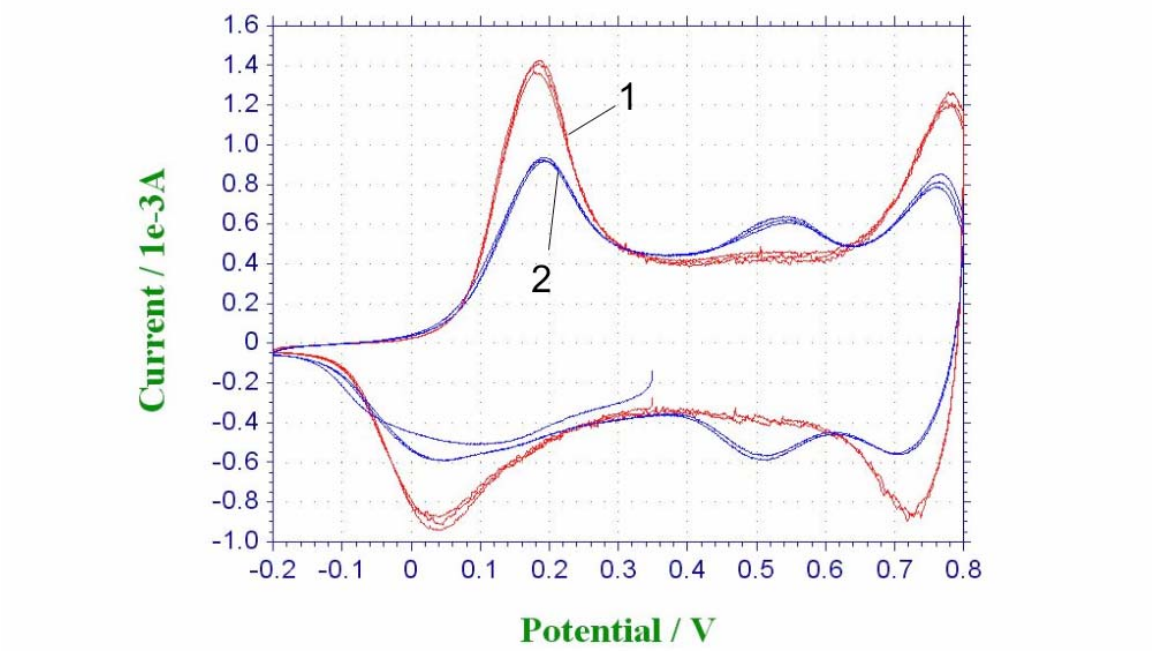

Figure 4.2: Cyclic voltammograms of polyaniline recorded at Pt electrode in 1M HCl at 20 mV/s (1) before Au deposition (2) after Au deposition.

4.1.1 Preparation of Gold/Polyaniline Composite

The objective of this work has been to achieve controlled growth of un-capped Au clusters using polyaniline as the deposition matrix. Because forming Au particles are separated from each other by the delocalized π-electron polymer chain network a spontaneous aggregation similar to that seen in formation of Au colloids does not take place. Formation of gold/polyaniline composites by reacting aniline with haloaurate in acidic medium has been reported.[78] In such preparations chloroaurate is acting both as

the oxidizing and the complexing agent. In our study we have used exclusively polyaniline formed by electropolymerization. The involvement of $AuCl_4^-$ is then described by Eq. 3 and Eq. 4.

4.1.2 "Top-down" Approach

When ES is exposed to acidic aqueous solution containing haloaurate anions a spontaneous formation of gold clusters takes place.[79] That reaction is predicated on difference of >400 mV between the open cell potential of ES and the redox potential of $AuCl_4^-$. Under such conditions Au clusters are formed and their sizes range from few nm to hundreds of nm. A detail study of the spontaneous formation of Au(0)/PANI from [ES $*AuBr_4^-$] has been performed to evaluate the change of work function of the composite materials with its metal content. In that work the time of exposure of PANI to the bromoaurate solution was varied and the work function of the final composite was correlated with the amount of the bromoaurate remaining in the supernatant, which was determined spectrophotometrically. As expected the work function of the composite, measured with Kelvin probe, increased linearily with the amount of Au in the composite.[79] In a further attempt to control their size and dispersity, the gold clusters were formed electrochemically by *in situ* generation of $AuCl_4^-$ from gold electrode coated with electrochemically polymerized polyaniline in chloride containing electrolyte.[68,78] In those experiments the advantage has been taken of the switching between conducting and non-conducting forms of polyaniline as observed during chronopotentiometric stripping of thin layer of sacrificial gold deposited on Pt electrode. The phenomenon of "*moving electrochemical interface*"[76] has been observed in those experiments.[69] The characterization of such *in situ* electrochemical preparations has been

done by high resolution tramsmission electron microscopy (HRTEM), by FTIR and by high resolution photoelectron spectroscopy (HRXPS).[80] Under optimized pulsed potentiostatic control it has been possible to narrow the cluster distribution to within 1-6 nm, Figure 4.3. The attempts for direct visualization of the sub-nanometer particles by HRTEM failed due to the limited resolution (electronic shimmer) caused by the conducting polyaniline matrix. Nevertheless, it has been determined by HRXPS that decreasing the size of the clusters from 5 to 1 nm increases the binding energy of the Au 4f photoelectrons by nearly 500 meV.[80] In other words the work function of Au increases with the decrease of the cluster size. Similar "nanoeffect" has been predicted by theoretical calculations[81] and confirmed by XPS experiments as size-dependent shift of the binding energy of the Au 4f photoelectron.[82] In the polyaniline/gold composite similarly observed shift of binding energy can be explained by formation of the contact potential between Au and PANI matrix and by increasing electrostatic repulsion of the charges at the surface of the Au particle as its size decreases to ~1 nm.[80]

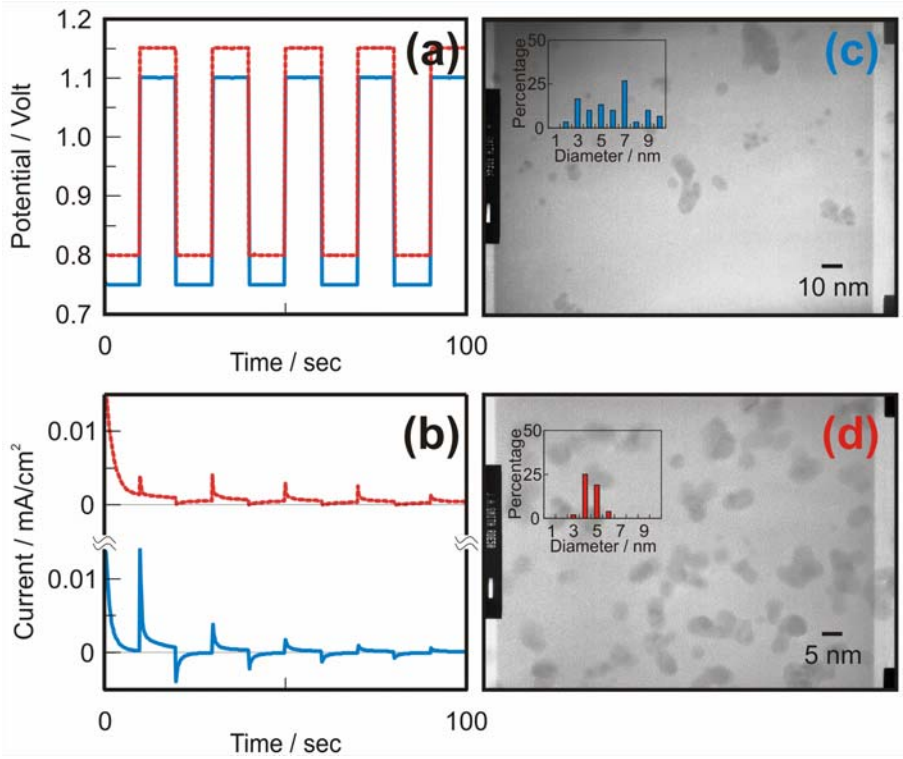

Figure 4.3: Electrochemical control of the size distribution achieved by proper selection of the pulsing regime.[68] The optimum results were obtained when the potential was pulsed between +1.15 and +0.80 V vs. Ag/AgCl, 1M KCl//1 M KNO_3// reference electrode.

Further attempts to prepare truly monodisperse gold clusters and/or to control their size to sub-nanometer dimensions proved to be unsuccessful. The fundamental question then remains – what is responsible for the formation of these multiatomic particles, since the elementary process (Eq. 5) clearly involves one $AuCl_4^-$ per one repeat unit of PANI? Spontaneous aggregation, similar to aggregation of unprotected gold colloids, although unlikely, is one such possibility. Another one is the "catalytic" mechanism leading to cyclical, multiple atom deposition on the same imine nucleation site. In order to resolve this issue a "bottom –up " approach based on the controlled electrochemical/chemical procedure has been studied.

4.1.3 "Bottom-up" Approach

The design of that experiment has been based on the assumption of stoichiometry of reactions (3) and (5) and on the high formation constant of the [PNS *$AuCl_4^-$] complex (Eq. 3). After the $AuCl_4^-$ has been reduced to, electrically neutral Au metal atom the corresponding imine site becomes free to bind another chloroaurate ion. As long as the electrons and chloroaurate ions are available the reduction can proceed in a "catalytic fashion" depicted in the reaction sequence I. – V. shown in Figure 4.4, resulting in the growth of large clusters. This mechanism would partly explain the formation of large Au clusters.[79]

A process for controlled, atom-by-atom growth of Au clusters in PANI template based on this sequence has been formulated (Figure 4.4). In that scheme one turn of the cycle should result in deposition of one Au atom. In this work, we have used either chemical or electrochemical means to affect the oxidation and reduction steps. They are specified in the description of the respective experiments.

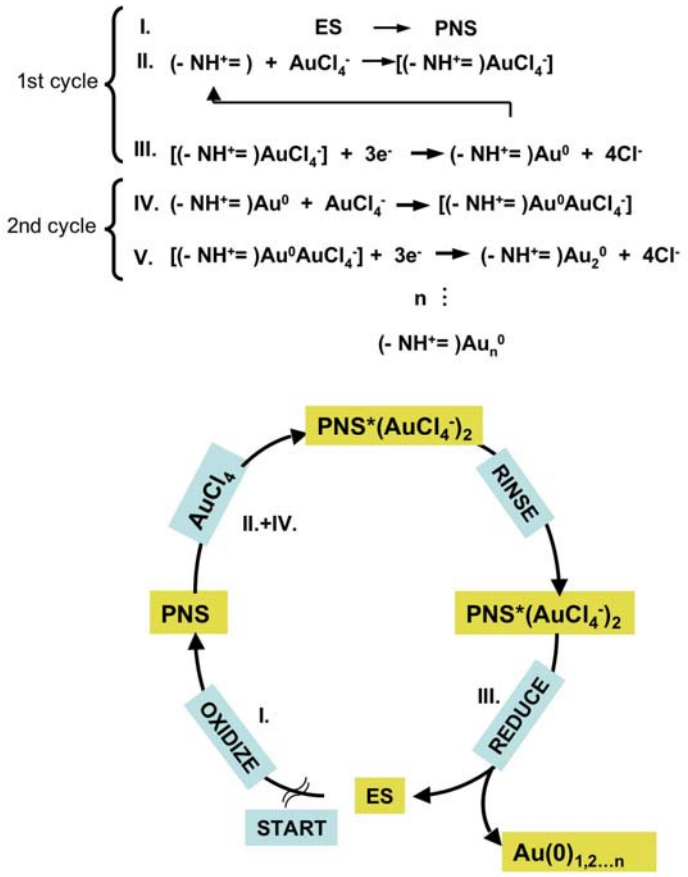

Figure 4.4: Proposed mechanism of sequential formation of $Au(0)_n$PANI composite.

4.2 Experimental

4.2.1 Chemical Preparation of Gold/Polyaniline Composite

A thin PANI film was deposited potentiodynamically on Pt-foil from solution containing 0.1 M aniline and 2 M HBF_4 within the range of -0.2 V to + 0.8 V. The electro-polymerization was conducted by running 25 cycles at 20 mV/s. The oxidation-reduction treatments of the PANI films were carried out chemically, using Ce(IV) and hydrazine, respectively. The first step (Figure 4.4) consisted of a 20 s treatment with

0.025 M $Ce(SO_4)_2$ in 1 M HCl. In that step the PANI film was oxidized from the emeraldine salt (ES) to the pernigraniline salt (PNS). The film was then immersed in a 10^{-5} M $KAuCl_4$ in 1M HCl for 30 s (Step II), It was then treated with a fresh solution of 0.025 M $Ce(SO_4)_2$ in 1 M HCl for 5 minutes, followed by 5 min rinsing with deionized water in order to wash out the unreacted $AuCl_4^-$. Following 20 s treatment with 0.1 M hydrazine dichloride reduced $AuCl_4^-$ to metallic Au^0 (Step III). The same cycle was repeated for deposition of next Au atom (step V).

4.2.2 Electrochemical Preparation of Gold/Polyaniline Composite

Polyaniline films were also prepared electrochemically from 0.1 M aniline in 1 M dichloroacetic acid. Those films were prepared by applying a constant potential of 0.7V to give a final charge of approximately 0.6 C. The films were then cycled in 1 M dichloroacetic acid from which the charge under the proton anodic peak was extracted. This value was then used to normalize the gold oxidation shown in Figure 4.5b. In addition, the oxidation and reduction of the films were carried out electrochemically by applying 0.7 V for 40 s in 1M HCl to oxidize the film and then scanning to -0.2V to reduce the film as shown in Figure 4.5a.

4.2.3 Characterization of Gold/Polyaniline Composite

The characterization of the prepared materials was done by cyclic voltatmmetry, by ashing/anodic stripping voltammetry, by Raman spectroscopy and by HRXPS. The XPS experiments were performed using a Physical Electronics Quantum 2000 Scanning ESCA Microprobe. This system uses a focused monochromatic Al Kα x-rays (1486.7 eV) source and a spherical section analyzer. The instrument has a 16 element

multichannel detector. The x-ray beam used was a 100 W, 100 μm diameter beam that was rastered over a 1.4 mm by 0.2 mm rectangle on the sample. The x-ray beam was incident normal to the sample and the photoelectron detector was at 45° off-normal. Wide scan data was collected using a pass energy of 117.4 eV. For the Ag $3d_{5/2}$ line, these conditions produce FWHM of better than 1.6 eV. Narrow scan or high energy resolution data is collected using a pass energy of 46.95. For the Ag $3d_{5/2}$ line, these conditions produced FWHM of better than 0.98 eV. The binding energy (BE) scale is calibrated using the Cu $2p_{3/2}$ feature at 932.62 ± 0.05 eV and Au 4f at 83.96 ± 0.05 eV for known standards.

The Raman spectra were obtained using a Research 785 Raman microscope made by Kaiser Optical Systems, Inc., with a 10x objective. Approximately 3mW of laser light was focused onto the films.

Several other characterization techniques have been used including HRTEM, TOF-SIMS, Laser ablation-MS, and ICP-MS. However, due to the small size (angstrom level) of the gold clusters these techniques proved ineffective in detecting or identifying the atomic clusters.

4.3 Results and Discussion

4.3.1 Electrochemical Analysis

The prepared PANI-Au materials were characterized by recording cyclic voltammograms in 1 M HCl solution. Not surprisingly, the reduction peak of [ES $^*AuCl_4^-$] (Eq. 5) remains essentially unchanged (Figure 4.5a).

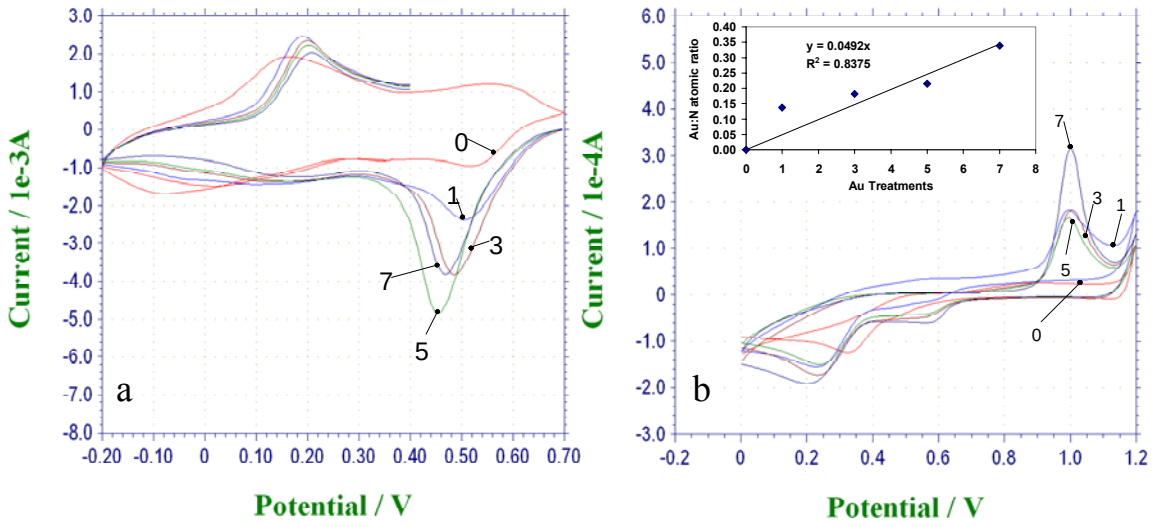

Figure 4.5: a) Cyclic voltammograms corresponding to sequential deposition of 1 - 7 atoms of Au according to Figure 4.4. in 1M HCl and 0.025 M $Ce(SO_4)_2$. and 10^{-5} M $KAuCl_4$. The scan rate was 20 mV/s. Curve 0 corresponds to zero concentration of $AuCl_4^-$. b) Cyclic voltammograms of oxidative stripping of deposited Au in 0.01 M HCl, after "ashing" of PANI residuum. Insert shows the atomic ratio Au : N obtained from the normalized peak areas.

The total gold content was then determined by "flaming off" the Au/PANI composite in a Bunsen burner and performing the anodic stripping voltammetry of the remaining metallic gold at the Pt electrode.[83] The stripping cyclic voltammograms are shown in Figure 4.5b. They correspond to oxidation of Au in chloride containing medium (Eq. 3).[83] The peak areas were normalized to the area of the proton uptake peak of untreated PANI (at +0.2V, Figure 4.5a), which can be used to quantify the amount of PANI in the individual preparations. The results of these experiments show that, as expected, total gold content increases with the number of deposition cycles.

4.3.2 HRXPS Analysis

Further proof of progressive incorporation of Au has been obtained from HRXPS measurements. The ratio of Au 4f peaks and N1s also shows increasing content of Au with increasing number of cycles (Figure 4.6a) while the ratio of N : C intensities remains essentially unchanged (Figure 4.6b).

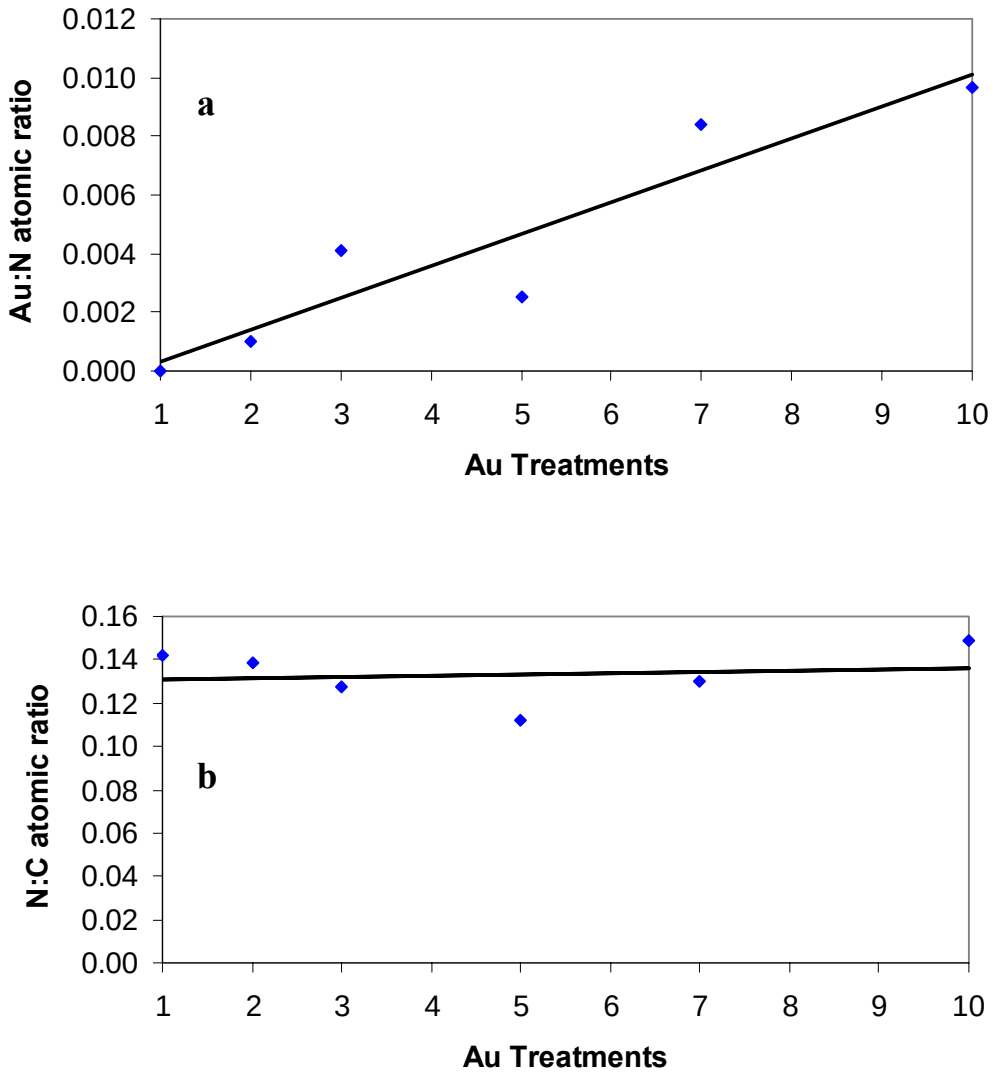

Figure 4.6: a) Atomic ratio Au : N obtained from peak intensities of Au 4f line and N 1s line, indicating increasing amount of Au. Plot b) shows that the ratio of intensities of N 1s : C 1s lines change only very little.

A hint of size dependence is seen in plot of binding energies against the number of cycles referenced to N 1s line (Figure 4.7). The trend of decrease of the binding energy with increasing number of Au atoms is consistent with the similar trend observed for the electrochemically prepared nanometer size Au clusters.[80]

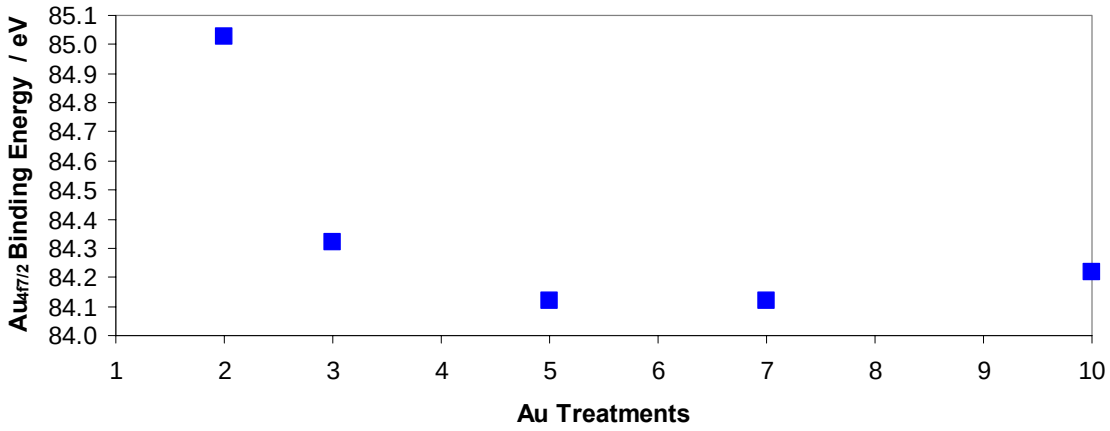

Figure 4.7: Shift of the Au 4f binding energy with the number of deposition cycles referenced to the N 1s line.

The electrochemically prepared materials were characterized by Raman spectroscopy (Figure 4.8). The C—H bending modes are occurring at 1176 cm^{-1}, the ring C—C stretching at 1595 cm^{-1}, and the different C—N stretching modes (amines, imines and polarons) between 1210 and 1520 cm^{-1}.[84] As can be seen from Figure 4.8, the Raman intensity is also increasing with consecutive Au treatments.

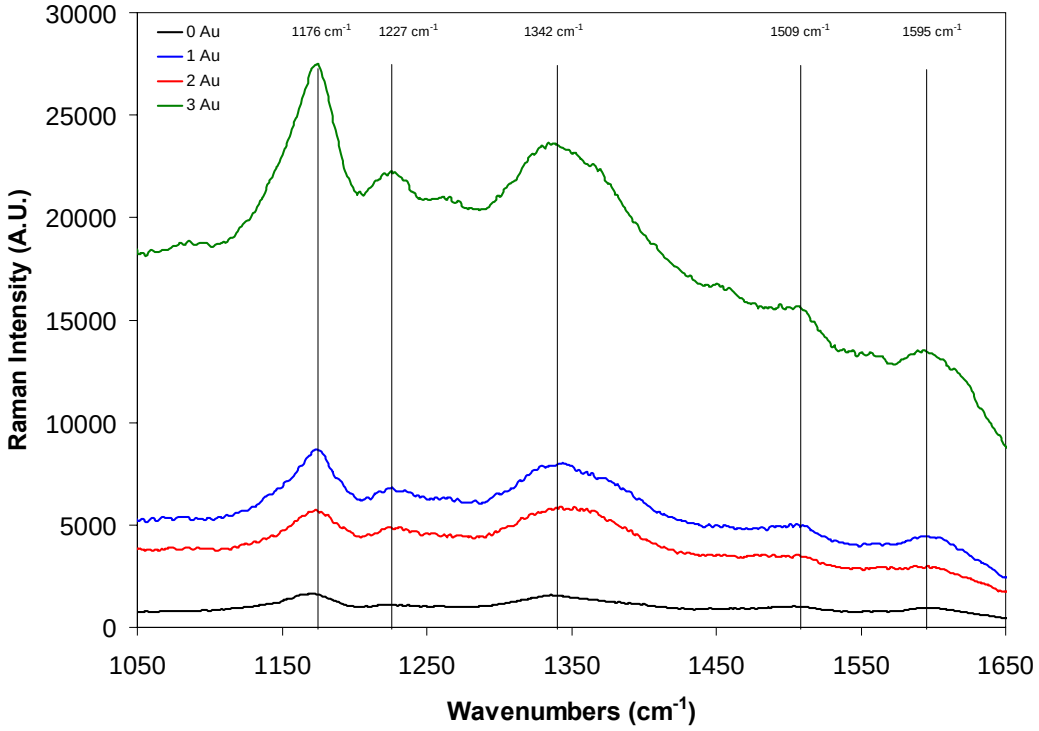

Figure 4.8: Raman spectra obtained from films in which the redox reactions were performed electrochemically.

4.4 Conclusions

The two approaches to forming Au/PANI composites with the controlled size of the uncapped metal clusters as the experimental parameter show some common trends, namely the increase of the work function with decreasing size of the metal cluster, as evidenced by the increase of the binding energy of the Au 4f photoelectron. This size dependent change of work function has its origin in the electrostatics of the contact potential that forms between gold and electronically conducting polyaniline matrix. The fact that the overall work function of the Au/PANI composite increases with the content of the gold agrees with the contact potential concept. It has been confirmed by the Kelvin

probe measurements.[79] The shift of the Au photoelectron binding energy is referenced to the N 1s line of polyaniline. Since both elements are in the same conducting phase the change of work function of the entire composite which is due to the changing amount of Au does not affect this shift.

The attempts to visualize or positively identify low Au atom clusters in the materials prepared by the bottom-up approach have been so far unsuccessful. Only strong circumstantial evidence shows that in these sequential treatments the amount of gold increases and that the binding energy of Au so prepared decreases with the increasing number of cycles and presumably, with increasing number of Au atoms in the cluster (Figure 4.7). The atomic ratio, Au : N, in the materials prepared by purely electrochemical means and determined from the cyclic voltammetry/ashing (Figure 4.5b insert) is well below the theoretical value of 0.25/Au. The atomic ratio determined from the integrated intensities of the Au 4f and N 1s XPS peaks of materials prepared by chemical oxidation/reduction is even lower (Figure 4.6a). It again raises with the number of deposition cycles. It can be concluded from these results that only a fraction of imine sites participates in the complexation reaction II (in Figure 4.4), depending on the experimental conditions.[75]

It is important to realize that a spherical 200 nm diameter Au particle contains approximately 250 million atoms of Au, which corresponds to 11.9 nC of charge, while a 1 nm diameter cluster contains approximately 30 metal atoms. Since Au particles of those sizes are formed spontaneously in the top-down approach[79] the most puzzling question remains – where do the electrons necessary for the reduction of chloroaurate anion come from? The most likely reducing agent in the system is water. That explanation begs

another question and that is why would such spontaneous reduction stop once the Au clusters reach certain size. Further studies are needed to answer these intriguing questions.

CHAPTER V

CHEMICALLY SENSITIVE FIELD-EFFECT TRANSISTOR WITH POLYANILINE-IONIC LIQUID COMPOSITE GATE

5.1 Introduction

Properties of organic semiconductor (OS) polymer layers such as the response time, dynamic range of the response, sensitivity and the operating temperature play a crucial role in gas sensor performance. Some OS polymer sensing layers are difficult to process due to their highly aromatic nature, interchain hydrogen bonding and charge delocalization. Generally, the cast material on any sensor platform is described as a "hybrid film", implying that the polymer or the solvent is the major component of the system.[85] However, as the casting solvent leaves, the cast layer solidifies. That process is often the determining factor of the gas sensor performance since it is responsible for the rate of uptake/release of the gas analyte by the polymer-matrix.

In this work, we have explored the development of a sensing layer "gel hybrid material". It is based on a mixture of polyaniline (PANI) and room temperature ionic liquid (IL). The use of ILs as a substitute for organic solvent is of great interest because of their low vapor pressure, nonvolatility, good solubility of gases and thermal stability.[86,87] The ILs have been already used to prepare gel-like materials. Some of the approaches combined IL with a gelator, such as gelatin and carbon nanotubes as the supporting matrix,[88] or polymer electrolyte such as poly(ethylene oxide), PEO, poly(methyl methacrylate), PMMA, poly(vinylidene fluoride) PVDF[89], or just by grinding imidazolium-based ionic liquid with single-walled carbon nanotubes (SWNT).[90] From these studies, it has been found that the gel-state formation results not only from the

uniform dispersion of the gelators in the IL but also from the strong interaction between the IL and the added material.[90]

Gas diffusion through a gel-like polymer matrix follows a different mechanism as compared to a homogeneous solid polymer matrix since most of the interactions are between molecules and the pore walls. The Knudsen model should be well suited to describe diffusion in gels since the mean free path is usually significantly greater than the average pore diameter of the material. It has been shown that permeation of gas through a sol-gel silica membrane is enhanced by Knudsen diffusion for gases ranging significantly in their molecular weight, such as H_2 and Kr.[91]

The focus of our work is on PANI that has been generally cast in a wide range of aqueous and/or organic solvents or formic acid.[1,2] One of the major drawbacks in this type of process is the evaporation of the volatile solvent in which the OS is dissolved or for which the solvent acts as dopant such as formic acid.[92] In order to improve the general physical and chemical properties of the sensing materials, we investigated composite films containing PANI doped with the non-volatile camphorsulfonic acid (CSA) in the mol ratio of 1: 2 (CSA : aniline units).[74] That material showed significantly improved sensing properties, and long term stability. In order to further improve the speed of response we added the IL, 1-butyl-3-methylimidazolium bis(trifluoromethanesulfonyl)-imide [BMI(Tf_2N)], to the final composition. This IL was chosen for its zero vapor pressure, wide liquid range, good conductivity, hydrophobicity[7], miscibility with organic solvents such as acetonitrile[93] and solubility of various vapors and gases. Ammonia that has been used as the test gas in this study has a solubility of 13.7 mol% in EMI(TF_2N) at 298.4 K and 0.145 MPa.[94]

The solubility of gases in IL depends on the anion of the IL.[95,96] Therefore, besides the BMI(TF_2N) we also explored other ionic liquids such as BMI(PF_6) and BMI(BF_4). However, their inherent hydrophilicity increases absorption of water into the sensing layer resulting in the overall instability of the response.

The critical issue of this new approach is to find out if the presence of IL in the PANI matrix would facilitate the interaction between the ammonia gas analyte and the PANI matrix. A reduced transport time of the gaseous species through the gel like PANI sensing layer should result in shorter response time and possibly also in a wider dynamic range for the detection of the analyte.[97,98] This paper demonstrates that using a polymer matrix formed from polyaniline emeraldine salt and IL improves the response time of the CHEMFET layer. When IL is present in the sensing layer the detection limit is lower.

5.2 Experimental

5.2.1 Chemicals

Formic acid (88 %, Fisher Scientific), ammonium hydroxide solution (29.3 %, Fisher Scientific), and (1R)-(-)-10-camphorsulfonic acid (CSA) (Aldrich) were used as received. Polyaniline emeraldine base, (PANI-EB) powder (MW ca. 20K, Aldrich), was treated in ammonium hydroxide solution (28%, Fisher) for 2 hours (with stirring), filtered, and then extracted with deionized water and methanol.[99] The ionic liquid 1-butyl-3-methylimidazolium bis(trifluoromethanesulfonyl)-imide, BMI(Tf_2N), was synthesized according to the standard procedure.[58] In order to remove the halides from reaction, the product was dissolved in methylene chloride and multiple water extractions were performed. It was then purified by stirring it with activated charcoal overnight. The solution was then filtered through a celite filter to remove the activated charcoal. The

excess organic solvent was then evaporated at 10^{-2}-10^{-3} mbar in a vacuum oven for 12hr at 60ºC.

5.2.2 Preparation of PANI/IL Sensing Layer

The PANI/IL sensing layer was prepared by using two solutions. First, solution of 50 mg PANI-EB powder in 10 mL of formic acid was made and used to prepare a PANI·CSA composite mixture by dissolving 6.42mg of CSA in 1 mL of the PANI/HCOOH. The amount of added CSA was calculated to be in the ratio of two CSA molecules per four benzene units of the repetitive segments of the PANI chain. The second stock solution was made by adding 0, 0.5, 1, and 1.5 wt% ionic liquid into the formic acid. These solutions were then mixed in 1:1 ratio to give 0, 0.25, 0.50 and 0.75 wt% IL in the CSA-doped PANI in formic acid. The above solutions were drop-cast into the wells of CHEMFET array[100] using a glass capillary, with approximately 0.02 mm^3 orifice. The films were dried at 80 ºC for 24 h in vacuum oven. The drying removes the volatile solvent formic acid from the films. This results in final composition of the sensing layer containing mole fractions of IL, $\chi_{IL} = n_{IL} / (n_{IL} + n_{PANI}) = 0, 0.51, 0.68, 0.76$ in PANI·CSA.

5.2.3 Instrumentation

The thickness of the cast films were measured using a Dektak3ST surface profiler (Sloan/Veeco Instruments, Inc.) with a speed of 60 μm/sec and a stylus weight of 5 mg. The measurement was done by casting the films four times in the same FET well and dividing the measured value by four. UV-vis spectroscopy measurements were

performed on a Shimadzu UV-3101PC spectrometer. Absorption spectra were measured on spin coated films cast on quartz slides.

The work function (WF) measurement of each film was obtained using a Besocke Delta-Phi-Electronik Type S Kelvin probe. The contact potential difference (CPD) was measured in automatic balancing mode vs. a vibrating gold grid reference electrode.[97] The gas delivery system is shown in Figure 5.1. An Environics S4000 (Environics, Inc.) was used to deliver ammonia gas of controlled concentrations between 0.5 to 694 ppm in air to the sensor array with a constant flow rate of 50 cm^3/s. The CHEMFET was placed in a gas sensor chamber (1.1 cm^3 in volume) equipped with a micro-jet.[101] It took 20 ms to purge the cell with gas. The ammonia concentrations were varied by changing the flow rates by the mass flow controllers connected to the air (Airgas) and the ammonia (5.14 % and 0.05 %, Matheson, dry air carrier gas) gas tanks. The flow was programmed with the Environics Series 4000 software to deliver ammonia concentration steps from 0.5, 1.74, 2.6, 3.47, 5.2, 6.94, 15, 25, 35, 174, 260, 347, 520, and 694 ppm.

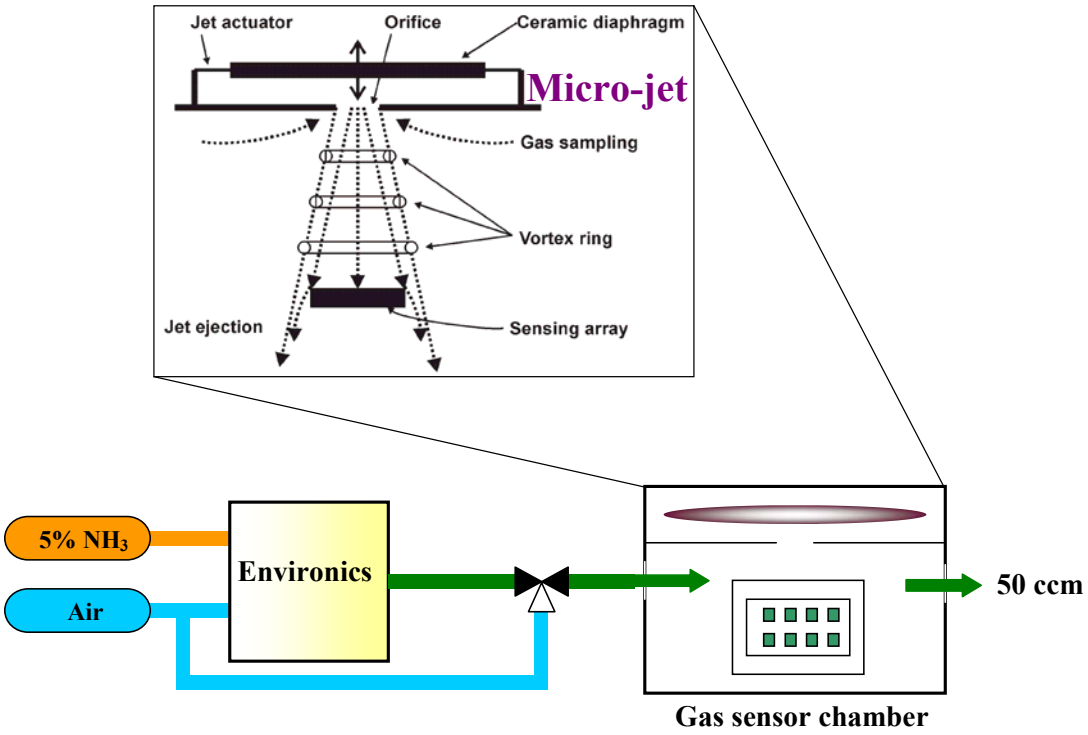

Figure 5.1: Experimental setup for the delivery of ammonia gas in air to the CHEMFET sensor array. Details of experimental testing set up can be found also in Ref. (101)

5.3 Results and Discussion

5.3.1 Material Properties

Optical micrographs of PANI layers between two gold contact electrodes of a CHEMFET cast with no IL (1) and different mol fractions of BMI(Tf_2N) in the layer (2) χ_{IL}=0.51, (3) χ_{IL}=0.68, and (4) χ_{IL}=0.76, are shown in Figure 5.2.

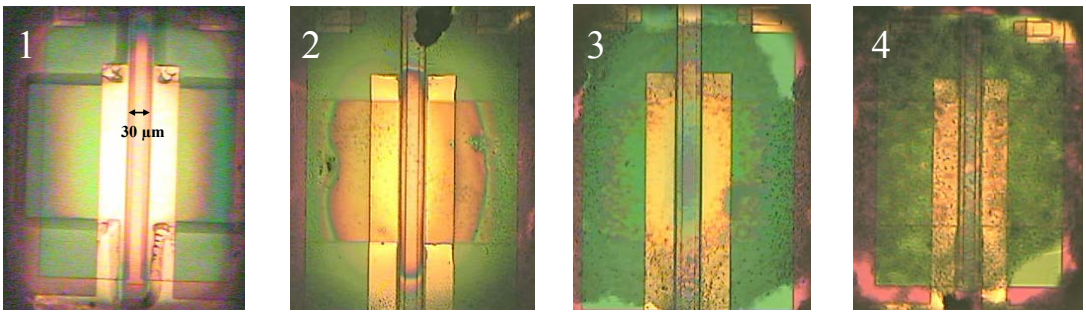

Figure 5.2: Optical micrographs of PANI·CSA films cast on the IGFET (GT03 platform[100]) (1) without IL and with (2) χ_{IL}=0.51, (3) χ_{IL}=0.68, and (4) χ_{IL}=0.76. The layer is cast on between two Au electrodes separated by 30 µm.

Table 5.1 summarizes the effect of the presence of IL in the gel like layer by keeping the doping level of PANI·CSA in the casting solution the same. With the increase of the mol fraction of BMI(Tf_2N) from 0 and 0.76, the thickness and roughness of the cast layers increases. The small discrepancy between the calculated theoretical thickness and the actual measured thickness can be attributed to the formation of meniscus at the walls of the CHEMFET well (Table 5.1).

Table 5.1: Physical characteristics of PANI·CSA layers prepared with IL's in different mol ratios, χ_{IL}.

χ_{IL}	film thickness (nm) measured / calculated	film roughness (nm)	$\tau_{90\%}$ / d step up	$\tau_{90\%}$ / d step down	δ step up	δ step down
0	200±10 / 250	9	1.74±0.26	1.19±0.06	0.55	0.77
0.51	500±25 / 750	112	0.11±0.02	0.17±0.01	0.60	0.50
0.68	1000±50 / 1250	255	0.05±0.02	0.07±0.01	0.61	0.59
0.76	1250±62 / 1750	545	0.07±0.01	0.12±0.01	0.49	0.42

[a]Calculated film thickness = d = PANI mass/[(PANI density)(FET width)(FET length)] + IL mass/[(IL density)(FET width)(FET length)].

To understand the effect of concentration of IL on the electronic properties of PANI·CSA/ BMI(Tf_2N) layer , optical absorption spectra for various mol fraction of IL in the film were recorded, Figure 5.3. With an increase of IL in the layer, a slight increase in the half width of the polaron band at 1.5 eV accompanied by a slight red shift (~0.05 eV) and the Peierls distortion occurring between 2.5 to 3 eV is observed. The

Peierls distortion mirrors the change in the alternating sequence of the benzenoid and quinoid rings.[102] The insert in Figure 5.3 shows the changes in the ratio of the bands at 1.5 eV (π- polaron transition) to 3.5 eV (π-π* transition). When IL is added to PANI in the ratio of χ_{IL}=0.51, the ratio of the two bands increases. However, further addition causes the band ratio to decrease. Since all the layers contain the same mol ratio of PANI to CSA (2 : 1), the observed changes in the two bands' ratio could possibly represent the changes in the electrostatic interactions between the PANI and the IL. This fact is supported by the work function measurements with the Kelvin probe (Figure 5.3). The addition of IL to the layer increases the work function (WF) of the layer measured against the gold electrode suggesting that the layer is changing to be more noble. Increase of work function of PANI·CSA/IL films upon addition of IL can be explained by the fact that imidazolium cation acts as an electron acceptor with respect to PANI.

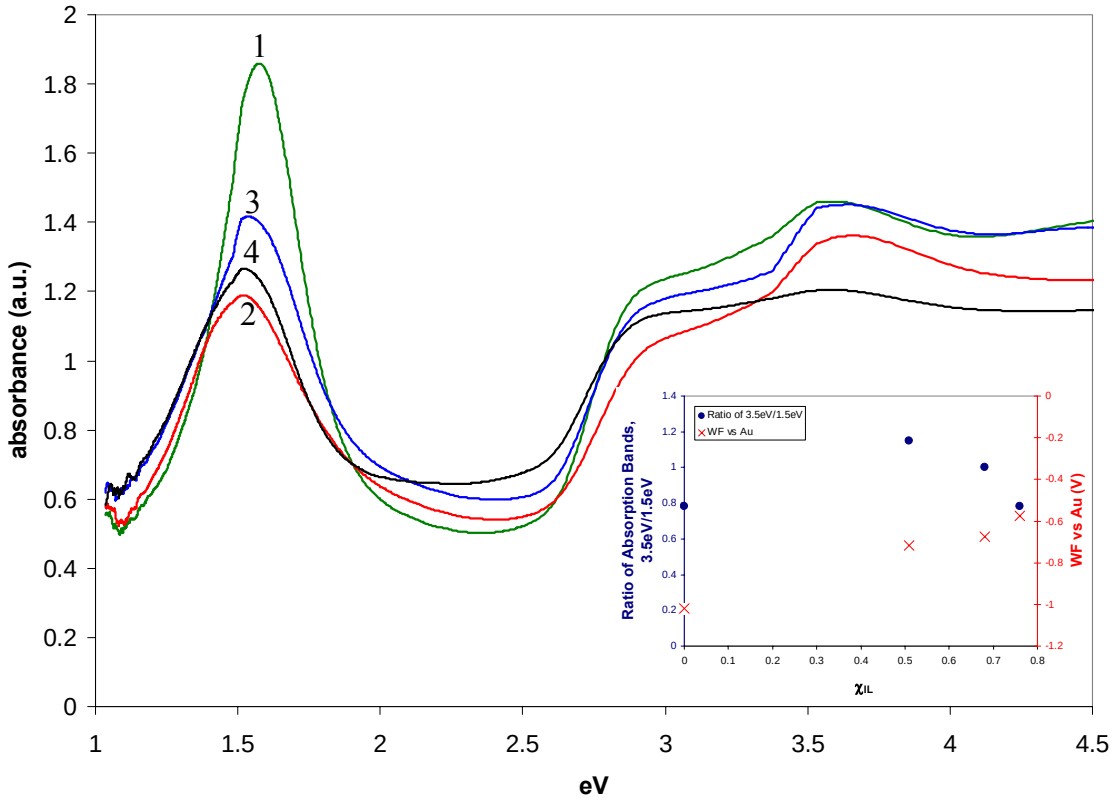

Figure 5.3: Optical absorption spectra of PANI cast on quartz crystal (1) without IL and with IL at concentrations (2) χ_{IL}=0.51, (3) χ_{IL}=0.68, and (4) χ_{IL}=0.76. Insert shows the ratio of absorbance at 3.5 to 1.5 eV and the WF versus Au.

5.3.2 Dynamic Behavior

The main objective of this work was to optimize the response time of the sensor by optimizing the amount of ionic liquid in the organic gel. The dynamic behavior is characterized as time for the sensor to reach 90% of its equilibrium value ($\tau_{90\%}$), for step changes of concentration of ammonia "up" (520 to 694 ppm) and "down" (694 to 520 ppm). In analogy with dynamic behavior of ion selective electrodes[24] the "step-up" times are shorter than the corresponding "step-down" times. This is consistent with different boundary conditions for these two changes.[103] The equilibrium response of WF

sensors is logarithmic, just as it is for ion-selective electrodes and for ion selective field-effect transistors (ISFET). In such potentiometric ion sensors the response originates at the interface of the thick (relative to Debye length) membrane with the sample while the bulk of the membrane remains electrically neutral. In contrast the response of WF CHEMFET involves interaction with the bulk of the membrane as well as with the membrane/dielectric interface to which the analyte must penetrate. This accounts for thickness-dependent response times of WF CHEMFETs. For this reason the 90% response times ($\tau_{90\%}$) reported in Table 5.1 were normalized to thickness. To our knowledge there is no exact expression yet that can describe the dynamic response mechanism of WF CHEMFETs. It is worth noting that the response time decreases with increasing content of IL despite the fact that the overall thickness of the membrane increases. Results shown in Table 5.1 demonstrate these opposing effects of increased content of ionic liquid: slowing down of the response due to larger thickness of the membrane compensated by the higher permeation rate. That fact can be attributed to the beneficial effect of the Knudsen diffusion of the analyte through the porous PANI/IL gel. Examples of the raw responses of the PANI·CSA/IL to "step-up" and "step-down" changes of ammonia are shown in Figure 5.4. In that case the step changes were made between two concentrations of analyte selected from within the dynamic range rather than between air (i.e. "zero gas") and some finite concentrations. The measurement of response times for concentrations selected from within the dynamic range is preferable due to the logarithmic nature of the sensor response.

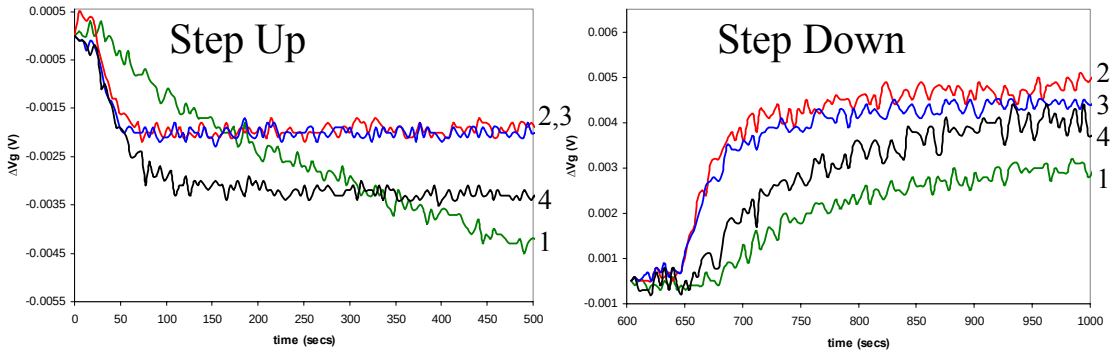

Figure 5.4: Raw responses of the PANI·CSA layers with and without IL as prepared in Figure 5.2 to ammonia for both "step-up" (520 ppm to 694 ppm) and "step-down" (694 ppm to 520 ppm).

5.3.3 Equilibrium Response

Modulation of Fermi level, E_F, of organic semiconductor by secondary doping with electron donor gas P_X has been described by the semiempirical equation :[104]

$$E_F = E_F^0 - \frac{kT}{2\delta}\ln(P_x + P_i)$$

where E_F^0 is the Fermi level of the organic semiconductor in the ambient of the inert gas P_i . Value of E_F^0 is given by its primary doping, and δ is a fractional charge donated by the donor gas X at partial pressure P_x. It is assumed that the relative shift of the Fermi level E_F due to this secondary doping is small compared to the intrinsic Fermi level value E_F^0. In other words, it is assumed that the overall electron affinity of the organic semiconductor remains essentially constant (i.e. E_F^0 = const.). That is the weakest assumption in that model but it can be justified if the overall excursion of E_F upon secondary doping is less than 100 meV.[97]

The Fermi level modulation due to the analyte gas interaction can be observed as the shift of the gate voltage, V_G, when the sensing layer is deposited on the CHEMFET. Such response is shown in Figure 5.5 for the CHEMFET modified with PANI·CSA/$IL_{0.68}$

layer. It can be seen that the sensor responds reversibly and reproducibly to stepwise changes of concentration of ammonia. It is possible to determine the value of δ from this plot. It has been tabulated in Table 5.1 for different concentrations of IL in the membrane both for "step up" and "step down." The change of slopes indicate that electron is donated from ammonia to PANI and also to the IL with a different value of δ. The decrease of δ with IL content correlates with the decrease of absorbance ratio as shown in Figure 5.3 (insert). The calibration curves for four different concentrations of IL are shown in Figure 5.6. They show that the films which contain IL have lower detection limit, albeit with different value of slope (sensitivity) due to large value of δ due to electron transfer to the IL.

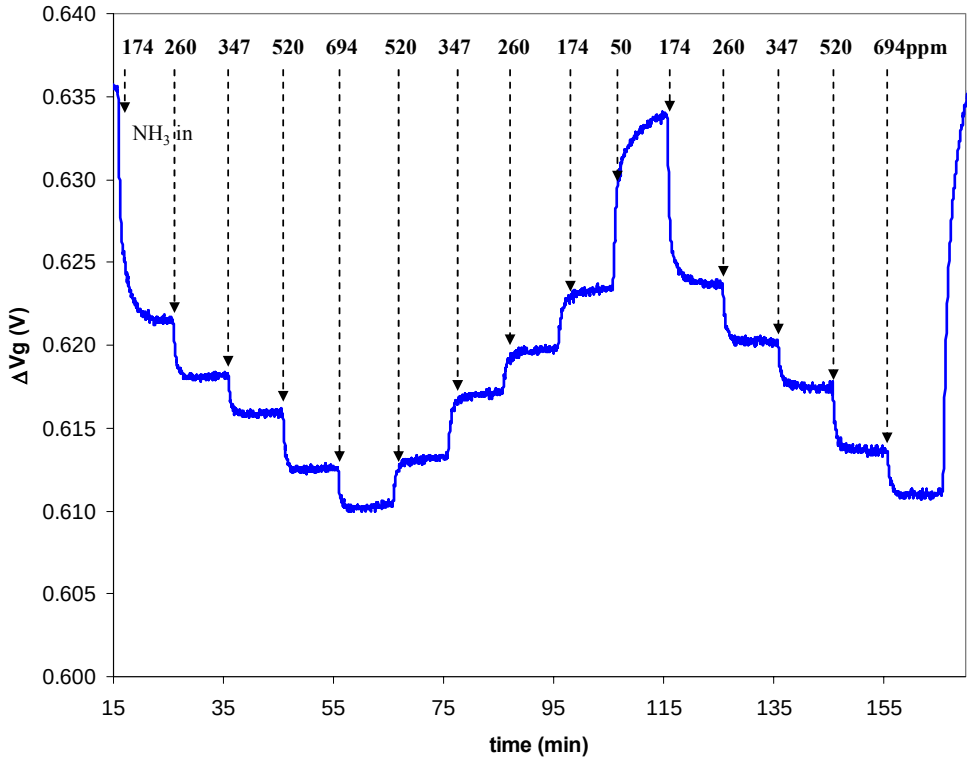

Figure 5.5: CHEMFET response to stepwise exposure of ammonia gas with PANI·CSA film containing IL of χ_{IL}=0.68. The individual step-wise changes of ammonia concentration are shown by arrows.

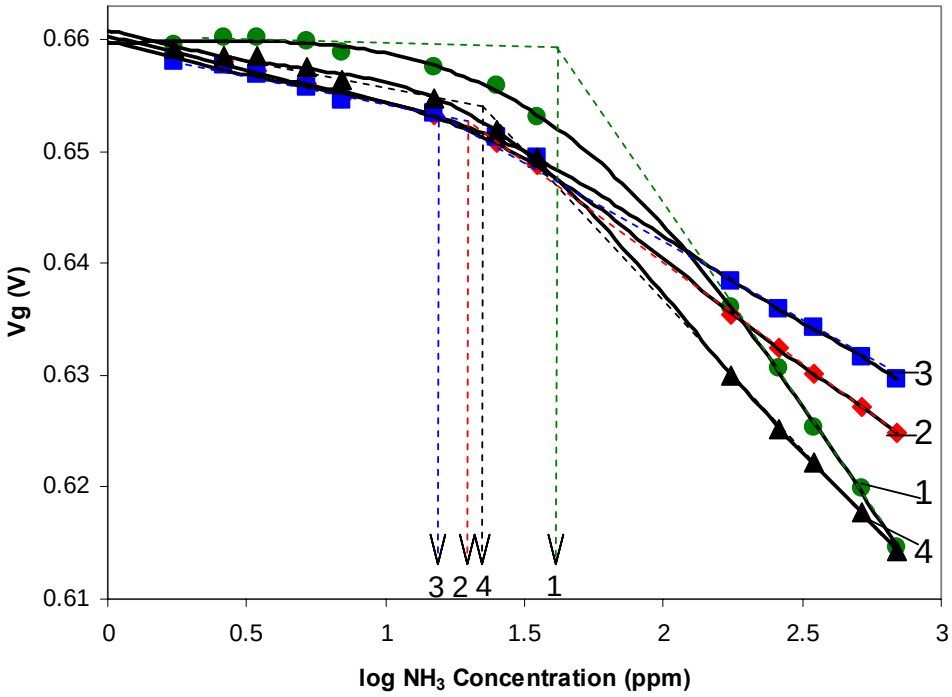

Figure 5.6: Calibration of PANI·CSA layers response to ammonia as a function of IL content in the film: (1) without IL and with IL (2) χ_{IL}=0.51, (3) χ_{IL}=0.68, and (4) χ_{IL}=0.76. The dashed lines indicate the estimated detection limit.

5.4 Conclusions

As demonstrated in this paper, considerable improvement is observed in the performance of gas sensors with PANI·CSA/IL layers. The gel-like sensitive layer results in faster response times as well as in somewhat greater sensitivity and lower detection limit. The optimum performance has been obtained for χ_{IL}=0.68 in PANI·CSA. The primary goal of this paper was to show how using a PANI/IL composite would enhance the general sensing properties of our CHEMFETs as opposed to testing for specific or interfering gases. Our measurements clearly show that evaluation of dynamic as well as equilibrium response of logarithmic sensors must be done from "step-wise" changes of concentration between two defined values within the dynamic range rather

than from the “zero gas” value. Nevertheless, sensor response observed from “zero gas” (i.e. baseline) value can be useful if the sensor is used e.g. as an alarm.

CHAPTER VI

FIELD-EFFECT TRANSISTORS WITH MIXED IONIC-ELECTRONIC GATE

6.1 Introduction

Both electrical and chemical properties of the gate material play an essential role for optimizing performance of work function chemically sensitive field-effect transistors (WF CHEMFET). The desired chemical selectivity can be achieved by rational choice of organic semiconductor (OS), by incorporation of selective binding sites into the electronically conducting matrix and by tuning its electron affinity.[97] These factors determine the initial value of work function of the gate material and thus determine the initial value of the threshold voltage. The electrical conductivity is not of the primary concern for CHEMFET operation since no current passes through the ideally designed CHEMFET. A leakage current passing through the gate dielectric is a sign of a problem, that may lead to experimental artifacts.[105-107] The absence of the current in the selective material is the most fundamental difference between CHEMFET and an "organic field-effect transistor" (OFET), in which current passes through the active, chemically sensitive layer. Because both work function and conductivity play an important role in the chemical response, the OFET used as chemical sensor is really a field-modulated chemiresistor. Both types of sensors belong to the relatively new class of active devices commonly known as "organic electronics".

Our recent approaches to tuning of chemical properties of the selective layer containing ionic liquids have been described in separate publications.[108,109] In this paper we examine the role of ionic and electronic conductivity of such gate materials and on the importance of the placement of the active material in the sensor structure. The relative

contribution of ionic and electronic conductivity has been varied by changing the ratio of room temperature ionic liquid (RTIL) to emeraldine salt of polyaniline (ES-PANI). This sensing material has been placed and studied on field-effect transistor structure in two different configurations. In the first it could be operated as an insulated gate field-effect transistor (WF CHEMFET) and in the second as a field-modulated chemiresistor (i.e. OFET). These studies have confirmed a fundamentally different role of operation of electronic materials when used in these two types of chemical sensors.

6.2 Experimental

6.2.1 Transistor Fabrication

The test platform shown schematically in Figure 6.1, has been designed and fabricated.[105] It has all the features of conventional silicon IGFET except that it has two gate contacts over which the layer of OS gate is deposited. A two-layer gate dielectric is formed by 80 nm of thermally grown SiO_2 and 80 nm of chemically vapor deposited, high-temperature silicon nitride, respectively.

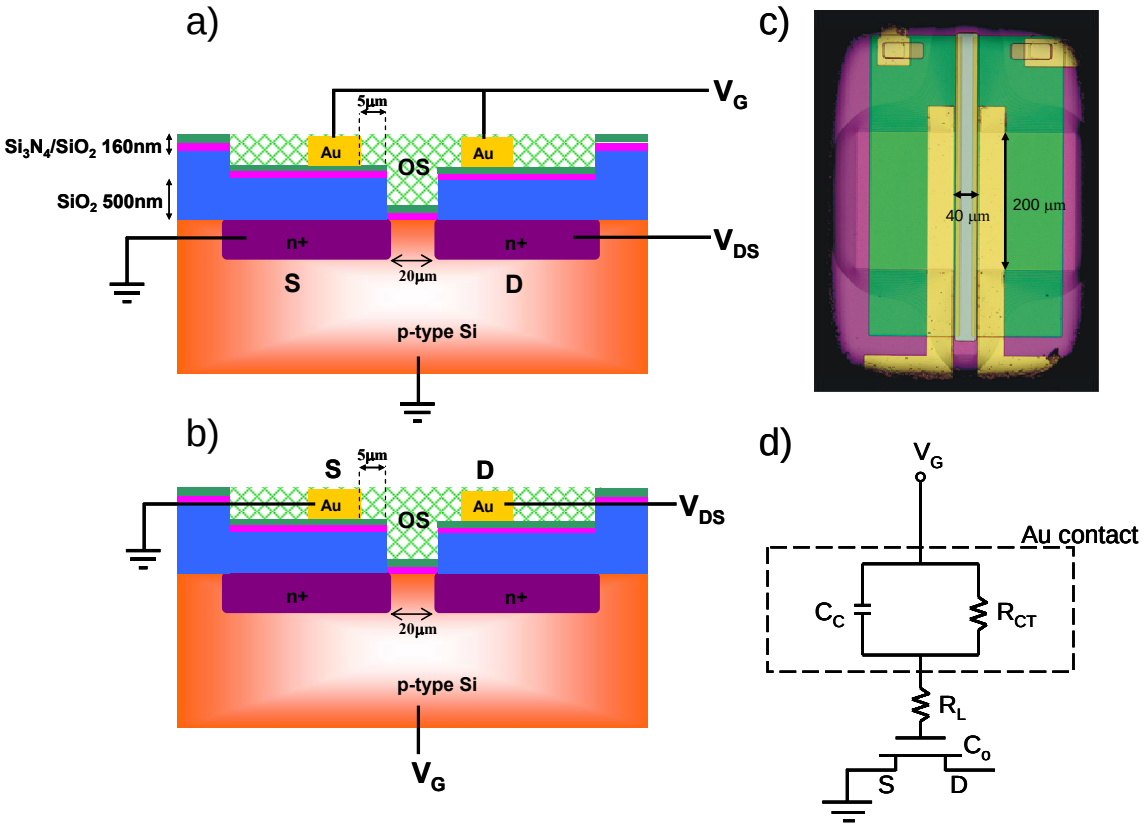

Figure 6.1: Schematic of the dual-purpose solid state IGFET/OFET chip used in this study.[105] The gate dielectric consisted of 80 nm of SiO_2 and 80 nm of Si_3N_4. Thickness of the field oxide was 500 nm . (a) In the IGFET configuration the Au serves as the gate contact. (b) in the OFET (chemiresistor) configuration the Au contacts serve as drain and source, respectively and the silicon substrate is used as a gate. (c) Top view of the IGFET/OFET chip. The oval border is the epoxy photoresist well used for drop-casting the gate material. (d) Equivalent electrical circuit representing CHEMFET gate connection and formation of the "virtual capacitive divider" (C_C+C_0).

The test platform can be operated as a regular IGFET as shown in Figure 6.1a, a common gate-to-source voltage, V_G, is applied to both contacts and drain-to-source current, I_D, flows in silicon, between n-doped drain and source electrodes. This platform can also be

used as an OFET when it is connected as shown in Figure 6.1b. In that case the two Au contacts (Ti 10 nm/Au 150 nm) are designated as drain and source, respectively, and V_G is applied to the p-Si substrate. The drain-to-source current then flows through the organic semiconductor, and the field modulation takes place in the OS, somewhere in the gate region above the gate dielectric.

6.2.2 Instrumentation

Transistor characterizations were performed on a Hewlett-Packard 4155A semiconductor parameter analyzer together with HP 16442A test fixture. IGFET measurements were performed of drain-source current, I_D, versus gate voltage with a constant drain voltage of V_D = 7 V and drain-source current versus drain voltage at different applied gate voltages. The $I_D - V_D$ and $I_D - V_G$ scans were performed at the scan rate of 400 mV s^{-1}.

6.2.3 Chemicals

Formic acid (88 %, Fisher Scientific), ammonium hydroxide solution (29.3 %, Fisher Scientific), and (1R)-(-)-10-camphorsulfonic acid (CSA) (Aldrich) were used as received. Polyaniline emeraldine base, (PANI-EB) powder (MW ca. 20K, Aldrich), was treated in ammonium hydroxide solution (28%, Fisher) for 2 hours (with stirring), filtered, and then extracted with deionized water and methanol.[99] The room temperature ionic liquid 1-butyl-3-methylimidazolium bis(trifluoromethanesulfonyl)-imide, BMI(Tf_2N), was synthesized according to the standard procedure.[58] In order to remove the halides the product was dissolved in methylene chloride and multiple water extractions were performed. It was then purified by stirring it with activated charcoal overnight. The solution was then filtered through a celite filter to remove the activated

charcoal. The excess organic solvent was then evaporated at 10^{-2}-10^{-3} bar in a vacuum oven for 12hr at 60ºC.

The PANI/IL composites were prepared by serial dilutions. First, a solution of 50 mg PANI-EB powder in 10 mL of formic acid was made and used to prepare a PANI·CSA composite mixture by dissolving 6.42mg of CSA in 1 mL of the PANI/HCOOH (Solution A). The amount of added CSA was calculated to be in the ratio of two CSA molecules per four benzene units of the repetitive segments of the PANI chain. The second stock solution (Solution B) was made by adding 1 wt% room temperature ionic liquid (RTIL) into the formic acid. The solution A was diluted with formic acid and then mixed with solution B in appropriate ratios to give 0, 0.01, 0.32, 1, 8, and 32 mol% ES-PANI in RTIL. The above solutions were drop-cast into the wells of FET array[109] using a glass capillary, with approximately 0.02 mm^3 orifice. The films were dried at 80 ºC for 24 h in vacuum oven. The drying removes the volatile solvent formic acid from the films.

6.3 Results and Discussion

6.3.1 IGFET Mode of Operation

Transistor with chemically sensitive layer drop-cast on top of the device depicted in Figure 6.1 can be used in CHEMFET (Figure 6.1a) or in OFET mode (Figure 6.1b). For the proper IGFET operation it is required that the gate is ohmic, meaning that at least some fraction of the conductivity is electronic. To put it in electrochemical terms the connection between the gate contact, i.e. Au electrode and the gate dielectric must be non-polarized. Ionic liquids are known to be excellent electrochemical media, highly conductive and with electrochemical window extending up to 5 V.[13,29] That means that in

the absence of some redox couple (depolarizer) the interface between the Au electrode and RTIL is almost ideally polarized. In such case the charge transfer resistance R_{ct} in the equivalent electrical circuit of the WF CHEMFET (Figure 6.1d) is very large and a virtual capacitive voltage divider is created from the contact capacitance C_C and gate capacitance C_0, which are in series. In electrochemical terminology, the contact capacitance C_C has the meaning of double layer capacitance. Presence of a capacitive voltage divider in potentiometric sensors violates the "one capacitor rule" of operation of potentiometric sensors[110] and leads to their unstable behavior. In order to avoid such problem the charge transfer resistance R_{ct}, at the Au/RTIL contact must have a finite value, even if such contact does not carry any net current during normal operation of the device. The bulk resistance of the selective layer, R_L, in the layers investigated in this study was always low and could be neglected.[109]

6.3.2 I_D-V_D Characterization

Effect of the gate contact resistance on the transistor characteristics is shown in Figure 6.2 and 6.3. Compositions of the RTIL/ES-PANI have been investigated in multiple steps, in the range between 0 mol% ES-PANI (i.e. pure RTIL) to 32 mol% ES-PANI. At the high loading of ES-PANI the value of charge transfer resistance is low and as expected the $I_D - V_D$ curves obey exactly the theoretical IGFET relationship (Figure 6.2a). Interestingly, even when the gate is made of pure RTIL and the Au/RTIL contact is capacitive the drain current reaches saturation in a curve that somehow resembles the theoretical $I_D - V_D$ relationship (Figure 6.2f). Nevertheless, there is a significant difference between the purely ionic and electronic layer. It is clearly seen in the dashed curves in Figure 6.2a, which belong to Figure 6.2f and were interposed into the Figure

6.2a panel. Furthermore, a more significant artifact is seen at the beginning of V_D sweep, between -2.0V and 0.0 V, which is most pronounced for higher values of applied gate voltages ($V_G > 3$). It is caused by the charging of the gate as the sweep of the V_D voltage is initiated and the gate voltage is changed abruptly from zero to some non-zero value. This charging effect on the gate, has no particular significance for I_D-V_D curves, but it further illustrates the presence of the capacitive gate contact and its role in the virtual capacitive divider.

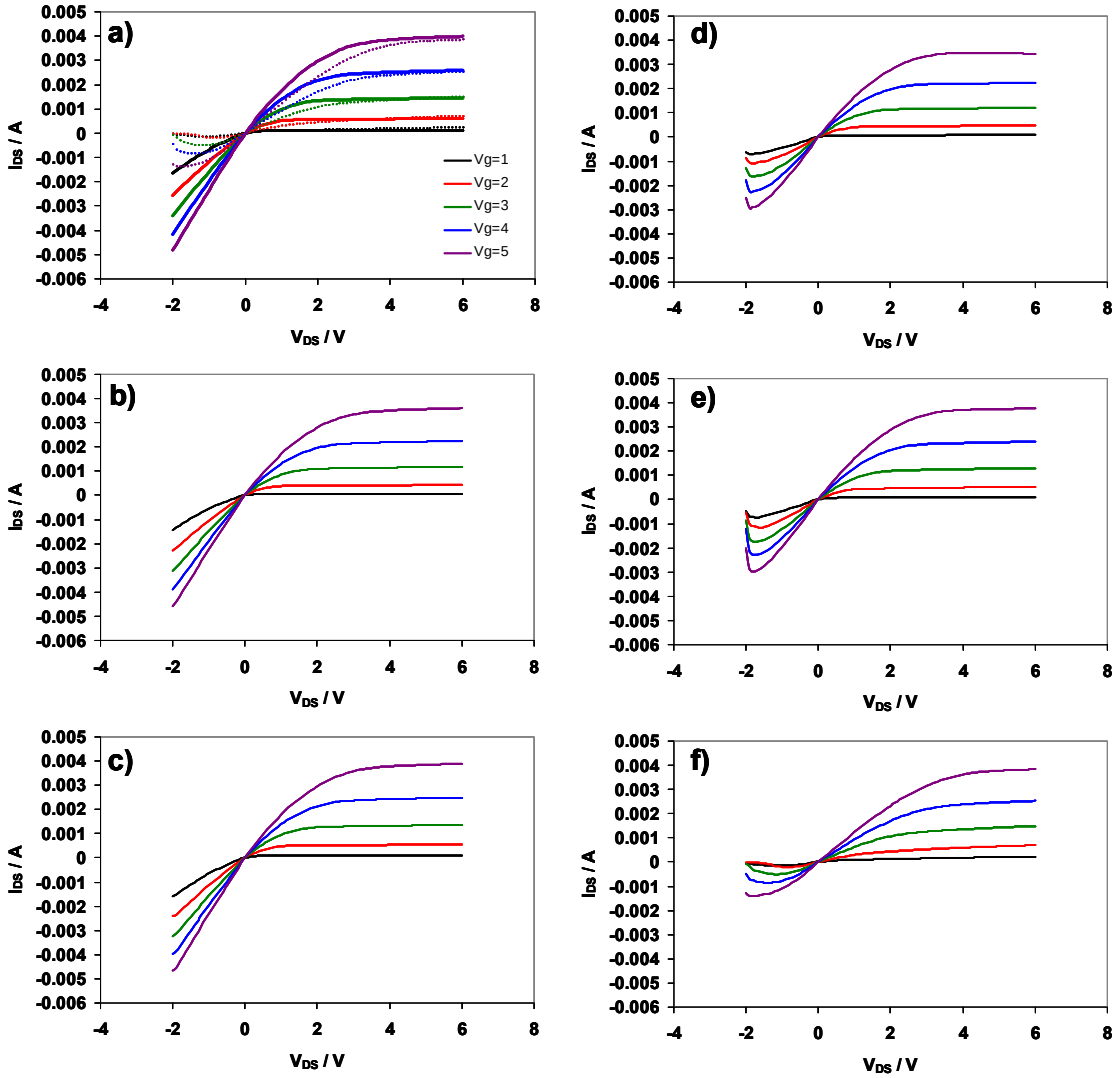

Figure 6.2: $I_D - V_D$ curves for the device tested in IGFET configuration with transistor gate material consisting of a) 32 mol% ES-PANI, b) 8 mol% ES-PANI, c) 1 mol% ES-PANI, d) 0.32 mol% ES-PANI, e) 0.01 mol% ES-PANI, and f) pure RTIL. The dashed lines in panel (a) are the $I_D - V_D$ curves shown in panel (f). They are show in order to highlight the characteristics of FET with pure RTIL.

6.3.3 I_D-V_G Characterization

On the other hand the effect of capacitive contact on the shape of $I_D - V_G$ curves is quite dramatic. The curves for 32 mol% ES-PANI, Figure 6.3a, again obey the theoretical IGFET characteristic. They overlap exactly for five repeated sweeps of gate voltage (Figure 6.3a). However, the $I_D - V_G$ curves for purely ionic gate (0 mol% ES-PANI) are random and completely irreproducible (Figure 6.3f). The minimum concentration of ES-PANI necessary to provide an ohmic contact and to yield reproducible and stable FET operation was found to be > 0.32 mol %. It is important to note that the ionic conductivity of the bulk gate material is high. Therefore the cause of this irreproducibility is the high value of the gate contact resistance.

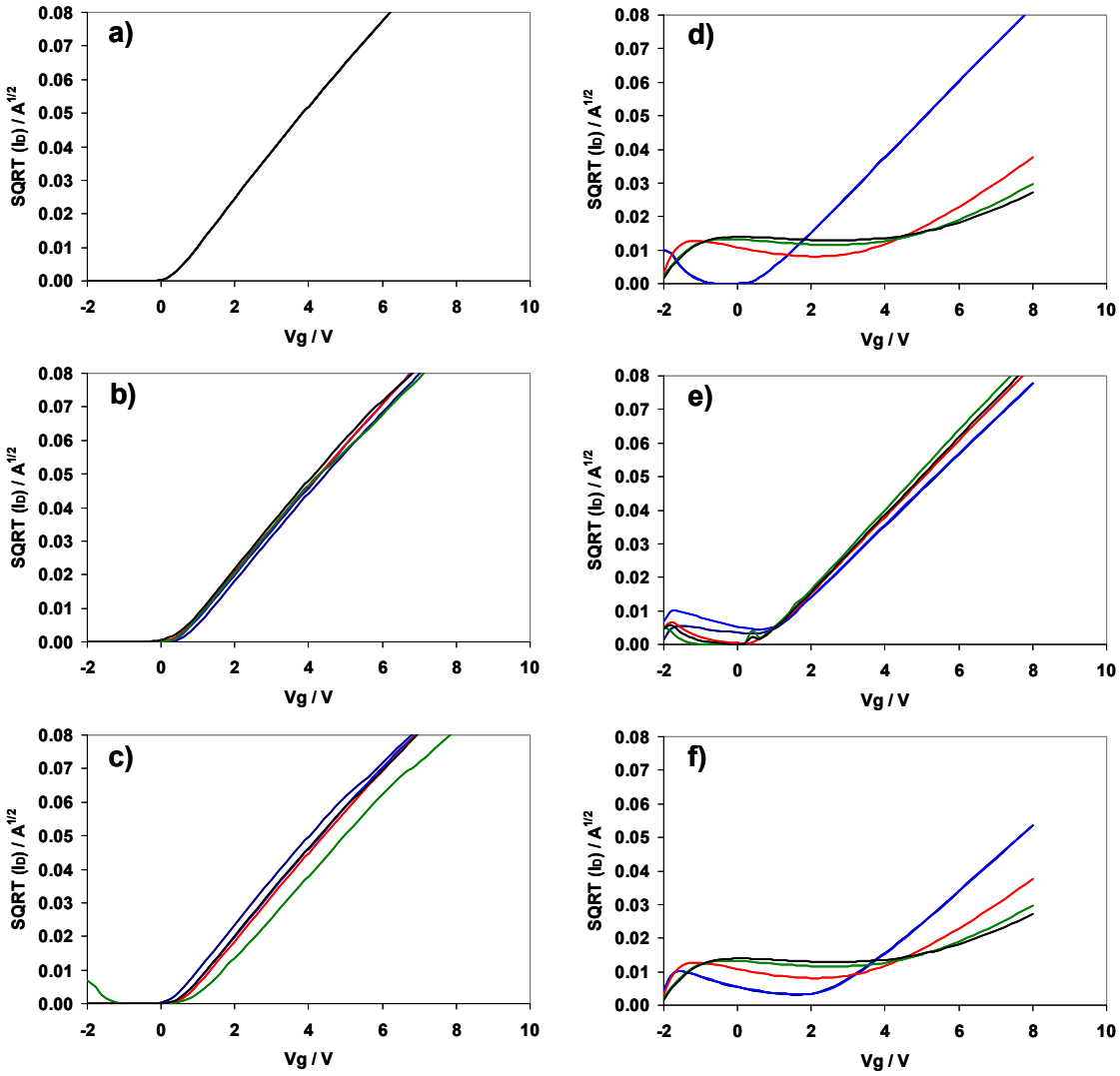

Figure 6.3: $I_D - V_G$ curves for the device tested in IGFET configuration with transistor gate material consisting of a) 32 mol% ES-PANI, b) 8 mol% ES-PANI, c) 1 mol% ES-PANI, d) 0.32 mol% ES-PANI, e) 0.01 mol% ES-PANI, and f) pure RTIL.

6.3.4 Work Function and Threshold Voltage

As expected, the work function of the RTIL/ES-PANI gate is affected by the composition. That effect has been first noticed in our study of optimization of the composition of such material for detection of ammonia where it was measured by the Kelvin Probe.[108] Increasing the concentration of RTIL increases the electron affinity (i.e. work function) of the material. Consequently, the threshold voltage of the WF CHEMFET shifts to the more positive values. Both the Kelvin Probe data and the threshold voltage data are shown in Figure 6.4.

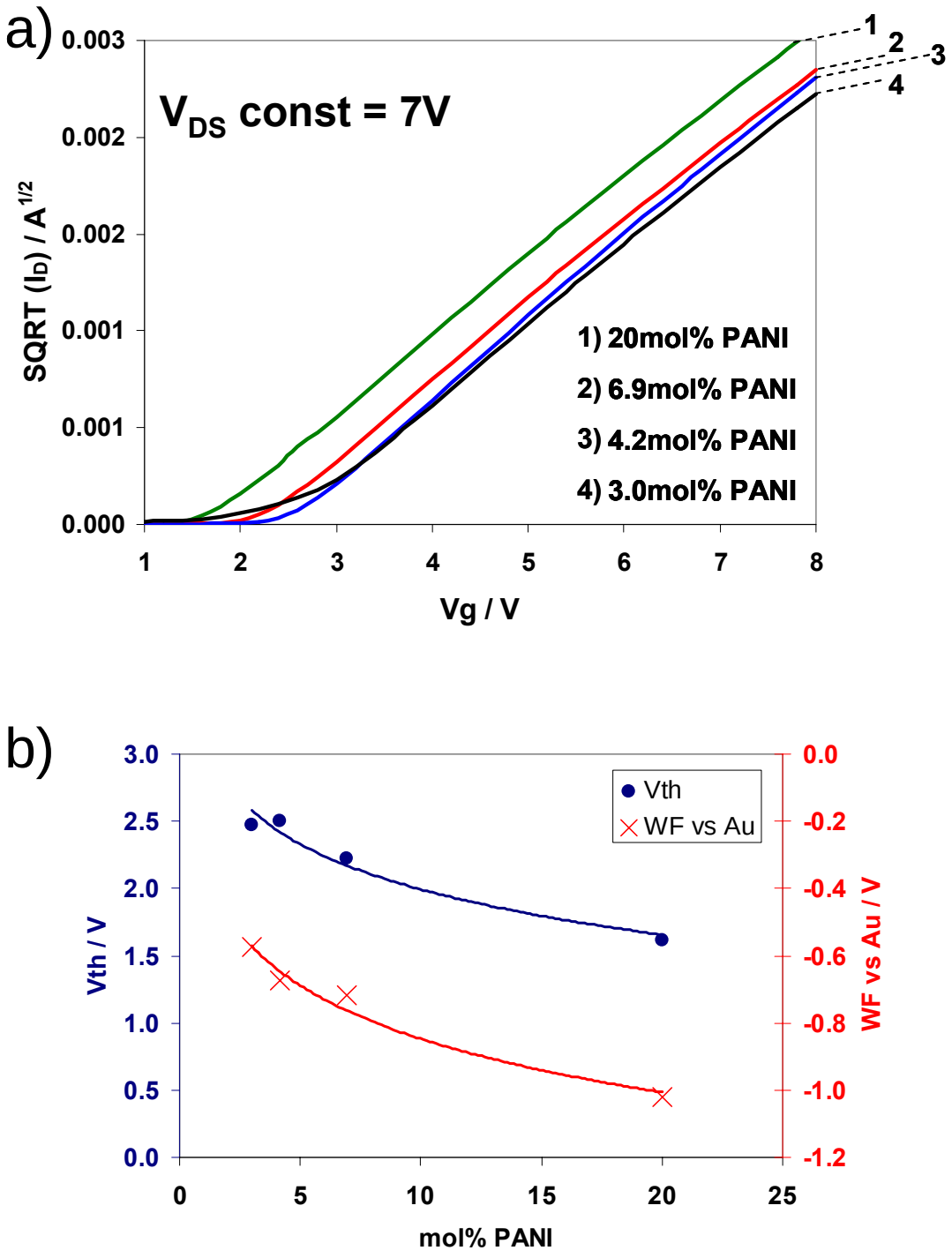

Figure 6.4: Dependence of (a) drain current – gate voltage curves for 1) 20mol% ES-PANI, 2) 6.9mol% ES-PANI, 3) 4.2mol% ES-PANI and 4) 3.0mol% ES-PANI and (b) threshold voltage (work function), on the composition of the gate material. The devices were operated in saturation (V_D= 7V).

6.3.5 OFET Mode of Operation

After the characterization as WF CHEMFET the devices were connected to the OFET configuration. This was done in order to verify the behavior of the same sensing layers under the conditions that would be encountered if they were used as chemiresistors, to our knowledge the RTIL/ES-PANI material has never been proposed as an OFET gate material. In fact, it is not a defined semiconductor with defined energy band structure, but rather a dispersion of a semiconductor (ES-PANI) in ionically conducting medium (RTIL). Nevertheless, it works quite well as a sensing material when properly located in the device structure. In the OFET configuration the current-voltage relationship shows more or less linear resistive and poorly reproducible behavior. There was no indication of any field-modulation of the overall resistance, up to -15 V of applied gate voltage. In order to further ascertain the possibility of field modulation we have used an interdigitated co-planar test structure that allows separation of contribution of the contact resistances from the resistance of the active material.[107] It can be also used to study the effect of added perpendicular electrical field on the value of such resistances. In the case of RTIL/ES-PANI material no field modulation has been found. That finding is not surprising because high conductivity of the ionic liquid precludes formation of space charge at the contacts. It corresponds to performing electrolysis in the presence of high concentration of inert supporting electrolyte. It is a very different situation from that when current is passed through the OFET with a genuine organic semiconductor, such as pure, undoped poly (3-hexyl thiophene) active layer. In such polymer the depletion layer was formed at the drain contact upon passage of drain current, resulting in formation of

the diffusion-depletion space charge, which is then modulated by the gate electric field.[107,111]

6.4 Conclusions

Several important points have been highlighted in this study. First, it has been shown that the ohmic gate contact, rather than bulk conductivity (ionic) of the gate material is the prerequisite for stable operation of WF CHEMFET. Second, it has been shown that a material that forms ohmically coupled gate contact satisfies the requirements to be used as a sensing material in the WF CHEMFET. The same material fails when it is used as a chemiresistor in the OFET configuration.[111] It is understood that the suspension of emeraldine salt of polyaniline (a semiconductor) in ionic liquid is a "poor conductor", rather than a semiconductor material with defined band structure. Therefore, the placement of the material in the field-effect structure and the electrochemical nature of the contacts to that layer are just as important as the properties of the material itself. If the contact is predominantly capacitive it forms a capacitive divider with the gate dielectric in series. That leads to irreproducible behavior of the device (Figure 6.2f and 6.3f). It is important to note that the commonly used "$I_D - V_D$ curves" have very little diagnostic value for visual identification of the proper field-effect behavior of transistors. It is so because the resistances, which are involved in the passage of current through most organic materials are non-linear with respect to the applied drain voltage, and always reach saturation. On the other hand, transistor $I_D - V_G$ curves are very sensitive indicators of the operation of the field-effect device, including of the nature of the gate contact.

CHAPTER VII

FUTURE WORK

7.1 Long-Term Stability and Performance of PANI/IL Sensing Layers

Having evaluated the dynamic and equilibrium response of the PANI/IL sensing layer, the next step is to examine the long-term stability and performance of the sensing layers under different conditions. Experiments would be conducted to determine how reproducible the sensor response would be after a period of several days to months. In addition, the sensors should be analyzed under varying operating conditions such as change in temperature, humidity, light exposure, etc.

7.2 Tuning of PANI/IL Sensing Layer WF

The objective of this thesis was to show how using a PANI/IL composite would enhance the general sensing properties of our CHEMFETs as opposed to testing for specific or interfering gases. However, the sensing layer can be tuned to be more selective or sensitive to certain gases by changing its work function. This can be accomplished in part by employing ILs with different cations and anions that accept or donate electrons to varying degrees. Therefore, by simply changing the IL structure in the PANI/IL sensing layer it is possible to change the work function of the material and hence its affinity for certain gases.

7.3 Synthesis of Nanoparticles from Ionic Liquids

Attempts to combine two cutting-edge topics, nanoparticles (NPs) and ionic liquids (ILs), have been intensively investigated.[112-115] Recently, alcohol ILs have been used in the preparation of metal NPs, causing the formation of monodisperse and

sizeselective metal NPs. The NP size and uniformity depend on the structure of the cation in ILs.[116] Preparation of these nanoparticles from ionic liquids would provide a new material that could possibly provide enhanced sensing capabilities, as the nanoparticles, i.e. Au clusters, have catalytic properties that can contribute to sensor applications.

APPENDIX A

CHEMISTRY OF POLYANILINE

A.1 Electrochemical Preparation of Polyaniline

In the electrochemical synthesis of polyaniline, the anodic oxidation of aniline is conducted on an inert metallic electrode, the most commonly used electrode material being platinum. One advantage of using this method is that the product from electrochemical synthesis is "clean" and does not necessarily need to be extracted from the initial monomer/oxidant/solvent mixture. Formation of the radical cation (step 1) of aniline on the electrode surface is considered to be rate determining step, shown in Figure A.1. This is followed by coupling of radicals, primarily *N*- and *para*-forms, and elimination of two protons. The dimer is then oxidized on the electrode surface with the aniline forming a radical cation which couples with an aniline radical cation to continue propagation of the chain as shown in step 4 of Figure A.1.

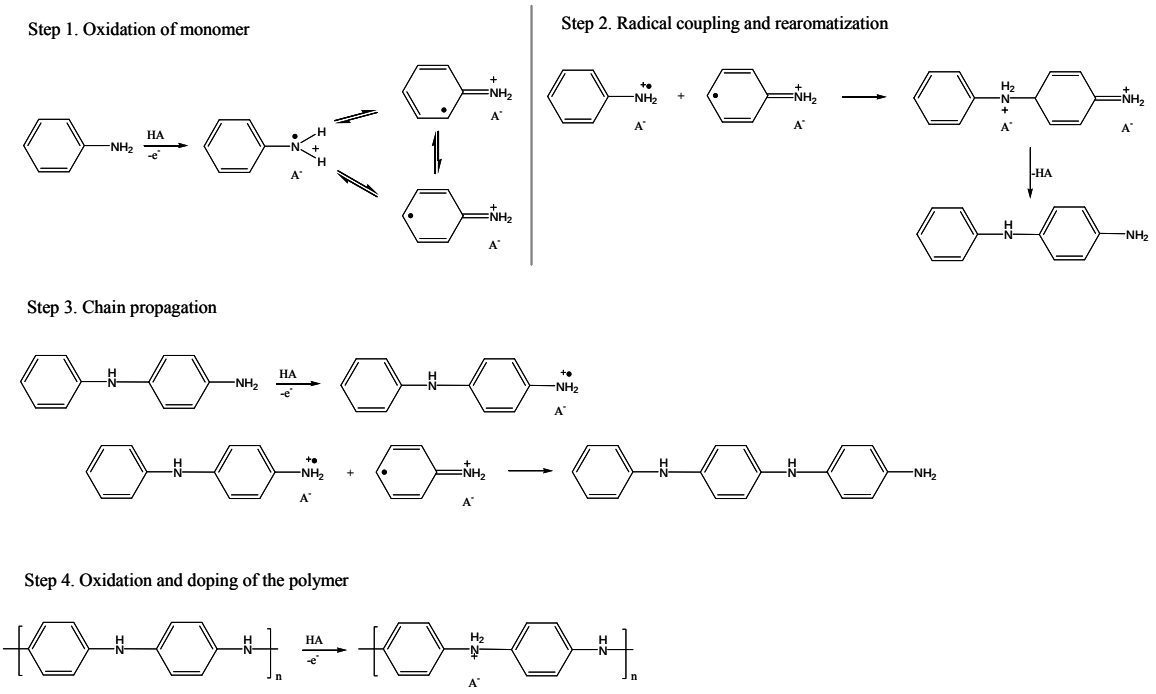

Figure A.1: Electropolymerization mechanism of aniline.[117]

A common technique used in the electropolymerization of aniline is cyclic voltammetry. The deposition of PANI by cyclic voltammetry has the advantage of a short exposure time at anodic potential and the reduction of the unreacted oxidized species during the cathodic scan. During electrochemical polymerization, three major oxidation peaks are observed during the anodic scan as shown in Figure A.2. The first two, A and B are attributed to changes in oxidation state of the polyaniline films: from leucoemeraldine to emeraldine (A), and from emeraldine to pernigraniline (B). Each electron in this process represents the presence of four aniline repeating units in the material on the electrode surface. This oxidation is reversible; two cathodic waves (A' and B') appear upon reversing the potential sweep resulting in reduction of the

polyaniline back to the leucoemeraldine state. This is further supported by a color change of the film from nearly transparent to dark green, and from dark green to dark blue, respectively. Peak C corresponds to over-oxidation of the polyaniline and takes place when the potential of the electrodes is raised above 800 mV resulting in irreversible and oxidative damage to the film. A very small oxidation wave (peak D) is located approximately at 440 mV and is attributed to oligomers or "living radicals" formed during the electropolymerization. In addition, during the reduction and oxidation of the polyaniline film uptake and expulsion of protons and anions occurs. The anodic peak (A) corresponds to the expulsion of protons.[74] It can be used to quantify the amount of polyaniline originally deposited at the electrode. The second anodic peak (B) corresponds to the uptake of the anions in the film. Its position and shape are strongly dependent on the type of the anion.[74] The reverse peaks, A' and B', occur in the reduction of the film corresponding to the uptake of protons and expulsion of the anions, respectively. Moreover, a cyclic voltammogram of the film grown in Figure A.2 was performed in 2M HBF_4 without the addition of aniline as shown in Figure A.3. As can be seen, the peak at 440 mV is significantly reduced indicating the film is homogeneous and that the oligomers responsible for the peaks around 440 mV have been removed. Studies also show the uptake and expulsion of the proton and anion depend strongly on the dopant acid used governing the redox peak potential and shape.[74]

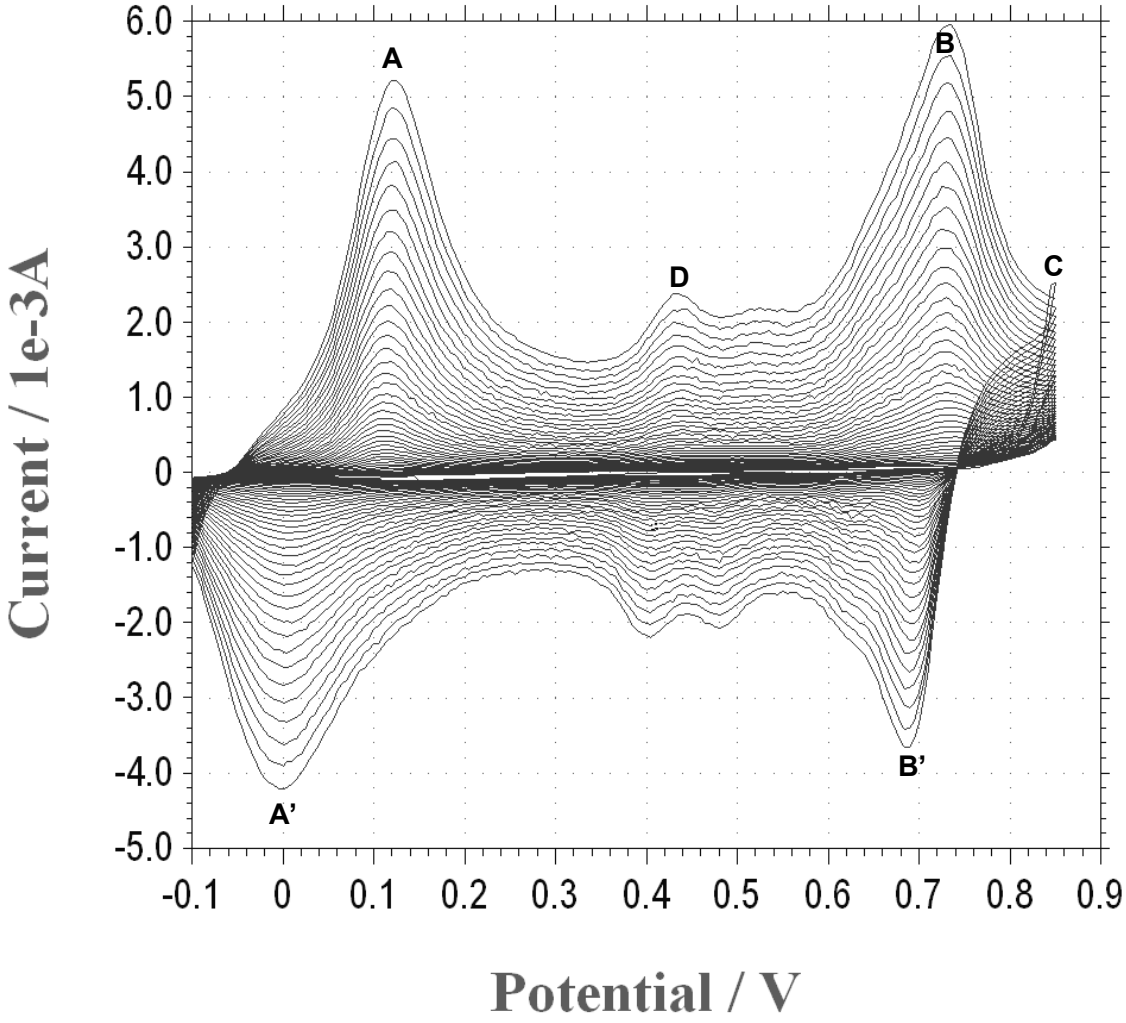

Figure A.2: Cyclic voltammograms of 0.1M aniline recorded at Pt electrode in 2M $H(BF_4)$ at 20 mV/s.

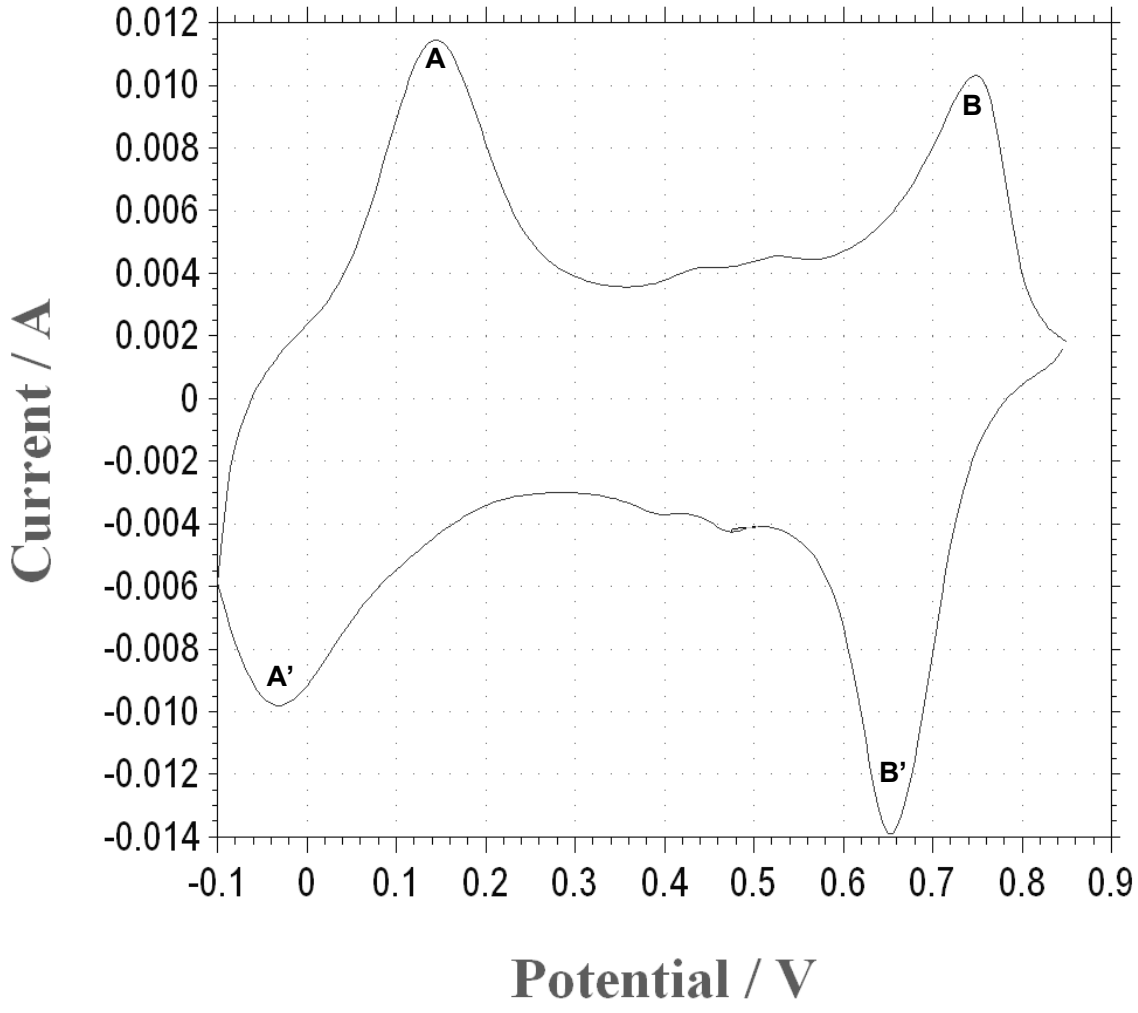

Figure A.3: Cyclic voltammogram of grown polyaniline film on Pt electrode in 2M HBF_4 at 20 mV/s.

A.2 Chemical Preparation of Polyaniline

In addition, polyaniline can be prepared by direct oxidation of aniline using an appropriate chemical oxidant. In the chemical synthesis, aniline is mixed with the chemical oxidant in a reaction vessel and left for a certain period of time. Various chemical oxidizing agents, the most commonly used being ammonium peroxidisulfate, $(NH_4)_2S_2O_8$, have been used and the reaction is mainly carried out in acidic conditions

(pH<3). Because the $S_2O_8^{2-}$ is a two-electron oxidizer, this allows the removal of two electrons for each aniline monomer during polymerization. In the first step of the polymerization, the aniline radical cation is formed which then couples with another radical cation with subsequent rearomatization of the dication of *p*-aminodiphenylamine. It then undergoes oxidation to the diradical dication which propagates the chain by reaction with a radical cation produced in the first step.

A.3 Electrochemistry of Polyaniline

A number of different oxidation states exist depending on the synthesis conditions of polyaniline. Each oxidation state can be doped to the corresponding salt form by protonic acid. While the electrical conductivity of most conducting polymers is related to the oxidation state of the polymer, in polyaniline the electrical conductivity is determined by two variables: the oxidation state and the extent of protonation. The base form of polyaniline can be generally represented as:

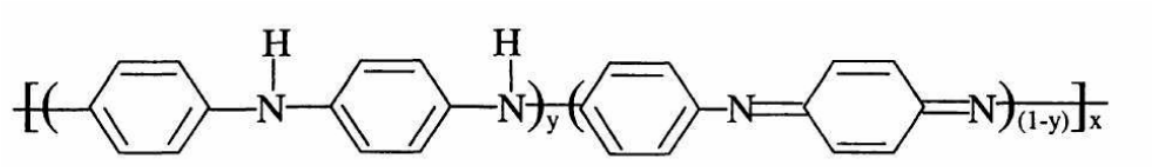

Figure A.4: Base form of polyaniline.

In the generalized base form shown above, (1-y) measures the fraction of oxidized units (imine species) on a macroscopic scale in a bulk sample whereas y measures the fraction of reduced units (amine species). (1-y) can be varied continuously from zero to give the completely oxidized polymer, to 0.5 to give the half oxidized polymer, to one to

give the completely reduced polymer. The various oxidation states of the polymer are summarized in Figure A.5.

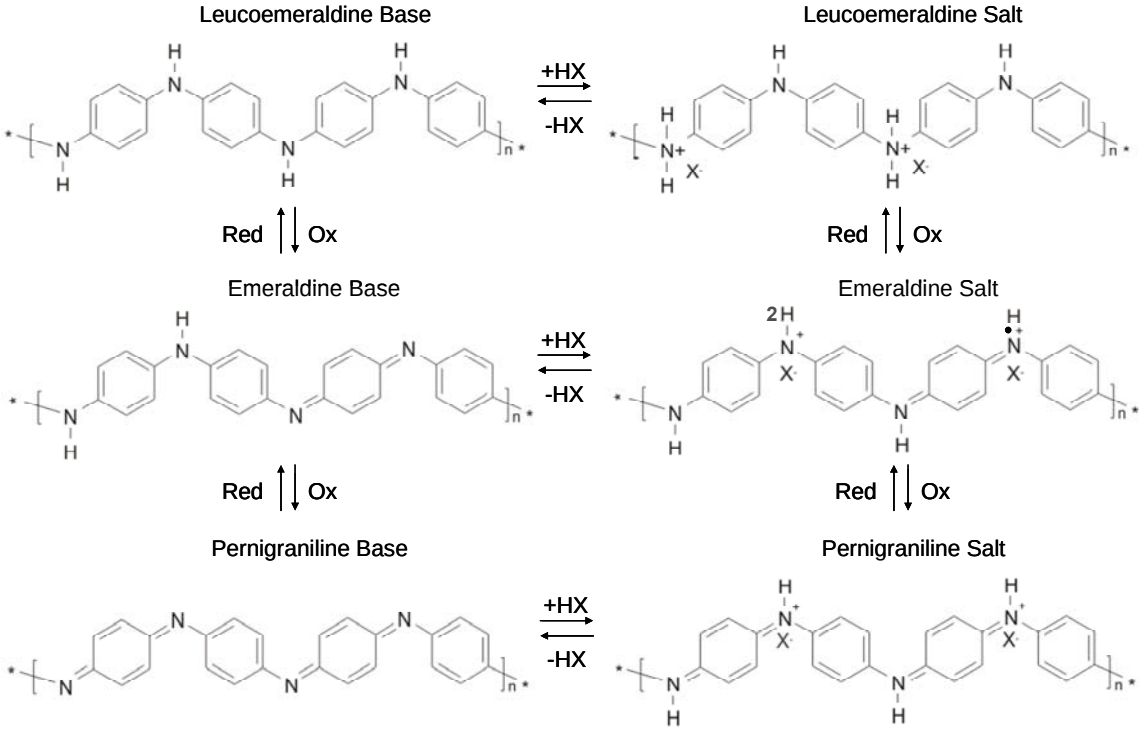

Figure A.5: The structures of polyaniline in different oxidation and protonation states.

The completely reduced polymer, where (l-y)=0, has no oxidized groups. All the nitrogen atoms are amine and all the aromatic rings are benzenoid rings. This form of polyaniline is commonly known as leucoemeraldine base. The completely oxidized polymer, where (l-y)=l, has only imine units. It has a one benzenoid ring to one quinoid ring structure and all the nitrogen atoms are imine. The polymer is referred to as pernigraniline base. It is very unstable and converts quickly to the lower quinoid stages. The half oxidized polymer, where (l-y)=0.5, has half oxidized units and half reduced

units. It has a three benzenoid ring to one quinoid ring structure and equal number of amine and imine nitrogen atoms and is referred to as emeraldine base. It is of special significance because the insulating emeraldine base becomes conducting when it is doped by protonic acid.

It is believed that all or some of the nitrogen atoms (imines or amines) in polyaniline can be protonated to yield a range of corresponding salts, the degree of protonation of the polymeric base depends on its oxidation state and on the pH of the aqueous acid. The protonation of polyaniline in the emeraldine oxidation state leads to a dramatic change in conductivity,[118] from ~10^{-10} S/cm for the unprotonated polymer to ~5 S/cm when "doped" by equilibration with aqueous acids at pH~0. The maximum conductivity occurs when polyaniline is 50% doped by protons to give the polaron lattice structure shown in the emeraldine salt form in Figure A.5. Under these condition, the polaron states overlap to form mid-gap bands allowing electrons to be thermally promoted at ambient temperatures to the lower energy unfilled bands resulting in conduction.[119] At doping levels higher than 50% some amine sites are protonated, and at levels lower than this some imine sites remain unprotonated. In both instances, delocalization of the charge carriers over the polymer backbone is disrupted, thereby reducing the polymer conductivity. The p*K*a values for the two acidic nitrogen groups within polyaniline have been determined by titration with NaOH to be 2.5 for the amine and 5.5 imine.[120]

REFERENCES

[1] J.C. Chiang and A.G. MacDiarmid, *Synth. Met.* 283, 102 (1998).

[2] J. Stejskal, D. Hlavata and P. Holler, *Polym. Int.* 294, 53 (2004).

[3] T. Skotheim, R. Elsenbaumer and J. Reynolds, *Handbook of Conducting Polymers*, Dekker, New York (1998).

[4] M. Freemantle, *Chem. Eng. News* 37, 78 (2000).

[5] P. Wasserscheid and W. Keim, *Angew. Chem. Int. Ed.* 3772, 39 (2000).

[6] K.R. Seddon, *J. Chem. Tech. Biotechnol.* 351, 68 (1997).

[7] P. Bonhôte, A.P. Dias, N. Papageorgiou, M. Kalyanasundaram and M. Grätzel, *Inorg. Chem.* 1168, 35 (1996).

[8] A. Elaiwi, P.B. Hitchcock, K.R. Seddon, N. Srinivasan, Y.M. Tan, T. Welton and J.A. Zora, *J. Chem. Soc. Dalton Trans.* 3467 (1995).

[9] H. Stegemann, A. Rhode, A. Schnittke and Fullbier, H., *Electrochim. Acta*, 379, 37 (1992).

[10] X. Li, D. Zhao, Z. Fei and L. Wang, *Science in China* 181, 35 (2006).

[11] D. Zhao, Z. Fei, T.J. Geldbach, R. Scopelliti and P.J. Dyson, *J. Am. Chem. Soc.* 126 (2004).

[12] R.Wang, T. Okajima, F. Kitamura and T. Ohsaka, *Electroanalysis* 66, 16 (2004).

[13] M.C. Buzzeo, R.G. Evans and R.G. Compton, *Chem. Phys. Chem*. 1106, 5 (2004).

[14] I.M. AlNashef, M.L. Leonard, M.A. Matthews and J.W. Weidner, *Ind. Eng. Chem. Res.* 4475, 41 (2002).

[15] M.C. Buzzeo, O.V. Klymenko, J.D. Wadhawan, C. Hardacre, K.R. Seddon and R.G. Compton, *J. Phys. Chem. A* 8872, 107 (2003).

[16] M.C. Buzzeo, O.V. Klymenko, J.D. Wadhawan, C. Hardacre, K.R. Seddon and R.G. Compton, *J. Phys. Chem. B* 3947, 108 (2004).

[17] D. Giovanelli, M.C. Buzzeo, N.S. Lawrence, C. Hardacre, K.R. Seddon and R.G. Compton, *Talanta* 904, 62 (2004).

[18] M.C. Buzzeo, C. Hardacre and R.G. Compton, *Anal. Chem.* 4583, 76 (2004).

[19] T.L. Broder, D.S. Silvester, L. Aldous, C. Hardacre and R.G. Compton, *J. Phys. Chem. B* 7778, 111 (2007).

[20] J.L. Anthony, E.J. Maginn and J.F. Brennecke, *J. Phys. Chem. B* 7315, 106 (2002).

[21] C. Liang, C.Y. Yuan, R.J. Warmack, C.E. Barnes and S. Dai, *Anal. Chem.* 2172, 74 (2002).

[22] X. Jin, L. Yu, D. Garcia, R.X. Ren and X. Zeng, *Anal. Chem.* 6980, 78 (2006).

[23] I. Goubaidoulline, G. Vidrich and D. Johannsmann, *Anal. Chem.* 615, 77 (2005).

[24] D.A. Buttry and M. Ward, *Chem. Rev.* 1355, 92 (1992).

[25] G. Sauerbrey, *Z. Phys.* 206, 155 (1959).

[26] L. Yu, D. Garcia, R. Ren and X. Zeng, *Chem. Commun.* 2277 (2005).

[27] E.D. Bates, R.D. Mayton, L. Ntai and J.H. Davis Jr., *J. Am. Chem. Soc.* 926,124 (2002).

[28] W. Lu, A.G. Fadeev, B. Qi and B.R. Mattes, *J. Electrochem. Soc.* 151, H33 (2004).

[29] T. Welton, *Chem. Rev*., 2071, 99, (1999).

[30] H. Olivier-Boubigou and L. Magna, *J. Mol. Catal. A-Chem.* 419, 182 (2002).

[31] J. Wilkes and *J. Mol. Catal. A: Chem.* 214, 11 (2004).

[32] A. Noda and M. Watanabe, *Electrochim. Acta.* 1265, 45 (2000).

[33] J. Dupont, R. F. de Souza and P.A.Z. Suarez, *Chem. Rev.* 3667, 102 (2002).

[34] P.A.Z. Suarez, S. Einloft, J.E.L. Dullius, R.F. de Souza and J.J. Dupont, *Chim. Phys.* 1626, 95 (1998).

[35] S.V. Dzyuba and R.A. Bartsch, *Chem. Phys.Chem.* 161, 3 (2002).

[36] S.V. Dzyuba and R.A. Bartsch, *Tetrahedron Letters*, 4657 (2002).

[37] Wen Lu, A. G. Fadeev, Baohua Qi, E. Smela, B.R. Mattes, Jie Ding, G.M. Spinks, J. Mazurkiewicz, Dezhi Zhou, G.G. Wallace, D.R. MacFarlane, S.A. Forsyth and M. Forsyth. *Science*, 983, 297 (2002).

[38] J.L. Anthony, E.J. Maginn and J.F. Brennecke, *J. Phys. Chem B.* 10942, 105 (2001).

[39] B.D. Fitchett, T.N. Knepp and J.C. Conboy, *J. Electrochem. Soc.* 151, E219 (2004).

[40] L. Xiao and K.E. Johnson, *J. Electrochem. Soc.* 150, E307 (2003).

[41] D. Zhang, T. Okajima, F. Matsumoto and T. Ohsaka, *J. Electrochem. Soc.* 151, D 31 (2004).

[42] A.D. Headley and N.M. Jackson, *J. Phys. Org. Chem.* 15 , 52 (2002).

[43] I.M. Alnashef, M.L. Leonard, M.C. Kittle. M.A. Mathews and J.W. Weidner. *Electrochem. Solid-State Lett.* 4, D16 (2001).

[44] Y. Katayama, H. Onodera, M. Yamagata and T. Miura, *J. Electrochem. Soc.,* 151, A59 (2004).

[45] D.T. Sawyer, *Oxygen Chemistry*, Oxford University Press, Oxford, England (1991).

[46] I.A. Koppel, R.W. Taft, F. Anvia, S.Z. Zhu, L.Q. Hu, K.S. Sung, D.D. DesMartenau, L.M. Yagupolskii, Y.L. Yagupolskii, N.V. Ignat'ev, N.V. Kondratenko, A.Y. Volkonski, V.M. Vlasov, R. Notario and P.C. Maria, *J. Am. Chem. Soc.* 3047,116 (1994).

[47] C. Lagrost, D. Carrie, M. Vaultier and P. Hapiot, *J. Phys. Chem. A*, 745, 107 (2003).

[48] A.E. Visser, R.P. Swatloski, W.M. Reichert, S.T. Griffin and R.D.Rogers, *Ind. Eng. Chem. Res.* 3596, 39 (2000).

[49] N.Gospodinova and L. Terlemezyan. *Prog. Polym. Sci.* 1443, 23 (1998).

[50] U. Schröder, J. Wadhawan, R.G. Compton, F. Marken, P.A.Z. Suarez, C.S. Consorti, R.F. de Souza and J. Dupont, *New J. Chem.* 1009, 24 (2000).

[51] K.R. Seddon, A. Stark and M.J. Torres, *Pure Appl. Chem.* 22075, 72 (2000).

[52] C.A. Wamser, *J. Am. Chem. Soc*., 409, 73 (1951).

[53] M. Anbar and S. Guttmann, *J. Phys. Chem.* 1896, 64 (1960).

[54] R. E. Mesmer, K.M. Palen and S.F. Baes, *Inorg. Chem.* 89, 12 (1973).

[55] R. E. Mesmer and A.C. Rutenberg, *Inorg. Chem.* 699, 12 (1973).

[56] R. J. Brown, P. J. Dyson and D. J. Ellis, *Chem. Commun.* 1862, 18 (2001).

[57] V. M. Hultgren, A. W. Mariotti, A. M. Bond and A. G. Wedd, *Anal. Chem.* 3151, 74 (2002).

[58] M. Quinn, Z. Ding, R. Moulton and A. J. Bard, *Langmuir* 1734, 18 (2002).

[59] Y. Yoshida, K. Muroi, A. Otsuka, G. Saito, M. Takahashi and T. Yoko, *Inorg. Chem.* 1458, 43 (2004).

[60] P. A. Suarez, V. M. Selbach, J. E. L. Dullius, S. Einloft, C. M. S. Piatnicki, D. S. Azambuja, R. F. D. Souza and J. Dupont, *J. Electrochim. Acta* 2533. 42 (1997).

[61] J.N. Butler, *Advances in Electrochemistry and Electrochemical Engineering*, (Eds. P. Delahay and C.W. Tobias), Interscience, New York, 77 (1970).

[62] P. Wasserscheid and T. Welton, *Ionic Liquids in Synthesis*, Wiley-VCH, Weinheim, Germany, 68 (2003).

[63] W. Weize, L. Wenjing, B. Han, T. Jiang, D. Shen, Z. Zhang, D. Sun and B. Wang, *J. Chem. Eng. Data*, 1597, 49 (2004).

[64] J. Zhang and A. M. Bond, *Anal. Chem.* 2694, 75 (2003).

[65] A.J. Bard, R. Parsons and J. Jordan, *Standard Potentials in Aqueous Solution*, IUPAC, Marcel Dekker, New York, (1985).

[66] M. Matsumiya, M. Terazono and K. Tokuraku, *Electrochimica Acta* 1178, 51 (2006).

[67] S. Strehlow, *The Chemistry of Non-Aqueous Solvents* (Ed. J.J. Lagowski), Academic Press, New York, 129 (1996).

[68] S. Eustis and M. El-Sayed, *Chem. Soc. Rev.* 209, 35 (2006).

[69] J.A. Smith, M. Josowicz and J. Janata, *Phys. Chem. Chem. Phys.* 3614, 7 (2005).

[70] G. Schmid, Ed., *Clusters and Colloids*, VCH, Weinheim, (1994).

[71] G.A. Ozin and A.C. Arsenault, *Nanochemistry,* RSC, Cambridge, (2005).

[72] U.Heiz and U. Landman, *Nanocatalysis*, Springer, New York, (2006).

[73] D.C. Trivedi, in: H.S. Nalwa (Ed.), Handbook of Organic Conductive Molecules and Polymers, John Wiley & Sons, New York, (1997).

[74] D.W. Hatchett, M. Josowicz and J. Janata, *J. Phys. Chem. B* 10992, 103 (1999).

[75] S. Kumar, R. Verma, B. Venkataramani, V.S. Raju and S. Gangadharan, *Solv. Extr. Ion. Exch.* 1097, 13 (1995).

[76] T. Johansson, N.K. Persson and O. Inganas*, J. Electrochem. Soc.* E119, 151 (2004).

[77] Y. Nagel and W. Beck, *Z. Anorg. Allg. Chem.* 529, 57 (1985).

[78] D.W. Hatchett, M. Josowicz and J. Janata, *Chem. Materials* 2989, 11 (1999).

[79] J.A. Smith, M. Josowicz and J. Janata, *J. Electrochem. Soc.* E384, 150 (2003).

[80] J.A. Smith, M. Josowicz, M. Engelhard, D.R. Baer and J. Janata, *Phys. Chem. Chem. Phys.* 3619, 7 (2005).

[81] R.C. Baetzold, *Inorg. Chem.* 118, 20 (1981).

[82] G.K. Wertheim, *Z. Phys. D* 319, 12 (1989).

[83] K. Jakub and Z. Sir, *Anal. Chim. Acta* 359, 172 (1985).

[84] M.C. Bernard, A.H. Goff, *Electrochim. Acta* 728, 52 (2006).

[85] J.P. Southall, H.V. Hubbard, S.F. Johnston, V. Rogers, G.R. Davies, J.E. McIntyre and I.M. Ward, *Solid State Ionics* 51, 85 *(*1996).

[86] J. Dupont and P. Suarez, *Phys. Chem. Chem Phys.* 2441, 8 (2006).

[87] J.L. Anderson, J.K. Dixon and J.F. Brennecke, *Acc. Chem. Res.,* 1208, 40 (2007).

[88] K. Hanabusa, H. Fukui, M. Suzuki, H. Shirai, *Langmuir* 10383, 21 (2005).

[89] S. Yeon, K. Kim, S. Choi, J. Cha and H. Lee, *J. Phys. Chem. B,* 17928, 109 (2005).

[90] H.B. Kim, J.S. Choi, S.T. Lim, H.J. Choi and H.S. Kim, *Synthetic Metals*, 189, 154 (2005).

[91] A. Fosmoe and L.L. Hench, *Chemical Processing of Advanced Materials*, Ed. by L.L. Hench and J.K. West, John Wiley & Sons, Inc., New York (1992).

[92] M. Zagorska, E. Taler, I. Kulszewicz-Bajer, A. Pron and J. Niziol, *J. Appl. Polym. Sci.* 1423, 73 (1999).

[93] A. Saheb, J. Janata and M. Josowicz, *Electroanalysis*, 405, 18 (2006).

[94] A. Yokozeki and M. Shiflett, *Ind. Eng. Chem. Res.* 1605, 46 (2007).

[95] J.L. Anthony, J.L. Anderson, E.J. Maginn and J.F. Brennecke, *J. of Phys. Chem. B*, 6366, 109 (2005).

[96] P.K. Kilaru, R.A. Condemarin and P. Scovazzo, *Ind. Eng. Chem. Res.* 900, 47 (2008).

[97] J. Janata and M. Josowicz, *Acc. Chem. Res.* 241, 31 (1998).

[98] J. Janata and M. Josowicz, *Nature Mater.* 19, 2 (2003).

[99] D.W. Hatchett, J. Janata and M. Josowicz, *J. Electrochem. Soc.* 4535, 146 (1999).

[100] B.J. Polk, J.A. Smith, S.P. DeWeerth, Z.P. Zhou, J. Janata and K. Domansky, *Electroanalysis,* 707, 11 (1999).

[101] I. Sasaki, J. Janata, M. Josowicz and A. Glezer, *Analyst*, 751, 131 (2006).

[102] W.P. Su and A.J. Epstein, *Phys. Rev. Letts.* 1497, 70 (1993).

[103] W.E. Morf, *The Principles of Ion-Selective Electrodes and Membrane Transport* Elsevier: Amsterdam, Chapter 14, (1981).

[104] J. Janata, J. *Anal.Chem.* 2546, 63 (1991).

[105] F. L'Hereec, Hang Chen, Zhipin Zhou and J. Janata, *J. Phys. Chem. B* 9042, 108 (2004).

[106] J. Janata, *Phys. Chem. Chem. Phys.* 5155, 5 (2003).

[107] Hang Chen, A. Rambhatla, J. Janata and K.P. Kamloth, *J. Electrochem. Soc.* H354, 154 (2007).

[108] A.H. Saheb, M. Josowicz and J. Janata, *Anal. Chem.* 4214, 80 (2008).

[109] I. Sasaki, J. Janata and M. Josowicz, *Polymer Degrad. Stabil.* 1408, 92 (2007).

[110] J. Janata, *Principles of Chemical Sensors*, Plenum, New York, 119 (1989).

[111] J. Janata and M. Josowicz, *J.Solid State Electrochem.* 2008, (in print).

[112] M. Antonietti, D. Kuang, B. Smarsly and Y. Zhou, *Angew. Chem., Int. Ed*., 2, 43 (2004).

[113] J. Dupont, G. S. Fonseca, A. P. Umpierre, P. F. P. Fichtner and S. R. Teixeira*, J. Am. Chem. Soc.* 4228, 124 (2002).

[114] K.-S. Kim, D. Demberelnyamba and H. Lee, *Langmuir*, 556, 20 (2004).

[115] R. Tatumi and H. Fujihara, *Chem. Commun.* 83, 126 (2005).

[116] Ki-Sub Kim, Sukjeong Choi, Jong-Ho Cha, Sun-Hwa Yeon and Huen Lee J. *Mater. Chem.* 1315, 16 (2006).

[117] P.C. Innis and G.G. Wallace, *J. Nanosci. Nanotech.* 441, 2 (2002).

[118] A. Ray, G. E. Asturias, D. L. Kershner, A. F. Richter, A. G. MacDiarmid and A. J. Epstein, *Synth. Met.* E141, 29 (1989).

[119] J. Tanaka, N. Mashita, J. Mizoguchi and K. Kume, *Synth. Met.* E175, 29 (1989).

[120] C. Menardo, M. Nechtschein, A, Rousseau and J.P. Travers, *Syth. Met.* 311, 25 (1988).